2013

High capacity digital beam steering technology

Daniel James Hebert
Louisiana State University and Agricultural and Mechanical College

HIGH CAPACITY DIGITAL BEAM STEERING TECHNOLOGY

A Dissertation

Submitted to the Graduate Faculty of the
Louisiana State University and
Agriculture and Mechanical College
in partial fulfillment of the
requirements for the degree of
Doctor of Philosophy

in

The School of Electrical Engineering & Computer Science

by
Daniel Hebert
B.S., University of Louisiana at Lafayette, 2004
M.S., Louisiana State University, 2007
August 2013

ACKNOWLEDGEMENTS

I would like to express how grateful and fortunate I am to receive professional and personal guidance, encouragement, and support from Professor Martin Feldman throughout the entire program. I'm grateful to Professors Theda Daniels-Race and Pratul K. Ajmera for advice and encouragement during the program. I would like thank committee members which include Professors John Dowling, Ashok Srivastava, and Carol Taylor (dean's representative) for the suggestions and support.

I would like to thank Marchelle Jones, Precious Cantu, Lakayla Greeup, Charlaya Washington, Ojala Obenga, Edwin Lee, and Cordell Scott for their work on the optical system. I would like to thank Dr. Pradeep Bathcheraya, Kenny Moses, and Tracy Jones, from the Department of Electrical and Computer Engineering at Southern University, for their time and effort in programming the processor and building the circuits for the optical system.

I am grateful to Mr. James Breedlove for the excellent work in building the fixtures and mounts that made this research possible.

I would also like to thank Charisma Edwards, Professor Wakeel Idewu, and Professor Brian Campbell for encouragement, advice, and help throughout the program.

I are thankful for the financial support from the U.S. Air Force Minority Leaders Program.

TABLE OF CONTENTS

LIST OF TABLES

LIST OF FIGURES

LIST OF SYMBOLS

θ : Common angular rotation of mirrors with respect to the polarizing beam splitter (PBS)
θ_R: Angle of Refraction
θ_1: Angular deflection for stage one
θ_n: Angular deflection at the nth stage
θ_N: Maximum angular separation at the last stage
R_s: Light horizontally polarized and transmits from the polarizing beam splitter.
T_p: Light vertically polarized and reflects through the polarizing.
n_{air}: Index of refraction for air
n_{PBS}: Index of refraction for a polarizing beam splitter
k: Illumination factor of a Gaussian beam of light brought to focus at a waist
λ: Wavelength of light
d: Incident beam diameter
β: Angular resolution and could equal θ_1.
NA: Numerical Aperture
f: Focal Length
L: Optical Path Length (OPL)
L_{PBS}: OPL for a polarizing beam splitter
L_{LC}: OPL for a liquid crystal cell
L_{QWP}: OPL for a quarter wave plate
L_{Epoxy}: OPL for epoxy
L_{Air}: OPL for air
N_{pair}: Number of vertical and horizontal deflector stage pairs
N: Number of stages in the one dimensional system.
x_n: displacement of the laser beam in the horizontal direction at the last stage resulting from the angular deflection at the nth stage
x: Maximum displacement in the horizontal direction is the sum of all displacements
y_n: displacement, of the laser beam in the vertical direction at the last stage resulting from the angular deflection at the nth stage
y: Maximum displacement in the vertical direction is the sum of all displacements
D_x: The width of the deflector at the last stage
D_y: The height of the deflector at the last stage

<u>LC material and cells</u>

$\Delta\varepsilon$: Dielectric constant within the LC material
$\varepsilon_{||}$: Dielectric constant perpendicular to the LC material's director
$\varepsilon_{\perp}$: Dielectric constant perpendicular to the LC material's director
ε_0: Dielectric constant in free space
Δn: Index of refraction within LC material
n_e: Index of refraction within LC material parallel to the director
n_o: Index of refraction within LC material perpendicular to the director
F: Elastic energy density of the LC material
k_{11}: Elastic coefficient for splay
k_{22}: Elastic coefficient for bend
k_{33}: Elastic coefficient for twist

k_{eff}: Effective elastic coefficient
$\hat{n}$: Director of the liquid crystal molecules
y_{eff}: Rotational viscosity of the LC material
t_{off}: Response time (relaxation time) required for a deformed liquid crystal to reach its equilibrium state
t_{on}: Response time required for the director to reorient to an applied electric field
d_{LC}: Thickness of the liquid crystal cell
V_{th}: Threshold voltage for parallel orientation of liquid crystal molecules
T: Transmitted Power (percent) after the beam passes through one LC cell.
u: Gooch and Tarry minimum
Δφ: Polarization after passing through the liquid crystal cell

Digital Operation

Y_a: Binary representation of output angles in the vertical direction
X_a: Binary representation of output angles in the vertical direction
$C_{n:}$ Binary label of the operation of the liquid crystal cell at the nth stage. Logic "0" is assigned when no signal is applied to the cell and logic "1" is assigned when a signal is driving the cells.
X_d: Binary label for the linear displacement in the horizontal direction is the binary sum of the horizontal displacements
Y_d: Binary label for the linear displacement in the vertical direction is the binary sum of the vertical displacements

Assembly tolerance

δ_{FT}: Angular offset for the LC cell from assembly to the deflector angle
x_{FT}: Centering offset for the LC cell from assembly to the deflector angle

Cross-talk

R_o : Cross-talk due to deviations in orientation angle
R_C : Cross-talk from the LC cell due to centering offsets during assembly
$R_{assembly}^{LC}$: Total Cross-talk from LC cell due to assembly tolerances.
R_{PBS}^{C}: Cross-talk in the polarizing beam splitter from input angles and assembly tolerances
$R_{Stage}(\theta_I, x)$: Cross-talk within a stage due to input angles and assembly tolerances
$R(t)$: Cross-talk from the LC cell due to switching speed

Circuits

I_n: Current from the quadrant detector (A)
f: Frequency (Hz)
R_f: Resistance (Ohms)
C: Capacitor (F)
V_{DC}: Voltage (V)

Appendix

I_V: Power of the vertically polarized incident beam.
T_V: Output power of beam which is vertically polarized
R_H:Cross-talk. Power of the unwanted beam which is horizontally polarized

ABSTRACT

A novel method is described in detail for steering light in many directions without moving mechanical parts. The method involves a combination of liquid crystal cells and polarizing beam splitters. The polarization at each beam splitter is controlled by applying a signal to its corresponding liquid crystal cell. A study of light steering techniques is described for efficient beam placement, in a line and plane.

These techniques permit accurate, non-mechanical, beam steering limited by the response time of the liquid crystal cells. A theoretical limit to the number of discrete directions is described and closely approached for the one dimensional system.

CHAPTER 1 INTRODUCTION

1.1 Importance of Non-Mechanical Beam Steering

The process of directing a beam of light from one point to another is called beam steering. One of the first and basic examples of a beam steering device is a two-axis gimbal scanner. A gimbal is a support that rotates an object (mirror) about an axis. Since the invention of gimbal scanners, the field of beam steering has increased substantially and numerous beam steering systems have been developed in almost every field. The fields include communications, imaging, integrated circuit, military, consumer electronics, orbital applications, etc.

For many years, the military has had interest in electro optic systems for identification, communication, air traffic, designation, and counter measures. All the systems mentioned require directing light in many directions. Due to advances in missile guidance systems, the military requires smaller, faster, lighter, accurate, and cheaper systems to place on planes for protection during flight missions. Also, each system should be capable of performing more than one function. A common tool currently used for beam steering is a two axis gimbaled scanner [1]. However, gimbaled scanners have slow response times, are large in size, expensive, and require routine maintenance.

Due to the limitations of gimbaled scanners, new methods for beam steering are currently being investigated. The systems are divided into two groups. The first group is labeled mechanical beam steering. A mechanical beam steering device is defined as a device that has a moving part (or parts) to direct a beam of light. Rotating prisms, MEMS mirrors, electro wetting prisms, and programmable phase arrays require the movement of components to steer a beam and are labeled mechanical beam steering systems [1-4]. The mechanical systems initially appear promising, however, the limitations of the devices are similar to gimbaled scanning systems.

The second group is non-mechanical beam steering devices. Non-mechanical beam steering devices direct a beam of light from one point to another without moving parts. Current methods for non-mechanical beam steering include Wollaston prisms, liquid crystal polarization gratings, volume holograms, liquid crystal phase arrays, and liquid crystal index of refraction modulation [5-9]. In recent reports, all three methods are capable for steering beam at large angles [6]. In comparison to mechanical beam steering devices, non-mechanical beam steering devices are cheaper, lighter, compact, accurate, and have faster response times.

Non-mechanical beam steering devices will replace mechanical beam steering devices for state of the art systems in the future. Due to the large number of systems requiring a beam steering device, many scientists and engineers are currently attempting to develop novel non-mechanical beam steering devices. While the fundamentals of physics form the basis for a particular non-mechanical beam steering device, its implementation and development must satisfy the specifications of industry and the military. The beam steering systems require a beam steering device capable of scanning at moderate frequencies over a large angular range with a high resolution. In many applications, the device must be compact, lightweight, and capable of working over a large range of wavelengths. The device is capable of performing more than one function. For example the device can detect and point to an object. The successful development of such a device will lead to state of the art communication systems and imaging systems.

The objective of this study is to address the development of novel non-mechanical beam steering devices, capable of steering either in a line or in a plane.

1.2 Preview of the Following Chapters

Chapter 2 reviews the “state of the art” mechanical and non-mechanical beam steering devices with an emphasis on non-mechanical beam steering devices involving liquid crystal cells. Therefore; a review of liquid crystal material and cells is discussed. Device limitations

and drawbacks are discussed while specifications required to overcome the problems (if possible) are provided.

Chapter 3 outlines the research goals and a summary is shown below:

1.) Study the principle of operation, theoretical limitations, and optimum design of a stage, one-dimensional, and two dimensional devices.
2.) Investigate the digital operation for a stage, linear, and planer system. A description and depiction of the liquid crystal cell logic for deflecting a beam of light in a line and plane is presented.
3.) Develop methods to measure and assemble a stage. Develop a one dimensional system which is composed of cascading stages.
4.) Develop a two dimensional beam steering device and compare to theory and alternative beam steering methods.

Chapter 4 discusses the principle of operation of a stage and system. A stage is composed of a liquid crystal cell and a deflector angle which consists of a polarizing beam splitter, two quarter-wave plates, and two mirrors. A system is composed of cascaded stages. The angular tolerances of the PBS and efficiency of the LC cell's polarization rotation are discussed with the cumulative effect of cascading stages. This chapter concludes with a description of the digital operation of a stage, one dimensional, and two dimensional systems.

Chapter 5 addresses theoretical limitations of a system which restricts the number of spots the system can resolve. The maximum deflection angle is $\sim \pm 15^{o}$ which is limited by the extinction ratio of the polarizing beam splitter and polarization efficiency of the liquid crystal cell. A study of the effect of cascading a large number of stages is presented. Increasing the number of stages by one increases the output directions by a factor of two. Increasing the

number of stages will increase the optical path length which corresponds to larger linear displacements at the last stage. Light must pass though the last stage. Increasing the incident beam width reduces the size of the resolved spots which increases the resolution. The beam width and the maximum linear displacement must pass through the last stage which is the theoretical limit. In the linear system the sum of the incident beam width and the total displacement must be smaller than the deflector width. The planer system requires the sum of the linear displacements and incident beam width must be smaller than the width and height of the polarizing beam splitter at the last stage.

Chapter 6 discusses the tools, systems, and methods for constructing a stage which include mirror/quarter-wave plate bonding using UV curing epoxy which is fixed to an L-bracket using candle wax. An optical system which can adjust and measure the angular deflection in the horizontal direction within an accuracy of ±10 μrad is discussed. The deflector angles are fixed using UV curing epoxy to bond the quarter-wave plates/mirrors to the polarizing beam splitter. An assembly was designed to hold the liquid crystal cell, at a 45 degree angle and centered with the polarizing beam splitter. Next the cross-talk due to the device and assembly tolerances is presented followed by the response time of the liquid crystal cell. Finally the stages power losses will conclude this chapter.

Chapter 7 discusses how to construct a system which is composed of several cascaded stages. The layout, tolerances, and adjustments are discussed. The problems encounter at the last two stages is described followed by two alternatives to overcome the problems (total displacement, active area of the liquid crystal cell). The first alternative is a reflective optical system between the last two stages while the second alternative uses liquid crystal cells with a larger active area. SU and LSU collaborated to design and implement the electronics for controlling the system.

The electronics used to test the system during assembly was a switch box and a processor and free-running oscillator was used to test the system after assembly.

The results of the linear array are provided in Chapter 8.The experimental results of a ten stage one dimensional beam steering device are presented with a discussion of the response time, cross-talk, and comparison to theory.

Chapter 9 reports an extension of a one dimensional beam steering system reported in chapter 7 to a two dimensional beam steering system. A two dimensional beam steering device consists of interleaved vertical and horizontal deflector stages. Modifications of the system layout were required to minimize periodic vertical offsets while a modification of the angular measurement technique was required to measure angular deflections along the horizontal and vertical directions. The experimental results of the two dimensional beam steering device are presented with a discussion of the response time, cross-talk, and comparison to theory. The chapter concludes with a comparison of the one and two dimensional beam steering devices.

Chapter 10 gives a brief summary of the results of the one and two dimensional beam steering devices with a comparison to alternative methods. The study ends with recommendations for future work.

CHAPTER 2 LITERATURE REVIEW

This chapter reviews the "state of the art" mechanical and non-mechanical beam steering devices. A brief discussion of mechanical beam steering systems which include two axis gimbaled scanners and rotating riley prisms is presented. Next, non-mechanical beam steering devices with an emphasis on devices involving liquid crystal cells are described in detail. Therefore a review of liquid crystal material and cells is discussed. Device limitations and drawbacks are discussed while specifications required to overcome the problems (if possible) are provided. The chapter concludes with a summary comparing the maximum angle, minimum angle, response time, resolution, scan rate, size, and cost.

2.1 Mechanical Beam Steering Devices

Mechanical beam steering methods include two-axis gimbaled scanners, rotating prisms, lenslet arrays, and MEMS. All mechanical beam steering systems methods use an actuator and/or an optical component for displacing a beam. In many cases a mirror, diffraction grating, lens, waveguide, or prism is integrated with an actuator. Applying an electric force, to the actuator, results in an angular or linear displacement of the optical component which results in a change in position for the beam. Vibrations from the actuator limit the resolution of the beam. In general, mechanical systems require routine maintenance or replacement.

2.1.1 Two Axis Gimballed Scanner/MEMS Mirrors

A two axis gimbaled scanner is composed of mirror fixed on actuator, rotary motor, etc. which is used to tilt the mirror at an angle. MEMS mirrors consist of a mirror fixed on an actuator which displaces or tilts the mirror, at an angle, when an electric force is applied to the actuator. The resolution of a gimbaled scanner is limited to vibrations from the actuator which restricts the resolution [9].

In recent developments a MEMS mirror device has a scanning range of 238 μrad in the horizontal direction and 197 μrad in the vertical direction. A time of 8 ms was required to scan the vertical range [10].

2.1.2 Rotating Riley Prisms

An alternative to changing the direction of a beam is to replace a mirror with a pair of prisms and the gimbal with a rotatory motor. Changing the angle of the prisms changes the angular displacement of the beam. The angular displacement of the beam depends on the prism's index of refraction, prism angle, and the incident angle. The rotating prism device is unable to move a beam in a straight line while changing the wavelength deflects the beam in a different direction (dispersive). Additional limitations include the size, cost, and complex control systems required to drive the mechanical rotating system. However it's important to emphasize that moving a beam in a straight line is the main limitation to this approach.

Optra Inc. has recently developed a rotating riley prism beam steering device which is composed of two prisms and two rotary motors to turn each prism [11]. In an attempt to reduce chromatic pointing errors a prism wedge was implemented. The prism wedge is composed of two prisms in which one prism is highly dispersive is combined with a low-dispersive prism. A scanning range of 120 degrees with an accuracy of 1 mrad and a response time of 110 ms was reported. However the device isn't capable of moving a beam in line. Instead, the direction the beam travels resembles the shape of a figure eight which is an improvement to prior methods which move the beam in a circle [12, 15]. Additional limitations include the lifetime of the bearings within the rotary motors and prism alignment within the system [49]. Mechanical system's which use rotary motors require routine maintenance to replace the bearings within the motor.

Ball Aerospace and Technologies Inc. have recently developed a 3-prism rotating riley system [13]. The system requires three rotary motors for turning each prism within the system. The group reports the third prism within the system enables beam deflection along a line. However the scanning range is reduced by a factor of 10 and the response time is 100 times slower (1 degree per second) compared to 2-prism rotating systems.

2.1.3 GRISMS

Raytheon Inc. has recently developed a new scanning system which is called a GRISM [14]. GRISM's is composed of two rotating prisms and a diffractive element which is usually a set of zone plates or a grating. The diffraction grating "somewhat" reduces the pointing errors by a factor of 10 compared to the two prism rotating system. However the diffraction efficiency changes with wavelength and incident angle. In the extreme case which involves wavelengths and incident angle outside the range can yield a ghost image.

2.1.4 Lubricated Adjustable Optical Wedge (LAOW)

MetaStable Instruments Inc., located in Missouri, has disclosed a "matched-lens" beam steering approach [16]. The wedge consists of a plano-concave lens, an index matched oil, and a plano-convex lens which is called a Lubricated Adjustable Optical Wedge (LAOW). The oil holds the two lenses in place and is a lubricant. The rotation of a lens results in a linear displacement. However, actuators are required to rotate one lens while contaminants in the oil will distort, if not ruin, the device.

2.1.5 Recent Developments

The Satellite and Wireless Communication Laboratory, at Ben-Guiron University of the Negev, has presented a mechanical beam steering device that changed the distance between two gratings [2]. Changing the distance, between the two gratings, results in coarse adjustments while

changing the wavelength gives fine adjustments. The reported accuracy was approximately 60 urad. Limitations include a large power loss (75 percent) from the gratings, the scanning range was 10 degrees, and coarse angle adjustments were observed for some wavelengths.

2.2 Non-Mechanical Beam Steering Devices

Non-mechanical beam steering devices include, birefringment and Wollaston prisms, LC phase arrays, LC variable index of refraction, LC polarization gratings, electro-wetting prisms, and holograms written into a LC cell [20-24].

2.2.1 LC Phase Arrays

Liquid crystal phase arrays consist of liquid crystal material and a liquid crystal cell. In their geometry liquid crystal phase arrays diffract light [34]. The two approaches for LC phase array steering include varying the blaze angle and varying the period [41].

Periodically varying the voltage between adjacent electrodes will change the index of refraction hence the optical path length within the liquid crystal cell. This approach is referred to variable beam steering throughout the literature [33]. The distance between adjacent electrodes require half-wave length spacing to steer at large angles [36]. Applying an electric force on one electrode can extend to neighboring electrodes which restricts the minimum spacing between electrodes (Fringing field effect) [35-36].

The liquid crystal cells are used to vary the blaze angle to reflect light at different angles [40, 17]. The smallest response times reported is on the order of milliseconds while poor steering efficiency for large angles is a major limitation [17, 37].

LC phase arrays have the potential to be used in all laser radio detection and ranging (RADAR) applications [38-40, 42].

2.2.2 Variable Index of Refraction

The liquid crystal cell can be used to deflect a beam of light at angle by changing the index of refraction. The method is composed of two beams and a nematic liquid crystal cell [18]. The two beams pass through the liquid crystal cell then cross paths (or collide) prior to exiting the liquid crystal cell. Beam 2 is reference beam and Beam 1 is incident beam. Changing the power of the reference beam changes the index of refraction of the liquid crystal cell which results in the deflecting the incident beam in a different direction. Also the maximum angular deflection depends on the reference beam diameter and the angle separating the two beams. The liquid cell doesn't need metal contacts to activate the liquid crystal material which have the potential to reduce or eliminate the majority of power losses, except refraction, associated with the liquid crystal cell.

Beam Engineering for Advanced Measurements Co. has demonstrated angular deflections of $\pm 12.4^{\circ}$ with a linear response (power vs. deflection angle) within angles of $\pm 9^{\circ}$ at a response time of ten seconds. However it's odd the author didn't make an effort to report the losses since the study included plots of input power vs. deflection angle. The authors report the smallest angular deflection was .5 degrees with large deviations in sequential angular deflections.

A liquid crystal cell is capable of deflecting a beam light at "large" angles by changing the power of a reference beam as opposed to applying a signal to cell. Since a signal isn't necessary to activate the liquid crystal material, the transparent conductive electrodes can be removed from the cell which will significantly reduce power consumption from the device. However the response time is very slow with non-linear deflections at larger angles while the smallest deflections were .5 degrees [18]. Therefore the technique isn't suitable replacement for

a two-axis gimbaled scanner currently used in communication systems. Also having reference laser source poses a risk for detection by an undesired party which could compromise a mission.

2.2.3 Holograms

The University of Michigan has demonstrated beam steering based on the principle of focal plane scanning [9]. The device is composed of a feed matrix, placed on the focal arc of filter lens array (FLA), fed by a feed network embedded by PIN diodes. A signal to the diodes determines which lens will release light which results in moving a beam. Beam steering at high frequencies was demonstrated (35 GHz) but, the beams wavelength is restricted to the millimeter range. Also, larger beam widths result in large losses, due to coupling, and smaller beam widths reduce the resolution.

2.3 Liquid Crystal Technology

2.3.1 Liquid Crystal Material

Liquid crystal materials contain characteristics of both a solid and a liquid within a range of temperatures. If the range is past the melting point, the material becomes a liquid. Liquid crystals consist of a group of organic molecules which contain a rod-like structure which changes orientation when an electric force field is applied. Liquid crystals are classified or labeled by the positional order and orientational order of the molecules within the material [19]. Nematic, Smectic, and Cholesteric are three main categories of liquid crystals.

2.3.1.1 Chemical Properties

The molecular structure of a rod like liquid crystal molecule is composed of a two or more ring system connected by a central linkage group [20]. The rings of the molecular structure define the range of molecular forces required to form the nematic phase. The electrical and elastic properties are also set by the rings of the molecular structure [21]. The central linkage group used to bond two rings affects the chemical stability of the liquid crystal molecule,

transition temperature, and resistance to moisture and radiation [21]. The terminal group ends the chain of liquid crystal has a large effect on the transition temperature and the electro-optic response of the material [22].

Smectic liquid crystals are similar to nematic liquid crystals. The molecules are parallel and arranged like tightly packed soda straws arranged in layers. In other words, smectic liquid crystals have a higher order, parallel alignment of molecules, and arranged in layers [23].

Cholesteric liquid crystals are arranged in layers aligned parallel and arranged in layers but the orientation slightly varies from one layer to the next forming a helical rotation [23].

2.3.1.2 Physical Properties

Nematic liquid crystals contain rod-like molecules (anisotropic shape) that are free to move around, as a liquid, but tend to remain oriented parallel to each other. The molecular orientation is not the same throughout the material. In addition, the molecules undergo thermal vibrations around an average direction, $\hat{n}$, which is defined as the director.

Nematic Liquid Crystals are uniaxially symmetric, due to the orientation order, with the symmetric axis parallel to the long axis of molecules [24]. The symmetry leads to different dielectric constants parallel and perpendicular to the director.

$$\Delta\varepsilon = \varepsilon_{\parallel} - \varepsilon_{\perp} \tag{2.1}$$

Also, the uniaxial symmetry leads to an optical anisotropy (or birefringence) with two principal refractive indices [24]. These two are the ordinary and the extraordinary index of refraction, for light with its polarization perpendicular and parallel to the director.

$$\Delta n = n_e - n_o \tag{2.2}$$

Therefore, the refractive index and electric permittivity, in both directions, depend on temperature, the order parameter, molecular structure, wavelength, propagation direction, polarization, and the frequency of the applied signal [25].

2.3.1.2.1 Threshold Voltage. The threshold voltage of a liquid crystal cell is set by the dielectric constant and elasticity of the liquid crystal material. The elasticity of the material is defined as the deformation (or distortion) from an external force and restoration to original shape after removing the applied force (voltage).

The elastic constants of the liquid crystal are material parameters that determine the threshold voltage [26]. When an electric field is applied to reorient the molecules to control the effective birefringence in an electro- optical device, it is the balance between the electric and elastic torque that determines the static deformation of the liquid crystal director. The three basic deformations are splay, twist, and bend. The elastic energy density, according to Oseen-Frank theory, of a deformed nematic liquid crystal can be expressed in vector notation as follows:

$$F = .5k_{11}(\nabla \cdot \hat{n})^2 + .5k_{22}(\hat{n} \cdot \nabla \times \hat{n})^2 + .5k_{33}(\hat{n} \times \nabla \times \hat{n})^2 \quad 2.3$$

The elastic coefficients k_{11} ,k_{22}, and k_{33} correspond to splay, twist, and bend. The minimum electric field (threshold voltage) required for parallel orientation of the liquid crystal molecules is related to the elastic constants and the dielectric response [26]. For small angles the minimum electric field is the following:

$$V_{th} = \pi \sqrt{\frac{k_{11}}{\varepsilon_0 \Delta\varepsilon}} \quad 2.4$$

2.3.2.1.2 Response Time. The thickness of the liquid crystal cell and the viscosity and temperature of the liquid crystal material determine the response time. There are two response

times associated with liquid crystals. The first response time is the time required for the director to reorient to an applied electric field (Equation 2.4) which is usually labeled as the time to activate or turn on the cell. Assuming the applied voltage is large compared to the threshold, the elastic terms can be neglected, therefore the response time is

$$t_{on} \cong \frac{y_{eff} * {d_{LC}}^2}{\varepsilon_0 \Delta \varepsilon V^2} \qquad 2.5$$

A nematic liquid crystal consists of three flow viscosities identified as Miesowisz viscosities. Additional viscosities are due to forces required to apply the liquid crystal between the plates which depends on the orientation of the liquid crystal molecules.

Viscosity is a measure of the resistance of the liquid crystals motion. The rotational viscosity, y_{eff}, defines the response times in liquid crystal cells in which high rotational viscosities correspond to slower response times and vice versa.

The second response time (relaxation time) estimates the time required for a deformed liquid crystal to reach its equilibrium state. Upon decreasing the voltage below the minimum (threshold voltage), for parallel orientation, the molecules start to deform or relax to the original orientation. The transition, or deformation, from parallel orientation to initial orientation is called the Freedericksz-transition [26]. In equation 2.5, an external force can't restore the liquid crystal to the initial state. Therefore, the cell thickness, rotational viscosity, and temperature determine the response time.

$$t_{off} \cong \frac{y_{eff} * {d_{LC}}^2}{k_{eff}} \qquad 2.6$$

2.3.2 Liquid Crystal Cells

The twisted nematic liquid crystal cells, which contain the liquid crystal material, consist of two pieces of glass, spacers, polyimide, and transparent conducting coatings, for example of

ITO or gold (Ag) [27]. The glass substrates are in coated with gold a conductive electrode. Next, an orientation layer is deposited on the surface (polyimide). Finally, the two substrates are rubbed while the rubbing direction of one substrate is perpendicular to the rubbing direction of the second substrate causing a helical orientation of the liquid crystal material within the liquid crystal cell [27-28].

2.4 Conclusion

Mechanical beam steering devices include gimbaled scanners and rotating risley prisms. MEMS mirrors reduce the device size. However vibrations from the actuator limit the resolution while the cost to build the device is very expensive. Rotating riley prisms are unable to move a beam in a straight line, are dispersive, and require routine maintenance.

Non-mechanical beam steering devices include Wollaston prisms, polarization gratings, variable index of refraction cell, and liquid crystal phase arrays. Wollaston prisms are large, expensive, and angular deflections change with wavelength. The fringing effects within adjacent electrodes restrict the scanning range of optical phase arrays to small angles. The diffraction efficiency of liquid crystal variable blaze arrays limit the number of output directions. Varying the index of refraction, within a liquid crystal cell, using a reference source has a linear response within a small range of angles with large response times. A summary of beam steering methods is shown below:

Table 2-1: Summary of Mechanical and Non-Mechanical beam steering devices.

Mechanical					
	Min Angle (urad)	Max Angle	Resolution	Dispersive (Y or N)	Response Time
Gimballed Scanner/MEMS mirrors	N/A	280 urad	N/A	N	8 ms
Rotating Prisms	N/A	± 2.09 rad	60 urad	Y	110 ms
Non-Mechanical					
	Min Angle	Max Angle	Resolution (mm)	Dispersive (Y or N)	Response Time (s)
Polarization Gratings	±87.3 mrad	±263 mrad	N/A	Y	N/A
Birefringment and Wollaston Prisms	±43.6 mard	±349 mard	N/A	Y	N/A
Liquid crystal devices					
Variable Blaze Gratings	34.9 mrad	104 mrad	N/A	N	<1ms
Variable Period	34.9 mrad	104 mrad	N/A	Y	<1ms
Variable Index of Refraction	8.73 mrad	±157 mrad	N/A	Y	10 s

CHAPTER 3 RESEARCH GOALS

Our goal is to complete a thorough study of a novel non-mechanical device which is organized into four mains categories listed below:

1.) Study the principle of operation, theoretical limitations, and optimum design of a stage, one-dimensional, and two dimensional devices.

2.) Investigate the digital operation for a stage, linear, and planer system. A description and depiction of the liquid crystal cell logic for deflecting a beam of light in a line and plane is presented.

3.) Develop methods to measure and assemble a stage. Develop a one dimensional system which is composed of cascading stages.

4.) Develop a two dimensional beam steering device and compare to theory and alternative beam steering methods.

CHAPTER 4 PRINCIPLE OF OPERATION

A non-mechanical beam steering device directs a beam a light with no moving parts. In principle, the combination of a liquid crystal cell and polarizing beam splitter can be used as a digital linear system. The polarizing beam splitter is used to deflect the beam at an angle while the liquid crystal cell selects (or controls) the direction. In this chapter, the concepts of the polarizing beam splitter and the liquid crystal cell are discussed in the detail. The first half of the chapter will discuss single-pass, double-pass, tolerances, and the cumulative effects of a polarizing beam splitter. The second half of the chapter focuses on the liquid crystal cells and digital operation.

4.1 Single-Pass Operation of a Polarizing Beam Splitter

Single-pass operation is defined as the beam of light making one entry and one exit though a polarizing beam splitter. A polarizing beam splitter is used in this work were composed of two prisms, made from crown glass called BK7, and thin films, composed of several layers of alternating index of refraction, which is illustrated in Figure 4.1 [43]. The beam of light maybe either horizontally or vertically polarized incident on the polarizing beam splitter.

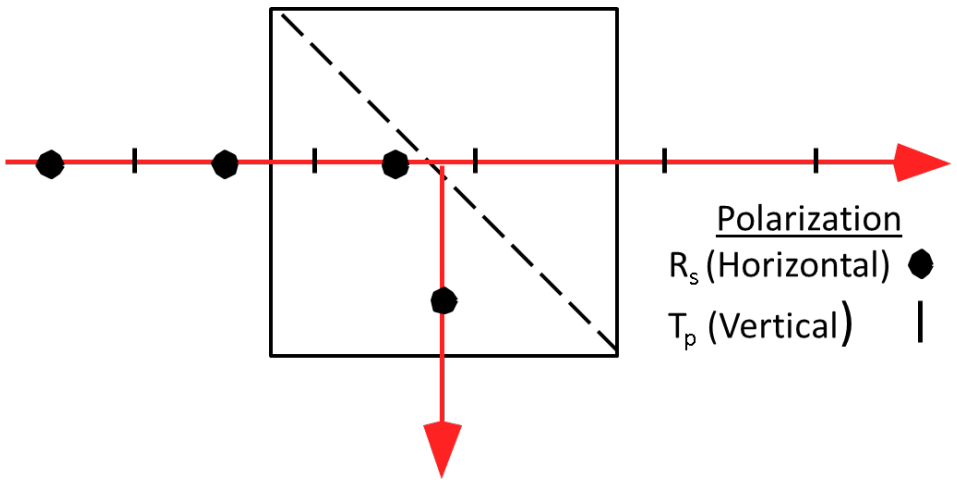

Figure 4-1: Polarizing Beam Splitter.

At the interface of the two prisms, the horizontally polarized, $R_{s,}$ component undergoes total internal reflection while the vertically polarized component, T_p, is transmitted through the second prism assuming the polarizing beam splitter is a perfect polarizer. If the input polarization is defined the beam will pass in one direction.

4.2 Double-Pass Operation of a Polarizing Beam Splitter

Double-pass operation is defined as the beam of light entering and exiting polarizing beam splitter twice. In figure 4.2, vertically polarized light is transmitted through the polarizing beam splitter and enters a quarter wave-plate with its fast axis at a 45 degree angle. Next, it's reflected by an aluminum coated first surface mirror, then passes through the quarter wave-plate again. The two passes through the quarter-wave plate change the vertically polarized light to horizontally polarized light. Upon re-entry to the polarizing beam splitter the beam is reflected by the polarizing beam splitter. Similarly, light horizontally polarized reflects through the beam splitter, polarization changes from horizontal to vertical after passing through the quarter wave-plates and the beam splitter.

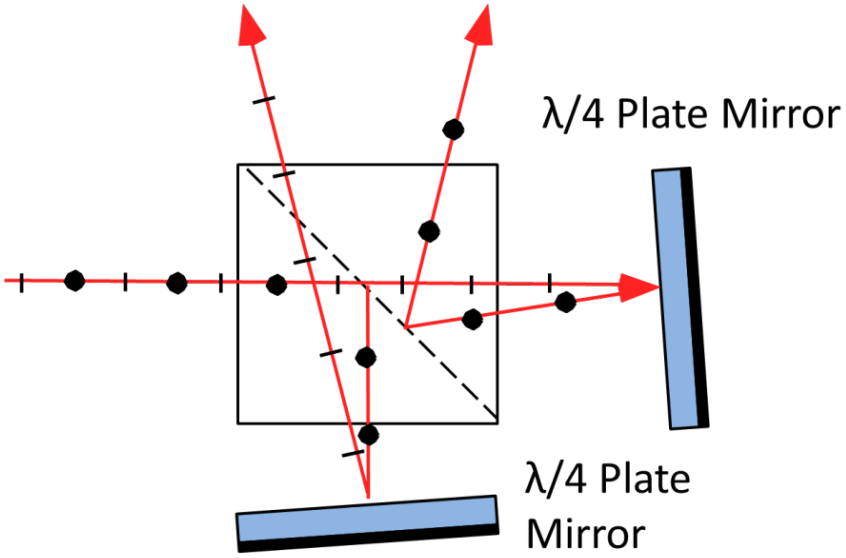

Figure 4-2: Double-pass operation of a polarizing beam splitter.

After passing through the system, the horizontal and vertically polarized beams exit at an angle 4θ with respect to each other. The quarter wave-plates and mirrors are fixed at 90 degrees to each other, at an angle θ to the beam splitter.

4.2.1 Horizontal and Vertical Angle's Between the Hypotenuse and Mirrors

The axis of rotation is parallel to the line formed by the intersection of the two mirror planes (Figure 4.3). The angle between the mirrors is fixed at 90^o. Also the mirrors are fixed at an angle, θ, with respect to the polarizing beam splitter. Common rotations to the mirrors change the angles between the mirrors and beam splitter. Therefore one angle becomes greater than 45^o while the other angle becomes correspondingly smaller. The angle of rotation, θ_{rotate}, between the mirrors and hypotenuse of the beam splitter determines the angular separation between the two beams.

$$\pm\theta = 45^o \pm \theta_{rotate} \qquad 4.1$$

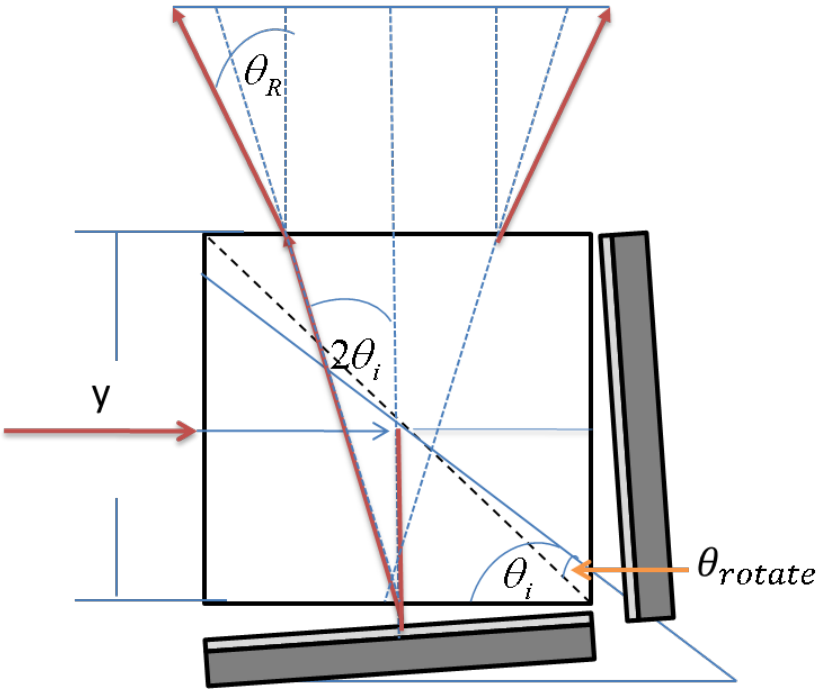

Figure 4-3: Effect of output directions of the beams as the beam splitter is rotated.

For example, a rotation of 1 degree from the nominal position results in angles of 44^o and 46^o between the diagonal and the external mirrors, leading to beam deflections of 88^o and 92^o within the beam splitter.

4.2.2 Effect on Output Directions

Refraction at the exit to the beam splitter further separates the beams, so that for example, if the index of refraction (n_{PBS}) is approximately 1.5, the total angle separation (θ_{TOTAL}) between the beams in the case above increases from 4^o to 6^o.

$$n_{air} \sin(\theta_{TOTAL}) = n_{PBS} \sin(2\theta) \tag{4.2}$$

$$\theta_{TOTAL} \cong 1.5 * \theta \tag{4.3}$$

Rotation of the mirrors about either axis perpendicular to their line of intersection must also be controlled, since it causes the plane of the two output beams to rotate. For displacements along a single line, errors in these angles cause displacements perpendicular to the line of deflected positions. The maximum angle is limited by cross-talk or power in the unwanted polarization which is discussed in Chapter 5.

4.2.3 Discussion

In double-pass operation the angular separation of the output beams is set by the mirrors instead of the wavelength of light. The angular separation of the output beams is $4n_1\theta$ times larger than the mirror angles. The plane of polarization of output beam changes by 90 degrees with respect to the input polarization. A change in the input beams polarization changes output direction.

The quarter wave plate is index matched on both sides. There are two reflections from the quarter wave plate, two reflections in the polarizing beam splitter, one reflection entering, and

one reflection exiting for one polarization in double pass operation which implies 8 unwanted reflections occur during double pass operation.

4.3 The Cumulative Effect of Binary Angular Addition

An angular deflection system is composed of N identical stages spaced apart by an optical path length L (Figure 4.4). The angular resolution of the system, β, is given by

$$\beta = \frac{k\lambda}{d} \tag{4.4}$$

where the wavelength of the light is λ, and the incident beam's diameter is d. For a Gaussian intensity distribution and small angles:

$$k = \frac{4}{\pi} \approx 1.27 \tag{4.5}$$

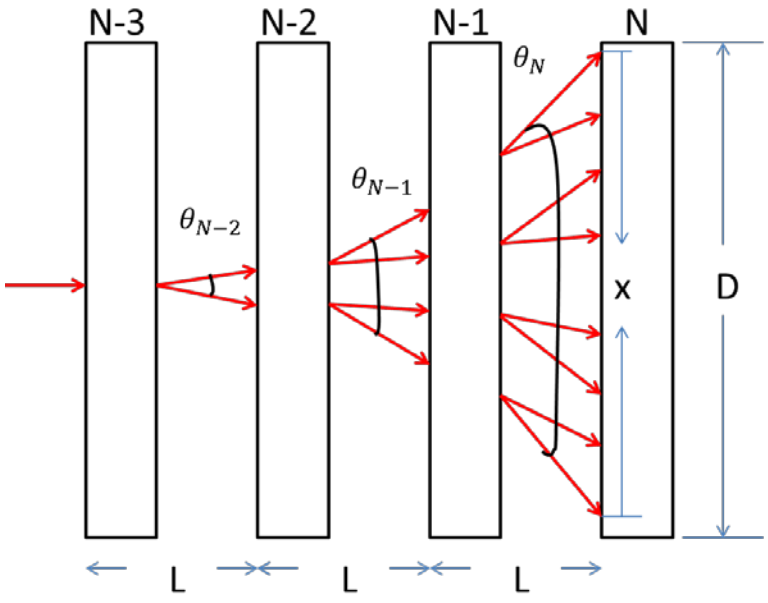

Figure 4-4: Cumulative effects of angular and linear displacements in a one-dimensional binary displacement system.

The deflection angle increases by a factor of 2 at each stage, so that after n stages there are a total of 2^n directions to which the beam may be deflected. The angular separation between deflections is equal to the angular deflection of the first stage, θ_1, where the separation between angular deflections has been set equal to the angular resolution ($\theta_1=\beta$), and θ_n is the deflection at the n^{th} stage, given by

$$\theta_n - \sum_{1}^{n-1} \theta_n \cong \theta_1 = \beta \tag{4.6}$$

$$\theta_n \cong 2^{n-1}\theta_1 \tag{4.7}$$

There is a displacement, x_n, of the laser beam at the last stage resulting from the angular deflection at the n^{th} stage. In the small angle approximation, and N stages,

$$x_n \cong (N-n)L\theta_n \tag{4.8}$$

Increasing the number of stages increases the number output directions by a factor of 2 per stage. The displacement at the last stage increases.

4.3.1 Need for Minimal Separation

The last stage must have a width, D, large enough to accommodate both the diameter of the beam, d, and the maximum displacement, x,

$$D = x + d \tag{4.9}$$

which limits the systems resolution and the number of output directions. The angles must be arranged from smallest to largest while minimizing the optical path length to reduce the displacements entering the last stage. A smaller resolution corresponds to larger beam width which increases the minimum deflector width. The theoretical limits are reserved for Chapter 5.

4.3.2 Extension to Two Dimensional Systems:

For two dimensional deflections the stages are arranged in pairs, N_{pair}, therefore, half the stages

deflect in the vertical direction and half deflect in the horizontal direction. The first stage in a pair deflects the laser beam vertically, and the second stage deflects it horizontally as shown in Figure 4.5.

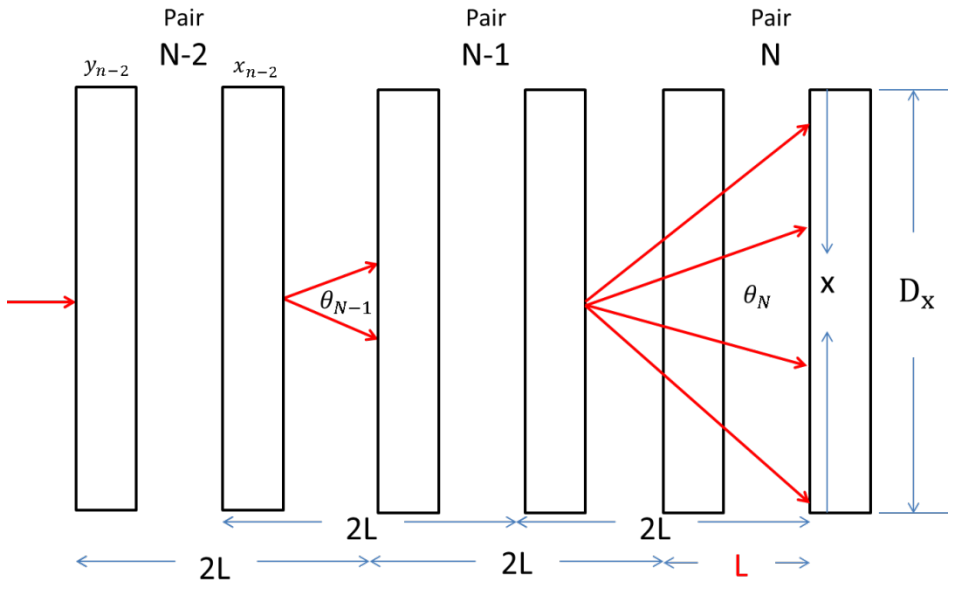

Figure 4-5: Cumulative effects of angular and linear displacements in the vertical direction for a two-dimensional binary displacement system. The horizontal displacements are omitted for clarity.

The deflection angle increase's by a factor of 2 after passing through a pair of stages, so that after N pairs of stages there are a total of $2^{N_{pair}}$ vertical directions and $2^{N_{pair}}$ horizontal directions to which the beam may be deflected. The angular separation between each pair of stages is equal to the angular deflection of the first pair of stages, θ_1, where the separation between angular deflections has been set equal to the angular resolution ($\theta_1=\beta$), and θ_n is the deflection at the n^{th} pair of stages, given by equation 4.7.

There is a displacement in the horizontal direction, x_n, and the vertical direction, y_n, of the laser beam at the last stage resulting from the angular deflection at the n^{th} stage pair. In the small angle approximation, and N pairs of stages,

$$x_n \cong (N_{pair} - n)2L\theta_n \quad 4.10$$

$$y_n \cong (N_{pair} - n)2L\theta_n + L\theta_n \quad 4.11$$

Interleaving the vertical and horizontal deflection angles doubles the optical path length between subsequent horizontal deflection angles and subsequent vertical deflection angles which doubles the displacement in the horizontal direction and the vertical direction.

4.4 Operation of liquid crystal cells

The operation of a twisted nematic crystal cell is shown in Figure 4.6. Assuming the wavelength, cell thickness, and index of refraction are designed to satisfy the design equation the liquid crystal cell rotates the plane of polarization 90^0 when no electrical signal is applied to the cell. For example, light vertically polarized incident to the cell rotates 90^0 exits horizontally polarized. Similarly, light horizontal polarization rotates 90^0 inside the cell and leaves the liquid crystal cell vertically polarized. No change in polarization occurs when the cell is activated. For our cells this consists of applying a 1 kHz square wave with a peak to peak amplitude of 6 volts.

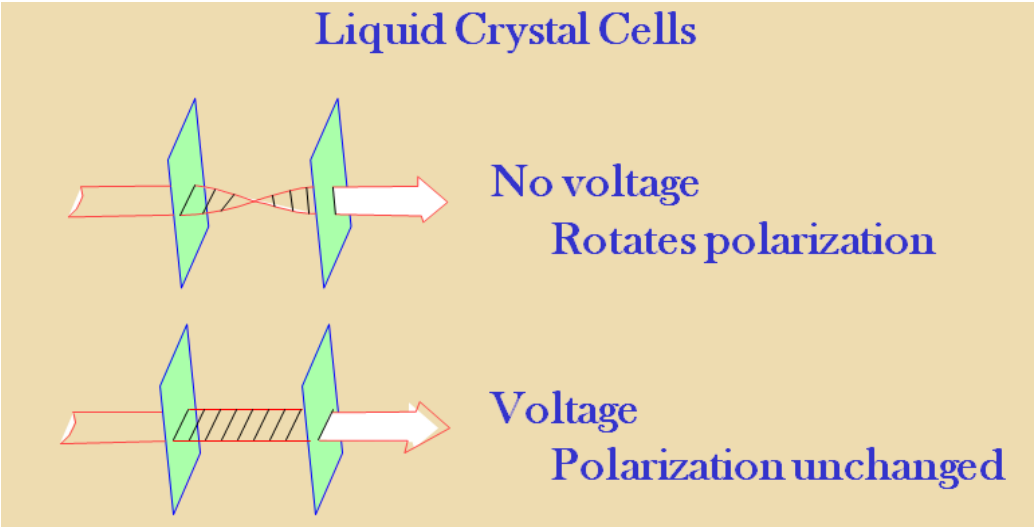

Figure 4-6: Depicts the effect of the field as it passes through the liquid crystal cells.

4.4.1 Transmission Efficiency and Polarization Rotation

The polarization state, $\Delta\varphi$, after passing through a liquid crystal cells is determined by the cell thickness d_{LC}, wavelength of light, and refractive index. Gooch and Tarry's derivation assumed parallel orientation of the polarizer transmission axis and the rubbing direction [26]. The transmission T of a polarized beam of light through a twisted nematic liquid crystal cell is shown below [25]:

$$T = \frac{1}{2}\frac{\sin^2(\frac{\mathrm{u}}{2} * \sqrt{1+\Delta\varphi})}{1+\mathrm{u}} \qquad 4.12$$

$$\mathrm{u} = 2d_{LC}\frac{\Delta n}{\lambda} \qquad 4.13a$$

$$\Delta\varphi = 2\pi d_{LC}\frac{\Delta n}{\lambda} \qquad 4.13b$$

where u is defined as the Gooch and Tarry minimum[26]. It's necessary to operate in the first or second minimum to maximize brightness, contrast, and viewing angle [26]. Also the cell thickness needs to be much larger than half the wavelength to avoid producing elliptically polarized light which will result in cross-talk.

4.4.2 Discussion

Combining a deflector angle, discussed in Section 4.2 with a liquid crystal cell can deflect a beam of light in different directions by controlling the polarization. The switching speed effect can be modeled as a RC circuit to estimate the cross-talk vs. switching speeds. The response time is limited by the relaxation time of the liquid crystal molecules after removing the signal.

4.5 Digital Operation

The purpose of this section is to discuss the algorithm and digital operation for a linear one and two dimensional laser beam steering device. The liquid crystal cells control the

polarization and output direction. However XNOR correction is required between consecutive stages so the position of the deflected beam corresponds to the binary input. This section is to discuss the digital operation for deflecting a beam of light for a one-dimensional and two-dimensional system. The output direction as function of binary input, referred to as the "liquid crystal cell logic", and code conversion for both systems is described.

A stage is composed of a liquid crystal cell and a deflector angle which was defined in sections 4.4 and 4.2 respectively (Figure 4.7)

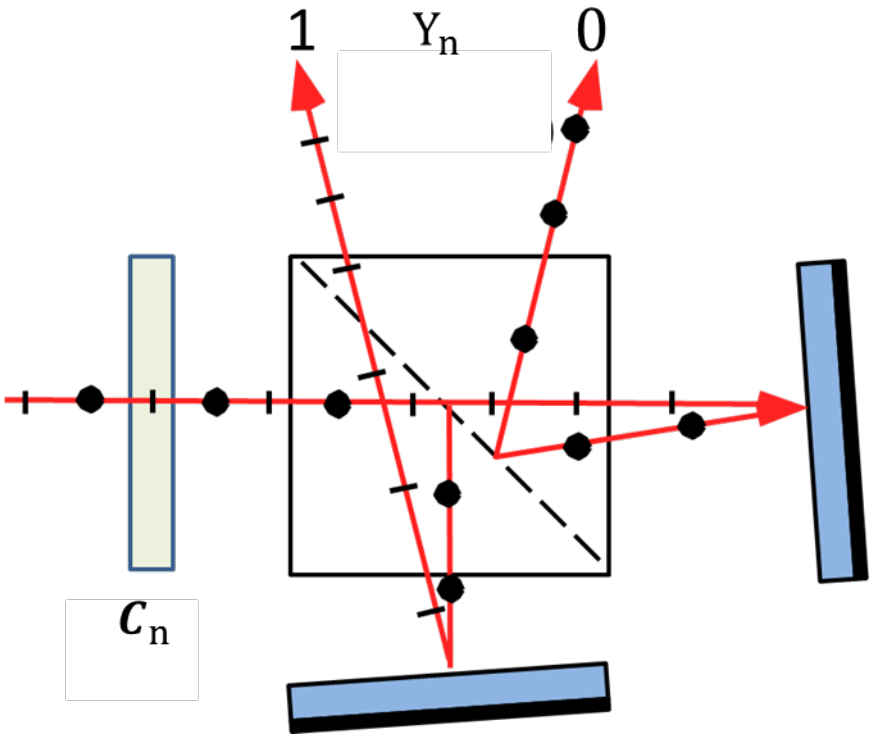

Figure 4-7: The digital operation consists of using the combination of a liquid crystal cell and a polarizing beam splitter. The deflector angle's mirrors and quarter-wave plates are not labeled for clarity.

4.5.1 Stage (Binary Unit):

Figure 4.7 depicts the digital operation of a stage which is labeled a binary unit. The binary label, C_n, describes the n^{th} state of the liquid crystal cell within the nth stage of the system. The binary bit, Y_n, is assigned to the n^{th} stage within the system.

For example a one stage binary deflection device has 2 output directions (Y_1 and Y_0) and is illustrated in Figure 4.7. Assume the incident beam is vertically polarized prior to entering the liquid crystal cell. If C_1=1; there is no change in polarization by liquid crystal hence no change in output direction (Y_0 =0). If C_1=0 the liquid crystal cell changes the polarization hence the output direction changes to Y_0 = 1. Therefore the corresponding liquid crystal cell logic is shown below:

$$C_1 = \overline{Y_0} \tag{4.14}$$

$$C_1 = \overline{Y_0 \otimes 0} \tag{4.14a}$$

4.5.2 One Dimensional System

This section will discuss the binary operation of a two stage system and the derivation for controlling a two stage and N stage system.

A two stage binary deflection system has 4 output directions and is illustrated in Figure 4.8. The second stage is rotated by 90 degree's in the XY direction then inverted in the XZ direction with respect to the first stage. The output directions after two stages are in the same plane at different angles to input direction.

A one bit binary number is assigned to the liquid crystal cell within each stage. The liquid crystal cell for the first stage is defined as the least significant bit (C_0) and the liquid crystal cell at the second stage is most significant bit (C_1). Two one-bit binary numbers assigned to the stages within the system (Y_0 and Y_1).

4.5.2.1 Derivation or Need for XNOR

A linear deflection in the vertical direction is the binary sum of the vertical deflections.

$$Y_{LIN} = \overline{Y_0 \otimes 0} + \overline{Y_1 \otimes Y_0} \tag{4.15}$$

$$Y_{LIN} = \sum_{n=0}^{N} C_{\mathrm{n}} = \sum_{n=0}^{N} \overline{Y_n \otimes Y_{n-1}} \tag{4.16}$$

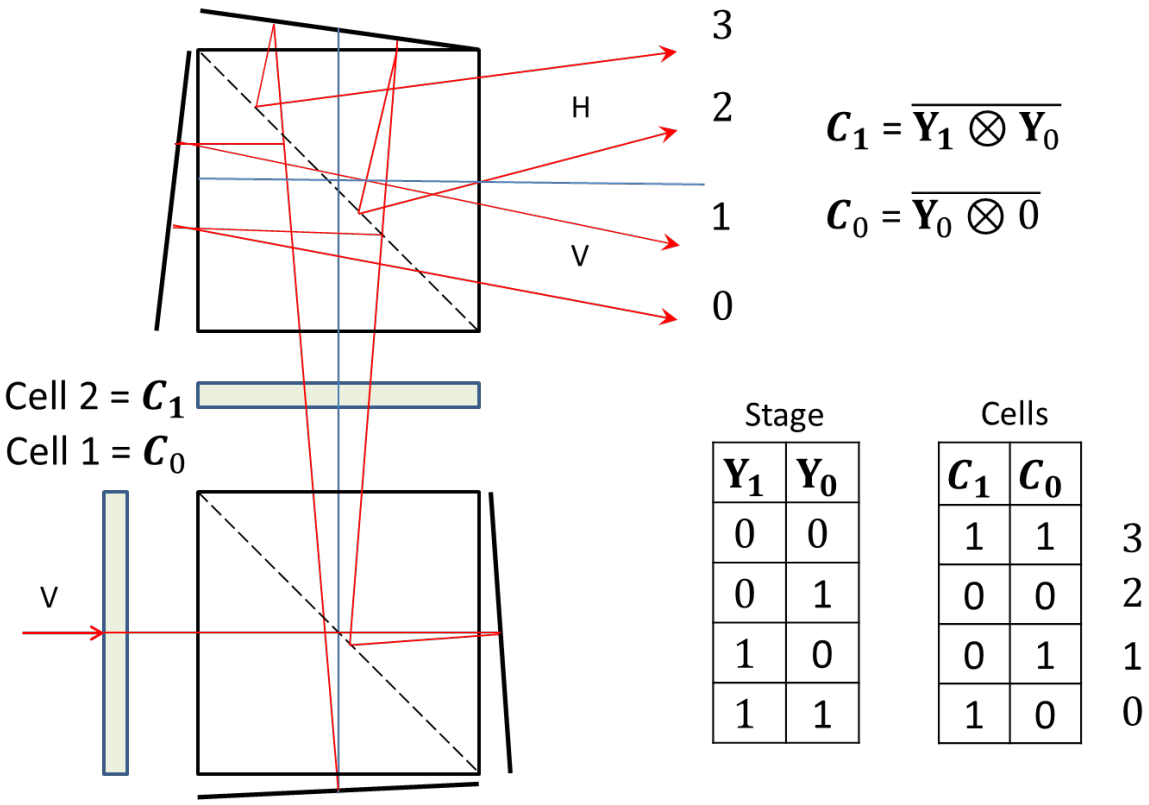

Figure 4-8: Digital operation of a two stage linear system. The figure depicts the output directions vs. a signal applied to the liquid crystal cell.

P_0 and P_1 are assigned to stages one and two account for polarization changes. The letter "N" is assigned when the liquid crystal cell within the stage doesn't change the polarization while the letter C is assigned when the liquid crystal cell changes the polarization. For example the initial output direction is obtained for a binary input of 11 for stages one and two (C_0 *and* C_1). The liquid crystal cells within stages one and two didn't change the polarization. Therefore P_0 =N and P_1 =N. The letter N corresponds to logic "0" for the binary address for stages Y_0 and Y_1.

An even number of polarization changes corresponds to C_n set equal to zero and an odd number of polarization correspond to C_n set to 1.

4.5.3 Extension to Two Dimensions

The purpose of this section is to discuss the algorithm for controlling a two dimensional laser beam steering device. The two dimensional system consist of interleaved vertical and horizontal stages. It's assumed the stage orientation doesn't change the deflection direction. This section will discuss the algorithm and gates required to move in vertical line, horizontal line, and angles (or slopes) for a 2-dimensional system. Also this section will discuss the algorithm to select a point within the array based on a known row and column.

Figure 4.9 shows the output for a six stage system, composed of three interleaved horizontal and vertical deflector stages, which is an 8 x 8 array of spots when the liquid crystal cells are driven in half voltage operation. The even stages are the horizontal stages while the odd stages are the vertical. The most significant bit (X_2) of the binary number is controlling the liquid crystal cell at stage 6 while the least significant bit controls the liquid crystal cell for the first stage (Y_0).

Horizontal Lines

1 →	0	6	24	30	32	38	56	62
2 →	3	5	27	29	35	37	59	61
3 →	12	10	20	18	44	42	52	50
4 →	15	9	23	17	47	41	55	49
5 →	48	54	40	46	16	22	8	14
6 →	51	53	43	45	19	21	11	13
7 →	60	58	36	34	28	26	4	2
8 →	63	57	39	33	31	25	7	1
	↑	↑	↑	↑	↑	↑	↑	↑
Vertical lines	1	2	3	4	5	6	7	8

Figure 4-9: Decimal equivalent of output directions for a two dimensional system.

The binary addresses for vertical and horizontal stages within the two dimensional system are shown in Figure 4.10.

C_5

0	0	0	0	1	1	1	1
0	0	0	0	1	1	1	1
0	0	0	0	1	1	1	1
0	0	0	0	1	1	1	1
1	1	1	1	0	0	0	0
1	1	1	1	0	0	0	0
1	1	1	1	0	0	0	0
1	1	1	1	0	0	0	0

C_4

0	0	1	1	0	0	1	1
0	0	1	1	0	0	1	1
0	0	1	1	0	0	1	1
0	0	1	1	0	0	1	1
1	1	0	0	1	1	0	0
1	1	0	0	1	1	0	0
1	1	0	0	1	1	0	0
1	1	0	0	1	1	0	0

C_3

0	0	1	1	0	0	1	1
0	0	1	1	0	0	1	1
1	1	0	0	1	1	0	0
1	1	0	0	1	1	0	0
0	0	1	1	0	0	1	1
0	0	1	1	0	0	1	1
1	1	0	0	1	1	0	0
1	1	0	0	1	1	0	0

C_2

0	1	0	1	0	1	0	1
0	1	0	1	0	1	0	1
1	0	1	0	1	0	1	0
1	0	1	0	1	0	1	0
0	1	0	1	0	1	0	1
0	1	0	1	0	1	0	1
1	0	1	0	1	0	1	0
1	0	1	0	1	0	1	0

C_1

0	1	0	1	0	1	0	1
1	0	1	0	1	0	1	0
0	1	0	1	0	1	0	1
1	0	1	0	1	0	1	0
0	1	0	1	0	1	0	1
1	0	1	0	1	0	1	0
0	1	0	1	0	1	0	1
1	0	1	0	1	0	1	0

C_0

0	0	0	0	0	0	0	0
1	1	1	1	1	1	1	1
0	0	0	0	0	0	0	0
1	1	1	1	1	1	1	1
0	0	0	0	0	0	0	0
1	1	1	1	1	1	1	1
0	0	0	0	0	0	0	0
1	1	1	1	1	1	1	1

Figure 4-10: Binary address for the liquid crystal cells at each stage within the two dimensional system.

4.5.3.1 Linear Deflection in Both Directions

A linear deflection in the vertical direction Y_{LIN}, is defined as the binary sum of the vertical deflections in which the horizontal stages have no effect on changing output direction and shown below:

$$Y_{LIN} = \sum_{n=0}^{N} C_{\mathrm{n}} = C_5 + C_3 + C_1 \qquad n - odd \qquad 4.16$$

$$Y_{LIN} = \sum_{n=0}^{N/2} \overline{Y_n \otimes Y_{n-1}} \qquad 4.17$$

This implies if the polarization changes within a vertical stage, the corresponding horizontal stages polarization must also change.

A linear deflection in the horizontal direction, X_{LIN}, is defined as the binary sum of the horizontal deflections in which the vertical deflection stages have no effect on the output direction and shown in equation 4.18.

$$X_{LIN} = \sum_{n=1}^{N} C_{\mathrm{n}} = C_6 + C_4 + C_2 \qquad n - even \qquad 4.18$$

$$X_{LIN} = \sum_{n=0}^{N/2} \overline{X_n \otimes X_{n-1}} \qquad 4.19$$

If the polarization changes for a horizontal stage, the subsequent vertical stages polarization must also change.

4.5.3.2 Selecting a Point within the 2D Array

Figure 4.11 depicts the algorithm for converting an ordered pair to an output direction on the 2D grid. Enter the row and column, invert the columns, interleave leave vertical and horizontal stages, and apply XNOR correction between adjacent stages as shown in the one dimensional system. the horizontal and vertical components are interleaved followed by XNOR correction. The output after XNOR correction is 000000 which is same as the measured position.

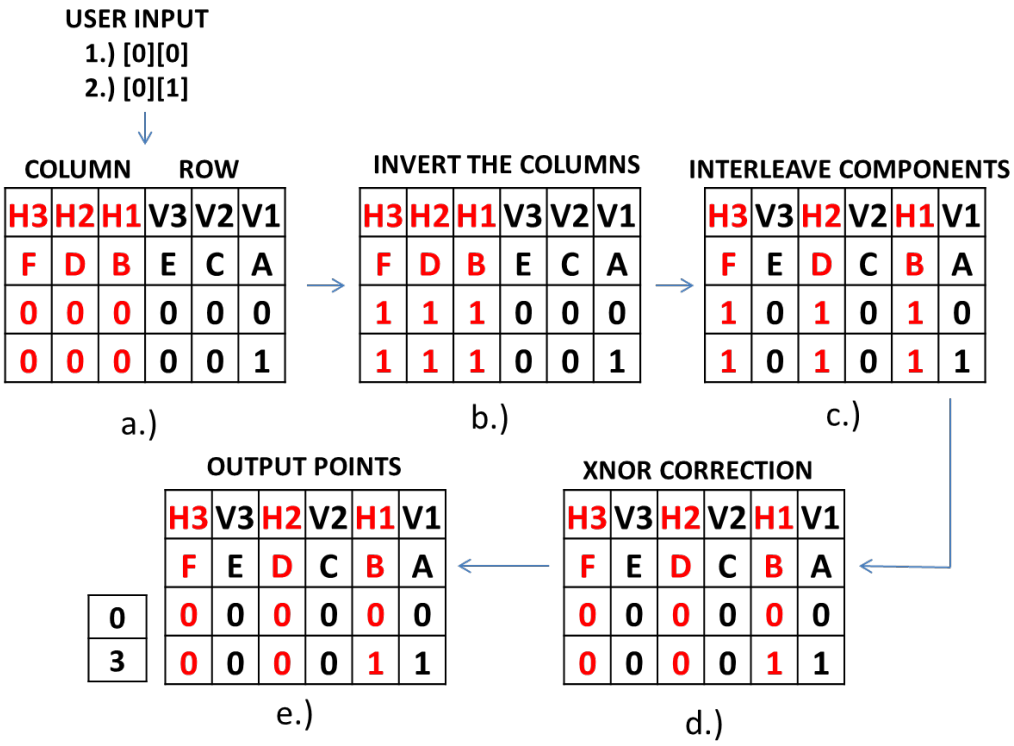

Figure 4-11: The algorithm for selecting a point in the planer system by entering a decimal number for the row and column

Sequential changes in linear deflections in the horizontal direction require XNOR correction when a signal is applied to all the horizontal stages. Also the vertical deflector stages can be used to define a row within the array of the planer steering system.

4.5.3.3 Scanning in Vertical and Horizontal Lines

Applying the algorithm discussed earlier the remaining vertical positions in column 0 are obtained by setting the horizontal stages (column) to 111 while incrementing or counting by 001 for the vertical stages (row) as shown in Figure 4.12.

Therefore scanning in a vertical line comes to the following:

$$y_{2d} = X_n^{LIN} \otimes Y_{n-1}^{LIN} \tag{4.20}$$

$$x_{2d} = \overline{X_n^{LIN} \otimes Y_n^{LIN}} \tag{4.21}$$

This can be accomplished by using two 3-bit binary counters to sequentially scan in the vertical direction for the entire array. The first counter is assigned to the stages that deflect in the vertical direction while the second counter is assigned to the horizontal deflection stages.

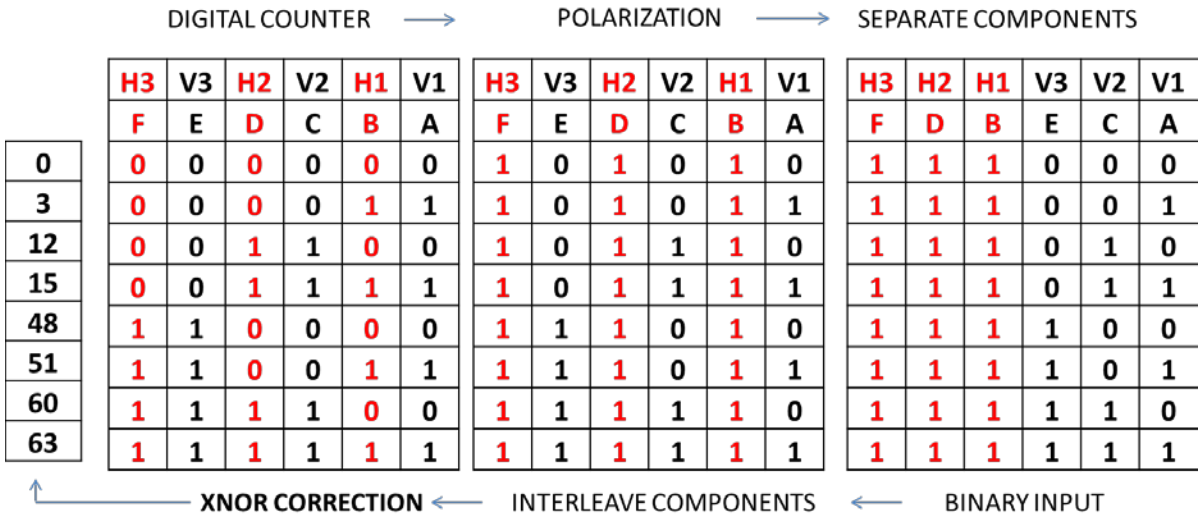

	H3	V3	H2	V2	H1	V1	H3	V3	H2	V2	H1	V1	H3	H2	H1	V3	V2	V1
	F	E	D	C	B	A	F	E	D	C	B	A	F	D	B	E	C	A
0	0	0	0	0	0	0	1	0	1	0	1	0	1	1	1	0	0	0
3	0	0	0	0	1	1	1	0	1	0	1	1	1	1	1	0	0	1
12	0	0	1	1	0	0	1	0	1	1	1	0	1	1	1	0	1	0
15	0	0	1	1	1	1	1	0	1	1	1	1	1	1	1	0	1	1
48	1	1	0	0	0	0	1	1	1	0	1	0	1	1	1	1	0	0
51	1	1	0	0	1	1	1	1	1	0	1	1	1	1	1	1	0	1
60	1	1	1	1	0	0	1	1	1	1	1	0	1	1	1	1	1	0
63	1	1	1	1	1	1	1	1	1	1	1	1	1	1	1	1	1	1

Figure 4-12: Scanning in a vertical line. The horizontal components polarization remains fixed while vertical components polarization increases by 1 from 000 to 111.

Assuming the horizontal stages remain fixed, counting by one for the vertical stages and taking the XNOR moves along a vertical line and changing the horizontal stages will cause the beam move/scan on a different vertical line. Similarly fixing the vertical stages while counting the horizontal stages scans in a horizontal line as shown in Figure 4.13.

4.5.3.1 Scanning at an Angle with a Positive and Negative Slope

Increasing the horizontal and vertical counts at the same time deflects the beam at an angle in the positive direction as shown in Figure 4.14

Angular scanning with a negative slope occurs by decreasing one counter while increasing the other as shown in Figure 4.15.

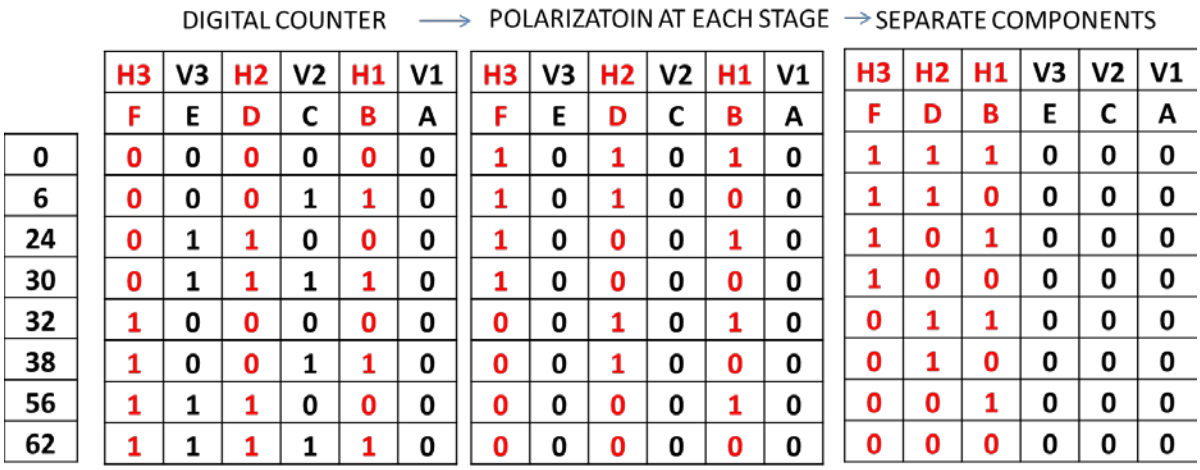

	H3	V3	H2	V2	H1	V1	H3	V3	H2	V2	H1	V1	H3	H2	H1	V3	V2	V1
	F	E	D	C	B	A	F	E	D	C	B	A	F	D	B	E	C	A
0	0	0	0	0	0	0	1	0	1	0	1	0	1	1	1	0	0	0
6	0	0	0	1	1	0	1	0	1	0	0	0	1	1	0	0	0	0
24	0	1	1	0	0	0	1	0	0	0	1	0	1	0	1	0	0	0
30	0	1	1	1	1	0	1	0	0	0	0	0	1	0	0	0	0	0
32	1	0	0	0	0	0	0	0	1	0	1	0	0	1	1	0	0	0
38	1	0	0	1	1	0	0	0	1	0	0	0	0	1	0	0	0	0
56	1	1	1	0	0	0	0	0	0	0	1	0	0	0	1	0	0	0
62	1	1	1	1	1	0	0	0	0	0	0	0	0	0	0	0	0	0

Figure 4-13: Scanning in a horizontal line

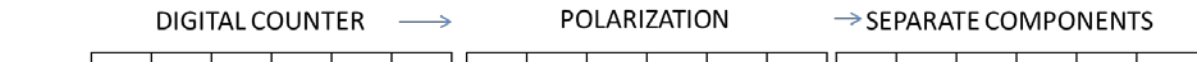

	H3	V3	H2	V2	H1	V1	H3	V3	H2	V2	H1	V1	H3	H2	H1	V3	V2	V1
	F	E	D	C	B	A	F	E	D	C	B	A	F	D	B	E	C	A
62	1	1	1	1	1	0	0	0	0	0	0	0	0	0	0	0	0	0
59	1	1	1	0	1	1	0	0	0	0	1	1	0	0	1	0	0	1
42	1	0	1	0	1	0	0	0	1	1	0	0	0	1	0	0	1	0
47	1	0	1	1	1	1	0	0	1	1	1	1	0	1	1	0	1	1
46	1	0	1	1	1	0	1	1	0	0	0	0	1	0	0	1	0	0
43	1	0	1	0	1	1	1	1	0	0	1	1	1	0	1	1	0	1
58	1	1	1	0	1	0	1	1	1	1	0	0	1	1	0	1	1	0
63	1	1	1	1	1	1	1	1	1	1	1	1	1	1	1	1	1	1

Figure 4-14: Linear scanning with a positive slope

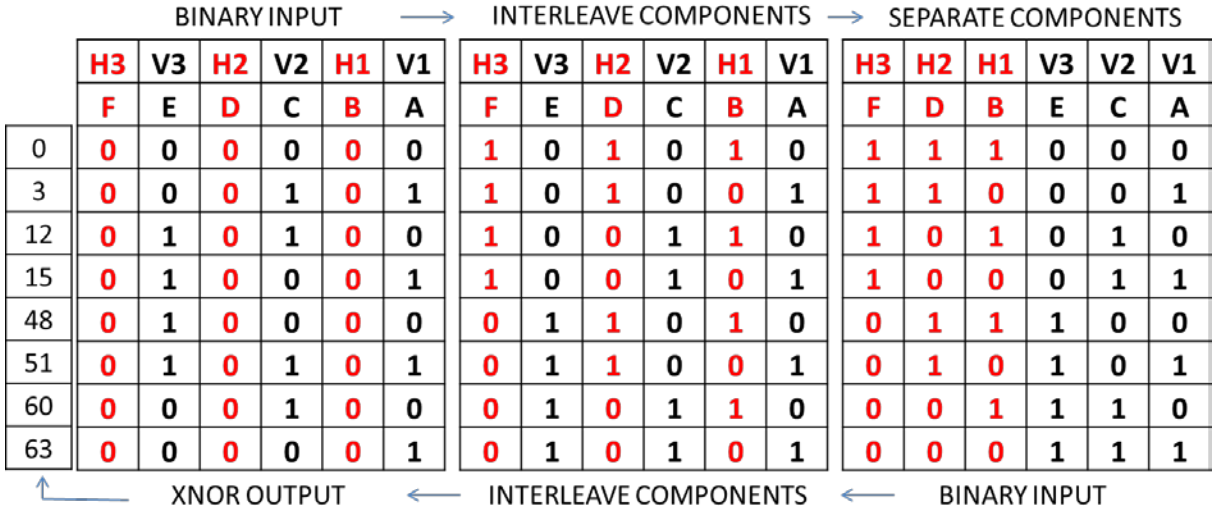

	H3	V3	H2	V2	H1	V1	H3	V3	H2	V2	H1	V1	H3	H2	H1	V3	V2	V1
	F	E	D	C	B	A	F	E	D	C	B	A	F	D	B	E	C	A
0	0	0	0	0	0	0	1	0	1	0	1	0	1	1	1	0	0	0
3	0	0	0	1	0	1	1	0	1	0	0	1	1	1	0	0	0	1
12	0	1	0	1	0	0	1	0	0	1	1	0	1	0	1	0	1	0
15	0	1	0	0	0	1	1	0	0	1	0	1	1	0	0	0	1	1
48	0	1	0	0	0	0	0	1	1	0	1	0	0	1	1	1	0	0
51	0	1	0	1	0	1	0	1	1	0	0	1	0	1	0	1	0	1
60	0	0	0	1	0	0	0	1	0	1	1	0	0	0	1	1	1	0
63	0	0	0	0	0	1	0	1	0	1	0	1	0	0	0	1	1	1

Figure 4-15: Linear scanning with a negative slope.

4.6 Conclusion

A stage consisting of a deflector and a liquid crystal cell is a digital non-mechanical beam steering device which changes the deflection direction by controlling the liquid crystal cell. The stage contains two mirrors and two quarter wave plates fixed at an angle with respect to the polarizing beam splitter used to set the angle separating two beams. The angular separation doesn't depend on the wavelength of the source. The angular separation between the beams is $4n_{pbs}$ times larger than the angle between the mirrors due to refraction at the output of the PBS. The maximum angle is limited by cross-talk.

A system is composed of cascaded stages. The number of output directions and angular range increases by a factor of 2 per stage. However the maximum linear displacement in the horizontal direction at the last stage increases with the number of stages. Double-pass operation within the polarizing beam splitter doubles the optical path length. Finer resolutions correspond to large beam diameters. The width of the polarizing beam splitter at the last stage must be large enough for the light pass through.

A twisted nematic liquid crystal cell is a voltage controlled polarizer that rotates the plane of polarization of light by 90^0 when no signal is applied to the cell and doesn't change the polarization for voltages greater than the threshold voltage. The response time of the liquid crystal is limited to the relaxation time, due the viscosity, of the liquid crystal molecules. The switching speed is limited to the relaxation time of the liquid crystal molecules.

The signals required to drive the liquid crystal cells require XNOR correction between adjacent stages to move in adjacent directions and for a binary input to correspond to deflection direction.

The theoretical limits for cascading stages, the maximum angle, resolution, etc. are presented in Chapter 5.

CHAPTER 5 THEORETICAL LIMITS

This chapter will focus on the theoretical limitations of a system which restricts the number of spots the system can resolve. The maximum deflection angle is ~ $\pm 15^{o}$ which is limited by the extinction ratio and polarization efficiency of the polarizing beam splitter and liquid crystal cell. A study of the effect of cascading a large number of stages is presented. The number of output directions increases by a factor of two per stage. Cascading additional stages increases the path length which corresponds to larger linear displacements at the last stage. The theoretical limit is set by the sum of the maximum displacement and the beam width which must pass though the last stage.

5.1 Maximum Angle

The maximum angle has a practical limit set by the multilayer coating at the hypotenuse. Single-pass and Double-pass operation in Chapter 4 assumed the polarizing beam splitter was a perfect polarizer and variation in the incident angle didn't cause cross-talk. There's an angular dependence on cross-talk and polarization efficiency as the incident beam deviates from the normal [32]. A small amount of power passes in the opposite direction and polarization within the PBS at the multi-layer thin film on the hypotenuse, and increases for angles which deviate from normal. As the angle increases the intensity of the unwanted light passing in the opposite direction increases while the transmitted light decreases until reaching the critical angle. The ratio of the power of light passing in the unwanted direction to power in the wanted direction is defined as cross-talk. There is a practical limit to the maximum angle due to degradation of extinction ratios of the polarizing beam splitter and liquid crystal cells at incident angles greater than $\pm 15^{o}$ [46].

5.2 Large Number of Stages

The maximum linear displacement, x, is the sum of the displacements, x_n. For a large number of stages, N, the maximum linear displacement x of the beam at the Nth stage approaches four times the displacement between the (N-1)st stage and the Nth stages (Figure 5.1).

$$x = \sum_{N}^{1} L(N-n)\,\theta_n = \sum_{N}^{1} L(N-n)\,2^{n-N}\theta_N \qquad 5.1$$

$$x = L\theta_N\left[0 + \frac{1}{2} + \frac{2}{4} + \frac{3}{8} + \frac{4}{16} + \cdots\right] \qquad 5.2$$

$$x \approx 2L\theta_N = 4L\theta_{N-1} = 2^N L\theta_1 \qquad 5.3$$

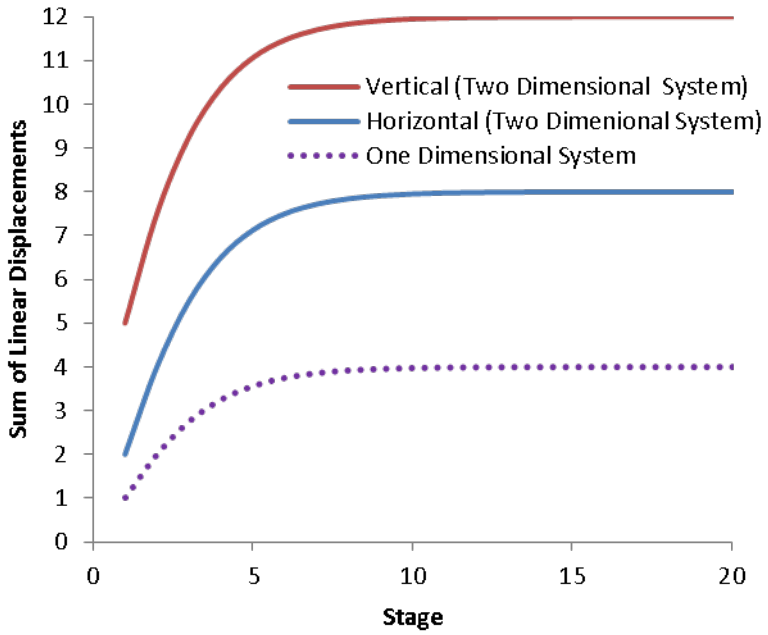

Figure 5-1: Summary of the cumulative effects for a one dimensional and two dimensional system

5.2.1 Two Dimensional System Extension

Assuming the distance between adjacent stages are identical and the average deflection is fixed the maximum linear displacement in the horizontal direction, x_{2D}, and the vertical direction, y_{2D}, is the sum of the horizontal and vertical linear displacements, $x_n$and y_n,

$$x_{2D} = \sum_{N}^{1} 2L(N-n)\,\theta_n = \sum_{N}^{1} 2L(N-n)\,2^{n-N}\theta_N \qquad 5.4a$$

$$x_{2D} = L\theta_N\left[0 + 1 + 1 + \tfrac{3}{4} + \tfrac{1}{2} + \cdots\right] \qquad 5.4b$$

$$x_{2D} \approx 4L\theta_N = 8L\theta_{N-1} = 2^{N+1}L\theta_1 \qquad 5.5a$$

$$y_{2D} \approx 6L\theta_N = 12L\theta_{N-1} = 3 * 2^N L\theta_1 \qquad 5.5b$$

The maximum linear displacements in the vertical and horizontal direction are 2 and 3 times larger than the one-dimensional system due to the increased optical path length after interleaving the vertical and horizontal deflector angles (Figure 5.1). The maximum linear displacement in the vertical direction is 1.5 times larger than horizontal direction and the 2D array of displacements forms a rectangle instead of a square. However the linear displacements in the vertical direction within the last stage would be ten times larger if the optical train was composed of all vertical deflector angles followed by horizontal deflector angles.

5.3 Need for Minimal Separation

The last stage must have a width, D, large enough to accommodate both the diameter of the beam, d, and the maximum linear displacement, x,

$$D = 2L\theta_N + \frac{k\lambda}{\beta} = 2^N L\beta + \frac{k\lambda}{\beta} \qquad 5.6$$

To the extent that the separation between stages is dominated by the size of the cube beam splitters, increasing their width will increase L proportionally. The increase in L affects the

width of the beam splitters as shown in Eq. (5.6). D varies slowly with β, but its minimum may be found by differentiating equation (5.6) with respect to β,

The minimum resolved angle is restricted to the width of the last deflector. Differentiating equation 5.6 with respect to the smallest angle gives

$$\frac{dD}{d\beta} = 0 \tag{5.7}$$

$$\frac{dD}{d\beta} = 2^N L - \frac{k\lambda}{\beta^2} \tag{5.8}$$

$$2^N L = \frac{k\lambda}{\beta^2} \tag{5.9}$$

$$\beta = \sqrt{\frac{k\lambda}{2^N L}} \tag{5.10}$$

However the number of deflector directions can be increased by a factor of 2^n by adding n stages at the start of the system. For the deflections to be resolvable, the width of the beam, d, must also be increased by the same factor of 2^n increasing the width of the beam splitters as shown in Eq. (5.6) and Figure 5.2.

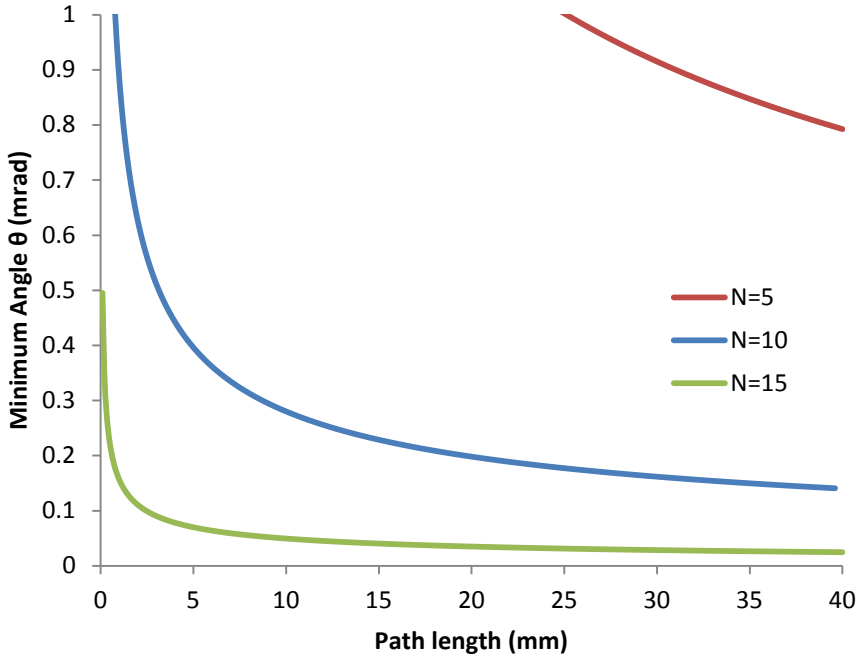

Figure 5-2: Plot of the path length vs. minimum angle. Increasing the path length reduces the minimum deflection angle and incident beam width.

Increasing the optical path length reduces the minimum angular displacement of the system. Figure 5.2 shows of the path length vs. the minimum deflection for a 5, 10, and 15 stage system at a wavelength 633 nm. A larger path length also implies larger incident beam diameters entering the system. For a ten stage system, Figure 5.3, the deflector width is restricted to the width of the incident beam for a fine resolution while the deflector width is restricted to the maximum displacement for larger initial angles.

.

.

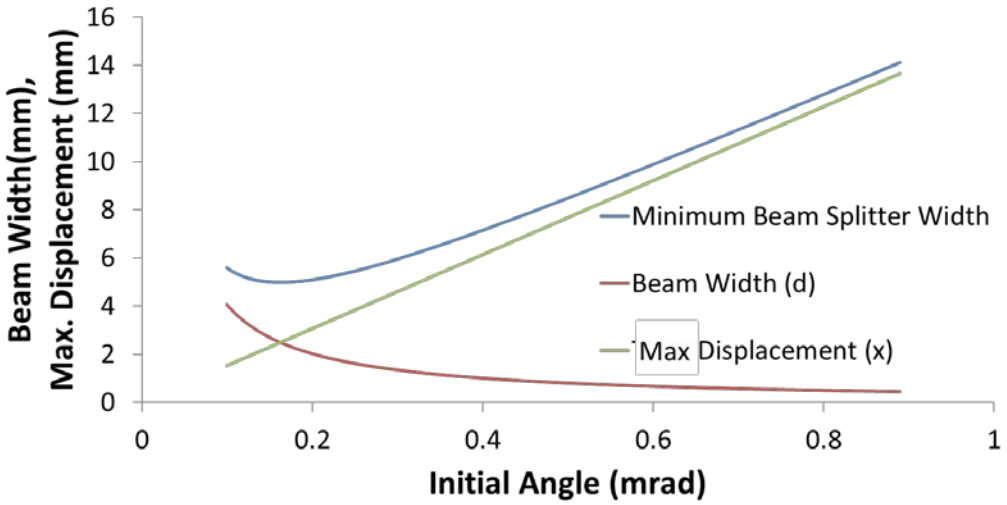

Figure 5-3: Plot of the deflector width vs. minimum angle. For small angles the deflector width for the last stage must accommodate for the beam diameter. For large initial angles the width of the deflector is limited the maximum displacement.

5.3.1 Extension to Two-Dimensional System

The last stage must have a width, D_x, and height, D_y, large enough to accommodate both the diameter of the beam and the maximum linear displacements in the vertical (y) and horizontal (x) directions,

$$D_x = x + d = 4L\theta_N + \frac{k\lambda}{\beta} = 2^{N+1}L\beta + \frac{k\lambda}{\beta} \qquad 5.11$$

$$D_y = y + d = 6L\theta_N + \frac{k\lambda}{\beta} = 3 * 2^N L\beta + \frac{k\lambda}{\beta} \qquad 5.12$$

Differentiating equation 5.8 *and* 5.9 with respect to the smallest angle gives

$$\beta_x = \sqrt{\frac{k\lambda}{2^{N+1}L}} \qquad 5.13a$$

$$\beta_y = \sqrt{\frac{k\lambda}{3 * 2^N L}} \qquad 5.13b$$

A two-dimensional system has the advantage of deflecting a beam of light in both directions but the angular range is reduced because of the increased optical path length.

5.3.2 Discussion

The last stage within the optical train defines the systems angular range and the first stage sets the angular separation between deflections. If there are too many stages, or if the path length is too long, the accumulated linear displacements can move the beam out of the area of the last stage. The first stage within the system will have the longest path length within the system therefore, the deflection angles must be arranged in order from smallest to largest to minimize the linear displacements. The maximum linear displacement and incident beam diameter entering the last stage must be smaller than the width of the deflector stage which limits the number of stages. The maximum linear displacement is minimized by reducing the optical path length. A detailed discussion of the optimum design and maximum number of resolvable locations are discussed later.

5.4 Optical Path Length

The optical path length (L) separating two stages will have a large effect on the linear displacement between stages. This section will discuss the optical path between stages in detail.

A beam of light passes through a polarizing beam splitter, quarter wave plate, UV curing epoxy, liquid crystal cell, and air. Recall from Chapter 4 that the beam makes two passes within the PBS for double pass operation, therefore the optical path length within the PBS doubles. The measured index of refraction of the polarizing beam splitter (n_{PBS}), is 1.57, and the optical path length path (L_{PBS}) within the polarizing beam splitter is the following:

$$L_{PBS} = 2\frac{n_{air}}{n_{PBS}}L_{air} \approx \frac{2L_{air}}{1.57} \qquad 5.14$$

For example if the width of the polarizing beam-splitter cube is 10 mm, the optical path length within the polarizing beam splitter 12.73 mm

The optical path length, L, the beam travels in optical components between two stages is the following

$$L = L_{PBS} + L_{LC} + L_{QWP} + L_{Epoxy} + L_{Air} \quad 5.15$$

The optical path separating adjacent stages is 22.2 mm when the thickness of quarter wave plates is 250 um, the epoxy thickness is 250 um, the liquid crystal cell's thickness is 2.25 mm, the polarizing beam splitter is 10 mm wide, and the air gap is 8.1mm.

5.4.1 Orientation Angle/Active Area of the LC Cell

The liquid crystal cells we used needed to be mounted at a 45^0 angle, which increased the distance between stages. For example a liquid crystal cell with a 20.25 mm length, 15.25 mm width, and 2.25 mm thickness that requires an orientation angle of 45^0 increases the distance between adjacent stages by 6.89 mm (Figure 5.4). The active area of the liquid crystal cells were 5 mm squares so the 45 degree orientation angle increased the active width to 7.07 mm as shown in Figure 5.4.

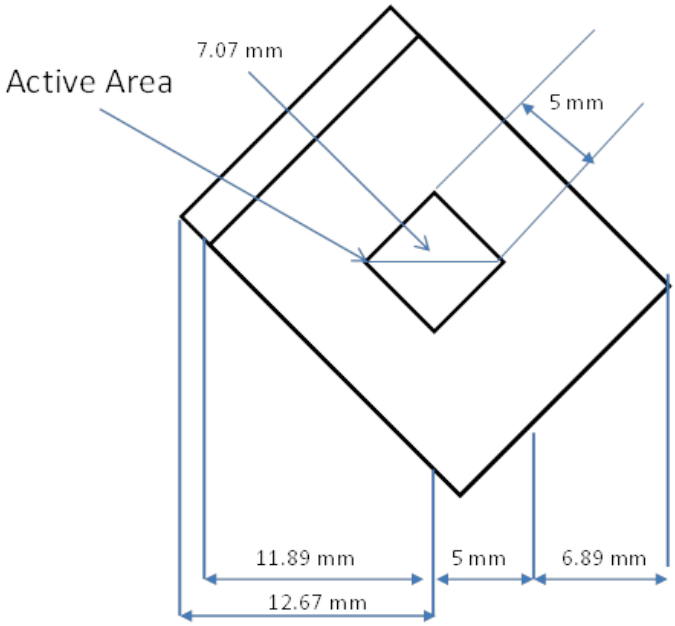

Figure 5-4: An illustration of a liquid crystal which requires an angular orientation greater than 90^0 with an active area smaller than the cell. The orientation angle increase's the distance separating stages while the active area restricts the maximum displacement.

The deflector width is restricted to the active width of the liquid crystal cell. Deviations from the 45 degree orientation angle with respect to the incident face of the polarizing beam splitter will result in crosstalk.

5.5 Number of Resolvable Spots

The output of the binary deflection system is brought to a focus using a lens at a distance F (Figure 5.5).

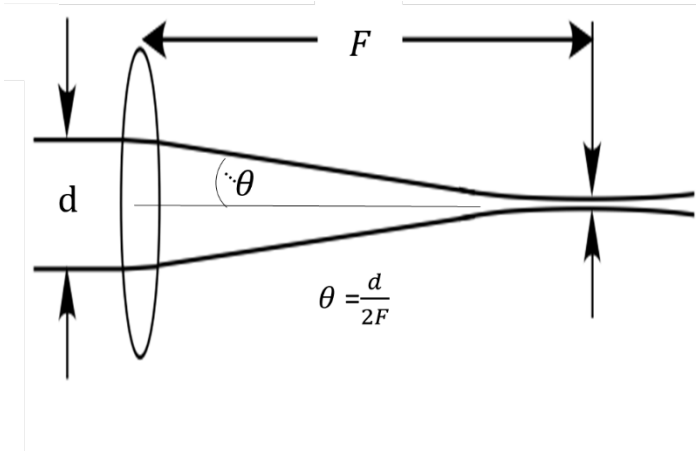

Figure 5-5: Angular Resolution of the focused laser beam.

The number of resolvable spots in the system is the ratio of the range to the resolution in which the range is the angular separation of the beams after the last stage. Therefore, the number of resolvable spots in the system is

$$NA = \frac{d}{2\mathrm{F}} \tag{5.16}$$

$$Resolution = \frac{k\lambda}{NA} \tag{5.17}$$

$$\#\ of\ resolvable\ spots = \frac{Range}{Resolution} \tag{5.18}$$

5.5.1 Practical System

For our ten stage system, the minimum angular separation of the first stage is 248 μrad, the optical path length separating adjacent stages is 22.2 mm, and the wavelength of light is 633 nm. The maximum linear displacement of the beam entering the last stage is 5.79 mm. If the incident beam diameter is set to 3 mm, the minimum width of the deflector (D) is 8.79 mm and the resolution is 260 μm at a focal length of about 1 meter. The system can resolve 1024 spots within a 0.25 meter line. Adding additional stages would increase the number of resolvable spots, but would also require a larger last stage to accommodate the increased displacements, and would increase cross talk since the angular range would be greater.

5.6 Conclusion

The maximum angle is limited to $\pm 15^0$ due to degradation of extinction ratios of the polarizing beam splitter and liquid crystal cell. The theoretical limit is light must fit within the deflector width of the last stage which includes the maximum displacement and the incident beam diameter. A smaller resolution corresponds to a wider beam while additional stages correspond to larger displacements entering the last stage. The optical path length separating two stages is limited by the size of the polarizing beam splitter cubes which affects the maximum linear displacement and the width of the deflector at the last stage. The optimum design for a practical system can't support an additional stage without increasing the size of polarizing beam splitter at the last stage and increasing the incident beam width entering the system.

CHAPTER 6 STAGE CONSTRUCTION

This chapter discusses the tools, systems, and methods for constructing a stage which include mirror/quarter-wave plate bonding using UV curing epoxy which is fixed to an L-bracket using candle wax. An optical system which can adjust and measure the angular deflection in the horizontal within an accuracy of ±10 μrad is discussed. The deflector angles are fixed using UV curing epoxy to bond the quarter-wave plates/mirrors to the polarizing beam splitter. An assembly was designed to hold the liquid crystal cell, at a 45 degree angle and centered with the polarizing beam splitter. Next the cross-talk due to the device and assembly tolerances is presented followed by the response time of the liquid crystal cell. Finally the stages power losses will conclude this chapter.

6.1 Mirror and Quarter Wave Plate Assembly.

Quarter wave plates between the beam splitters and the mirror were cut into 1 cm squares from sheet material 125 um thick[46]. The fast axis was oriented at 45^{o} to one side of the square. The quarter wave plates were bonded, with UV curing epoxy, to 1 cm square first surface mirrors (Figure 6.1) [47]. After an exposure time of five minutes, using a UV source (black light), the epoxy reaches a full cure and bonds the quarter wave plate and mirror (Figure 6.2).

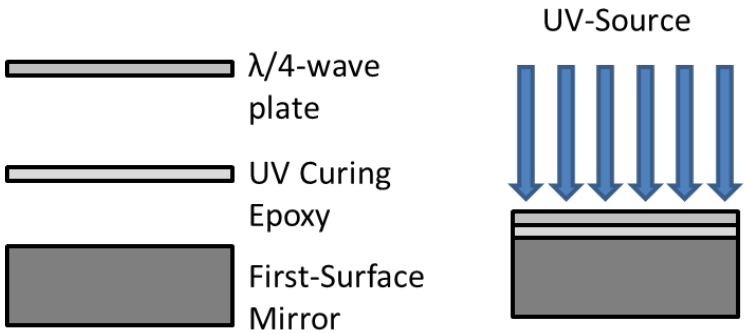

Figure 6-1: Illustration of bonding the quarter wave plate to the mirror using an index matched, UV curing epoxy.

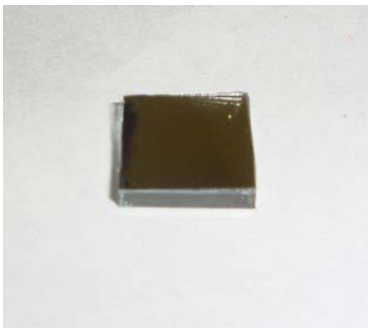

Figure 6-2: Photo of the quarter wave plate bonded to the mirror after a five-minute exposure to UV radiation.

The thickness of the UV epoxy is approximately 125 μm, therefore the optical path length after two passes through the UV epoxy (L_{Epoxy}) and quarter-wave (L_{QWP}) is the ratio of the index of refraction for air and the index of refraction of the quarter wave plate and epoxy which is shown below:

$$L = 2(L_{QWP} + L_{Epoxy}) \quad 6.1a$$

$$L_{QWP} = \frac{n_{air}}{n_{QWP}} L_{air} \approx \frac{1}{1.54} L_{air} \quad 6.1b$$

$$L_{Epoxy} = \frac{n_{air}}{n_{Epoxy}} L_{air} \approx \frac{1}{1.54} L_{air} \quad 6.1c$$

The index matched UV curing epoxy bonds the quarter-wave plate to the mirror, reduces unwanted reflections and minimizes the effect of the non-uniform "flat" surface of the quarter wave plate film, reduces the optical path length, and reduces reflection losses.

6.2 L-Bracket Assembly

Figure 6.3 illustrates the procedure for holding two mirrors at a 90 degree angle. Two mirrors, each bonded to quarter wave plates, were assembled at 90^{o} to each other on a bent metal L-bracket. Pellets of candle wax were first placed on the L-bracket (29 mm x 25 mm x 1 mm). Next, a hot plate melted the wax. After the wax melted, the mirrors were gently pressed in place on the L-bracket.

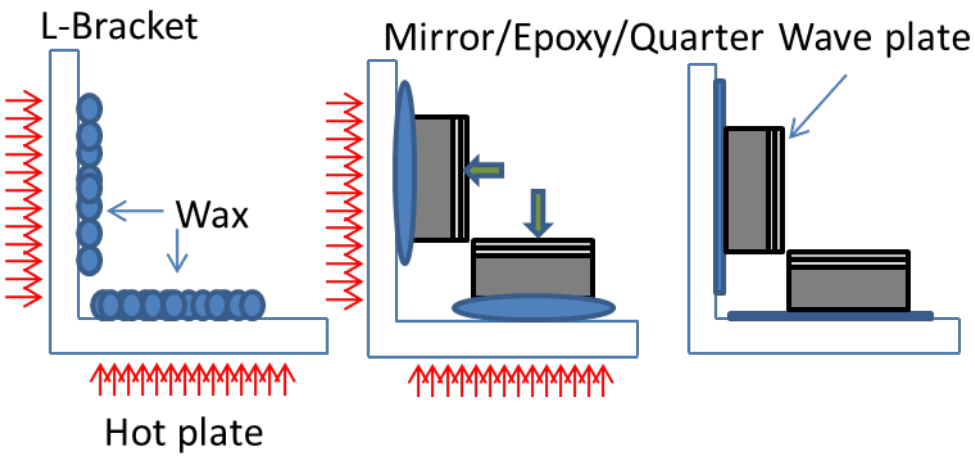

Figure 6-3: The procedure for assembling the mirrors and quarter wave plates to the L-bracket. a. Wax is placed on an L-bracket then heated on a hot plate. b. After the wax melts the mirrors are gently pressed in place. c. The assembly is removed from the heat.

The assembly was then removed from the hot plate with the mirrors held in place until the wax hardened. Latex gloves were required in this step to avoid fingerprints on the mirrors. A photograph of the completed L-bracket assembly is shown in Figure 6.4.

Figure 6-4: L-bracket assembly with two mirrors and quarter waveplates.

The L-bracket assembly was used to position the two mirrors during bonding to the polarizing beam splitter. Earlier attempts to attach the mirrors to the L-bracket used double sided tape or five-minute epoxy. The tape was insufficiently stable, so that the mirrors lost their

relative alignment. The five-minute epoxy maintained the mirrors in position, but the force required to remove the L-bracket from the mirrors after bonding was large enough to affect the alignment of the beams. The wax held the mirrors in position and with gentle heating permitted the L-bracket to be easily removed. The total thickness of the L-bracket assembly is 3.5 mm which includes the mirror, quarter-wave plate, epoxy, and wax assuming the thickness of the coat of wax is approximately 250 μm.

The L-bracket must be fixed at a 90 angle and a uniform coat of wax is required to hold the mirrors or unwanted angular offset is introduced prior to re-entering the polarizing beam splitter.

6.3 Assembly of Subassembly to the Beam Splitter

6.3.1 Description of Optical System and All the Adjustment Controls

The optical system for aligning and bonding the mirrors to the beam splitters is shown in figure 6.5. A vertically polarized beam from a He-Ne laser, at a wavelength of 0.633 um, exits a quarter wave plate circularly polarized and passes through a lens prior to entering the polarizing beam splitter. Within the beam splitter, the horizontally polarized component is reflected and the vertically polarized component is transmitted. Both beams exit the beam splitter, and are reflected back into the beam splitter by mirrors, after passing twice through quarter wave plates with their fast axes at 45^{o}. Their polarization is now changed, so that the beam which was initially horizontally polarized is now vertically polarized and therefore transmitted by the hypotenuse, and similarly the initially vertically polarized beam is reflected by the hypotenuse. The output beams reflect from a first surface mirror to a split photo diode, which is fixed on a digital caliper, 1.04 meter distant.

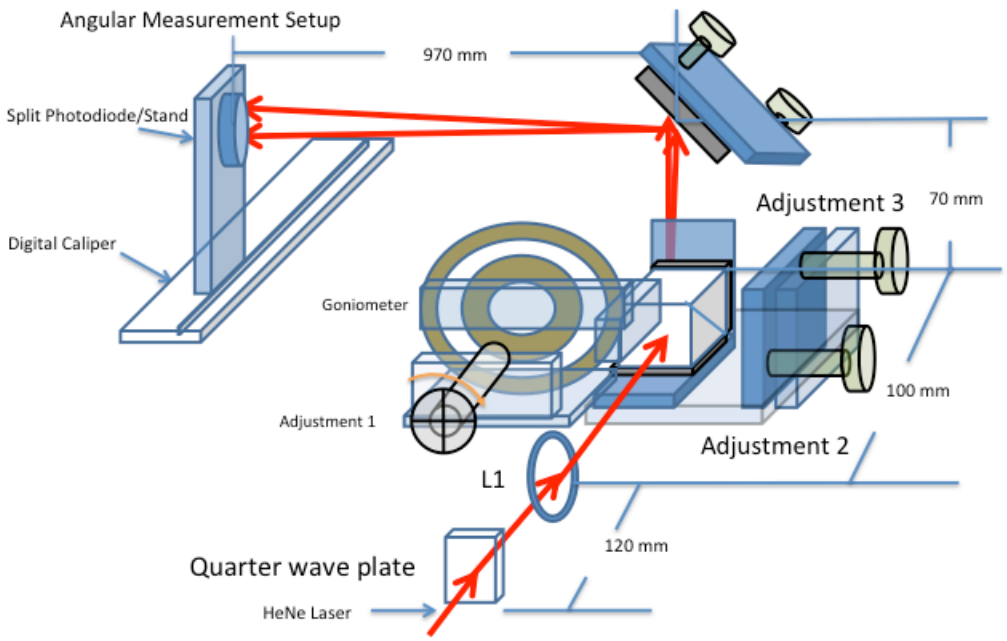

Figure 6-5: The optical system for bonding the beam splitter to the mirrors with an accurate angular displacement. For clarity the figure is not to scale, and the input laser has been omitted.

The polarizing beam splitter is mounted on the axis of a micrometer driven goniometer (See Figure 6.5 Adjustment 1). Rotating the goniometer clockwise increases the angle of the polarizing beam splitter with respect to the L-bracket assembly, which increases the horizontal angle between the two exiting beams. The accuracy of the angle between the beams is limited to the precision of the goniometer which is about 0.5 µrad. The L-bracket assembly, which contains the mirrors and quarter wave plates discussed in section 6.2, is mounted separately on a straight mirror mount, containing two 64-pitch mounting screws, to adjust the angles of the assembly (See Figure 6.5 Adjustment 2-3). Fine adjustments in the orientation of the mirror mount change the vertical angles of the exiting beams, permitting them to both be positioned in a horizontal plane. The precision of vertical offsets with each beam is limited to the mounting screws within the mirror mount which is 1 µrad. for a 64-pitch mounting screw.

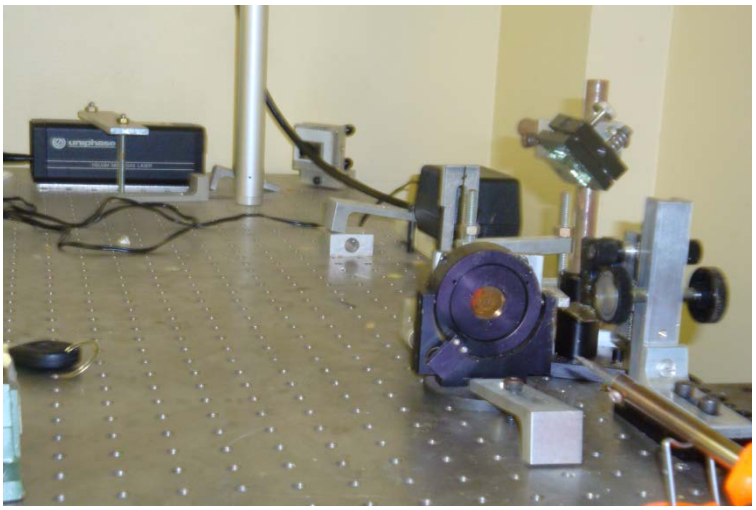

Figure 6-6: A photo of the optical system used to bond the quarter-wave plates/mirrors to the polarizing beam splitter.

6.3.2 Description of Angular Measurement Technique

Figure 6.7 is an illustration of the arrangement used to set the angle between the two beams exiting the polarizing beam splitter.

The two output beams exit the optical system, as discussed in section 6.3.1, and pass to the angular measurement setup (Figure 6.7). Initially, adjustments are made so the two output beams overlap each other prior to setting the angle. The microscope objective is used to expand the beams for crude alignment in the vertical direction prior to the setting the angle. The split photodiode is mounted on a digital caliper for moving the photodiode and measuring the horizontal distance between the beams. Figure's 6.8 and 6.9 depict the circuit diagram for the split photo diode and the response of the detector.

For small angular displacements, a polarizing filter is inserted at the input of the optical system to inspect one beam and rotated 90 degrees to inspect the second output beam. Rotating the goniometer changes the angular displacement between the beams and the digital caliper and

split photodiode measure the distance between them. The distance, from beam one to beam two, is the horizontal displacement.

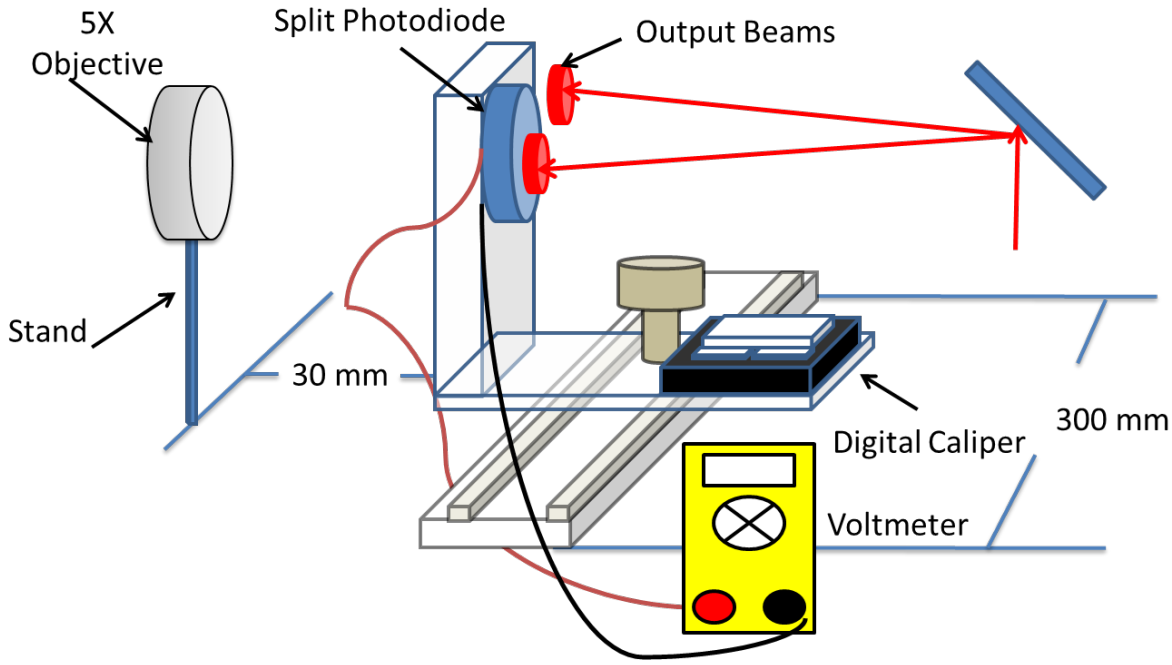

Figure 6-7: The setup for measuring the angular displacement of the two beams. A split photodiode is mounted on a digital caliper for horizontal alignment. The microscope objective behind the photodiode is used for vertical alignment.

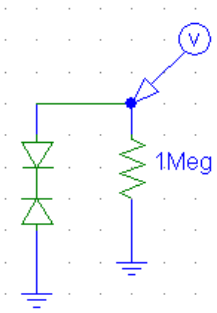

Figure 6-8: Schematic of the split photodiode used to measure the angular displacement.

The angular displacement can be determined since the tangent of the angular displacement is equal to the ratio of the horizontal (dx) displacement and distance from the beam splitters output to the detector (y). The digital caliper has a 300 mm horizontal range with an

accuracy of ±10 um. Therefore the system can measure angular displacements with an accuracy within ±10 urad.

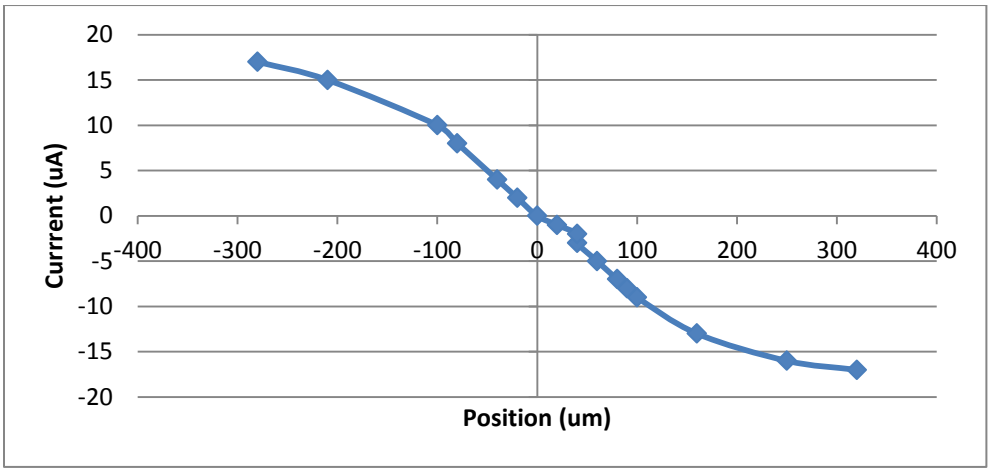

Figure 6-9: Measured response of the split photodiode.

6.3.3 Description of UV Epoxy Hardening Technique

The purpose of bonding the quarter-wave plate/mirror to the polarizing beam splitter is to fix the angular displacement of the beams and minimize power loss for the stage. The UV curing epoxy is applied in the space between the quarter wave plates and the beam splitter (Figure 6.10b) followed by alignment of both beams to set the angular displacement. After alignment is achieved, as described in the last section, UV light exposes and hardens the epoxy.

NOA 68 is an index matched, UV curing epoxy designed for bonding optical components [28]. The index of refraction for the epoxy, after full cure, is 1.54.

6.3.3.1 Curing Time

An exposure time of 3 minutes was required for bonding two microscope slides (Figure 6.10a). However, a longer exposure time was required for the epoxy to cure for bonding the mirror/quarter wave plates to the beam splitter.

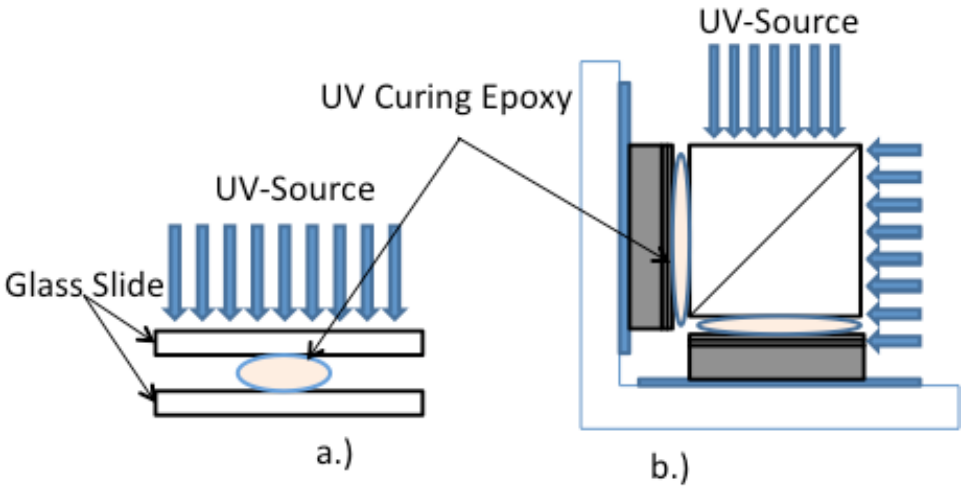

Figure 6-10: An illustration for the UV epoxy hardening technique for glass (a.) and for bonding the mirror/quarter wave plate to the beam splitter (b.).

The longer exposure time is required because the mirror mount holding the L-bracket blocks light entering one corner and the UV source could not be positioned directly on the beam splitter. Also several exposure intervals are required for realignment because the mirror mount would move while the epoxy hardened. A total time of thirty minutes was required for the epoxy to pre-cure. The epoxy was exposed to the UV source for one minute followed by realignment. This procedure was repeated thirty times to reach the pre cure. During this period, the change in horizontal displacements was large but coarse angle adjustments were possible. After the epoxy was pre-cured, the exposure intervals increased to five minutes followed by realignment. During the period from pre-cure to final cure, the change in horizontal displacements was very small or none occurred. However, fine angle adjustments are still possible during this period. The epoxy is fully cured when the beams don't move from exposure and fine adjustments. In many cases the time from pre-cure to final cure was three hours. The polarizing beam splitter with the quarter wave plates and mirrors are removed from the setup after the epoxy has reached a full cure as shown in Figure 6.11

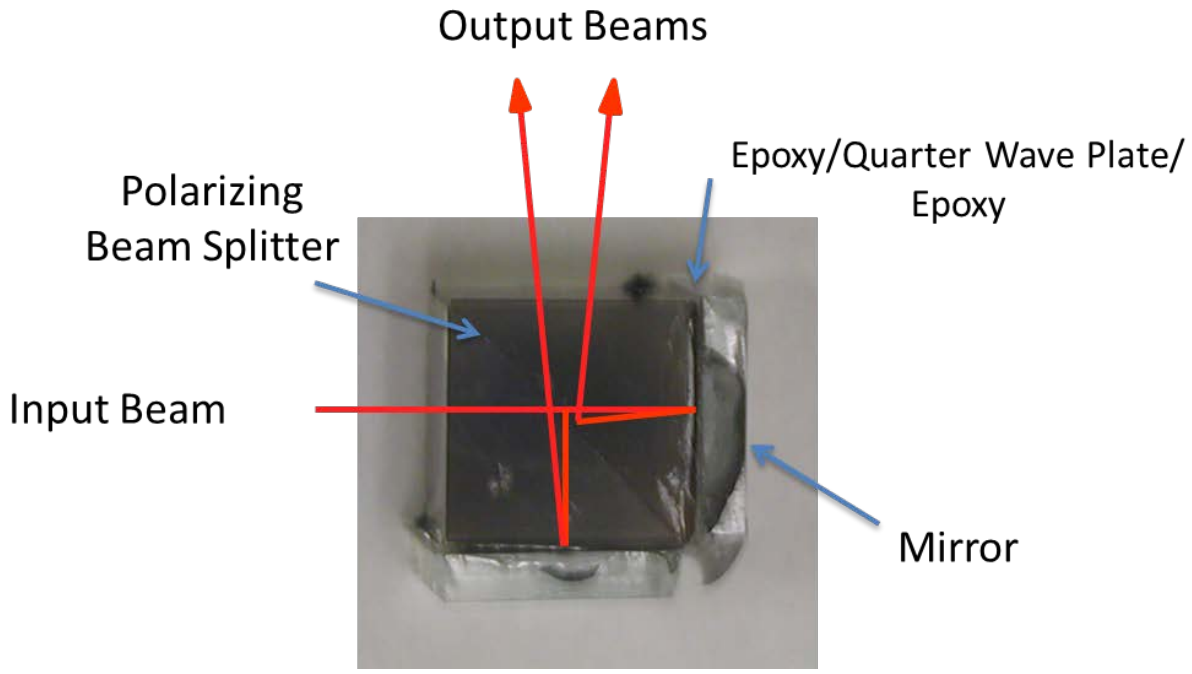

Figure 6-11: The mirror/quarter wave plates bonded to a beam splitter and removed from the setup.

6.4 Liquid Crystal Cell Assembly

The empty liquid crystal cells were purchased from Instec [16] and the liquid crystal material was provided by Teledyne Inc[48]. The active area of the liquid crystal cells purchased from Instec is 5x5 mm^2.

The empty liquid crystal cells contain two openings used for filling with the liquid crystal material. Prior to placing the material into the cell, wires were bonded to the liquid crystal cell contacts using a conductive epoxy. Next, the liquid crystal material was placed on one of the openings. The liquid crystal cell uses capillary forces to pull the liquid into the cell. The final step is sealing the two openings with a small amount of UV curing epoxy. Sealing the two

openings prevents any liquid crystal material from leaking out while protecting the material from debris, dust, etc. A photo of the finished liquid crystal cell is shown below (Figure 6.12).

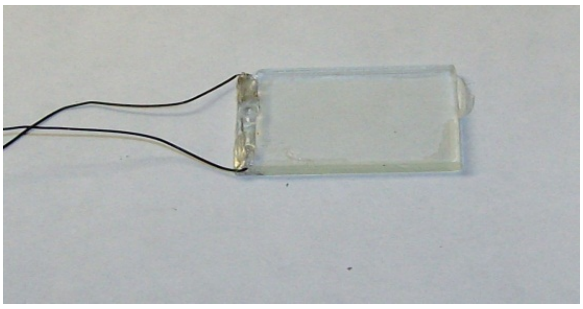

Figure 6-12: Liquid crystal cell filled with the liquid crystal material, wires bonded, and sealed prior to beam splitter assembly.

6.4.1 Assembly of the Liquid Crystal Cells to Beam Splitters

A fixture was designed to hold the beam splitter and liquid crystal cell in place during assembly (Figure 6.13).

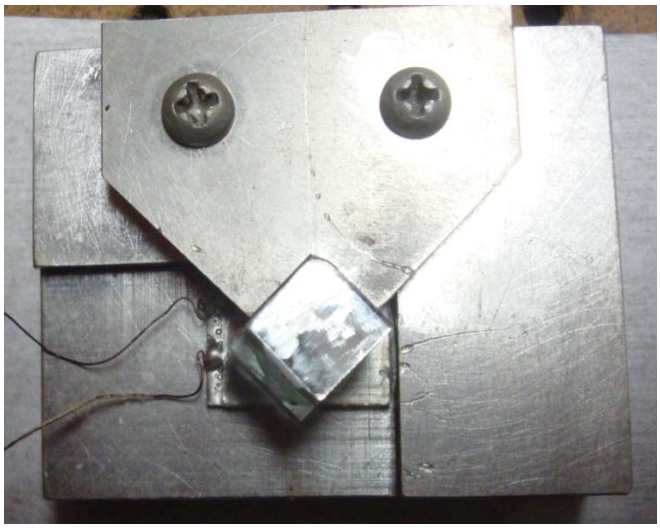

Figure 6-13: A picture of the assembly used to bond the liquid crystal cell to the polarizing beam splitter.

The liquid crystal cell was rotated to a 45 degree angle and the active area was centered on the beam splitter while on the mount. After placing both components on the fixture, a small

amount of epoxy was applied to the liquid crystal cell and the base of the beam splitter. A photo of the liquid crystal cell mounted to the polarizing beam splitter is shown below (Figure 6.14): The accuracy for centering the active area of the liquid crystal cell to the polarizing beam splitter was within $\pm$ 0.5 mm in vertical and horizontal direction. The accuracy fixing the liquid crystal cell at a 45 degree angle is less than 1 degree.

Figure 6-14: A picture of the assembly used to bond the liquid crystal cell to the polarizing beam splitter.

6.5 Tolerances

Errors in the positions of the deflected beams and cross-talk from unwanted polarizations are caused by tolerances in the devices and assembly of stages. This section reviews the cause of device and assembly tolerances while discussing the effect of assembly tolerances for a stage.

Device tolerances include the polarizing beam splitter and liquid crystal cell: Rotating the mirror angles changes the angular displacement but cross-talk restricts the maximum angular separation. Switching speeds faster than the liquid crystal cell's response time also cause cross talk. Errors in fixing the liquid crystal cell at a 45 degree angle cause cross-talk. A summary of

the assembly tolerances is shown below in Table 6.1. Angular offsets are un-centered angle or separation with respect to the input and output face of the polarizing beam splitter.

Table 6-1: Summary of assembly tolerances

Assembly Tolerances				
Deflector Angle	Angular Separation		Linear Displacement	
	Horizontal	Vertical	Horizontal	Vertical
	± .10 µrad	± .397 µrad	±10 µm	±397 µm
LC cell	Orientation Angle			
	$<1^0$			

Errors and angular separation and linear displacement have a cumulative effect within a system.

6.6 Response Speed

The response time of a stage is limited to the response time of the liquid crystal cells. Recall from chapter 4, the response time is defined as the time for the molecules to relax after removing the signal applied from the cell. If the time to switch from the on and off state is faster than the response time of the liquid crystal material cross-talk occurs. Appendix C describes an experiment for measuring the response time for liquid crystal cell. The response time measured for the liquid crystal cells from Instec was 20 ms.

6.7 Power Losses

Measurements were made of intensity losses of light passing through the various components in each polarizing beam splitter stage:

6.7.1 Liquid Crystal Cell

The measured transmission of an incident HeNe laser beam at 0.6328 microns varied with position, and was a maximum of 76% in one cell and 81% in another. Experiments with a

1.6 mm thick cell filled with liquid crystal material showed that 20% of the HeNe laser beam passed through as a narrow beam, while the remaining 80% was scattered through large angles. This implies the 6 micron thick cells used in the experiment the scattering loss in the liquid crystal material was only 0.6%. The remaining loss was apparently due to the nominally transparent electrodes.

6.7.2 Polarizing Beam Splitter

The measured transmission through beam splitters from two sources (Edmund and Casix) was 95% and 94% respectively [52, 44]. This was the same for both polarizations. When the input beams incident angle was set to the normal a cross-talk of about 0.1% was observed for both beam splitters. In each stage two passes are made through the beam splitter, so the final transmission was 90% and 88% respectively.

6.7.3 Quarter-Wave Plate.

The measured transmission of an available high quality quarter wave plate was 80%, of which 8% of the loss was due to reflections from the two surfaces [51] index of refraction. The inexpensive film type quarter wave plates actually used had a higher transmission, 91%, of which 7% of the loss was due to reflections [47]. In use two passes are made through the quarter-wave plates, but they are index matched so the reflective losses are minimal. The resulting transmission through the quarter wave plates is therefore 96%.

6.7.4 Mirrors

The specified reflectivity of the mirrors used in each stage is 96%. In principle multilayer mirrors are commercially available with reflectivity greater than 99.8%, but these are expensive and not readily available with the required dimensions.

The calculated best case transmission for each stage is therefore 0.81 x 0.90 x 0.96 x 0.96 or 67%. This corresponds to approximately 2% transmission through 10 stages. These results are summarized in Table 6.2.

Table 6-2: The power loss occurring in each component within a stage, the resulting transmission through a stage, and the corresponding transmission through 10 stages.

Component	**Component Loss (%)**	**Transmission in stage (%)**
Liquid Crystal Cell	19	81
Polarizing Beam Splitter	5	90
Quarter Wave Plate	2	96
Mirror	4	96
Transmission through one stage	-	67
Transmission through ten stages	-	2

6.8 Conclusion

Chapter 6 discussed the tools required to build a single stage. A single stage is composed of a voltage-controlled polarizer (liquid crystal cell) and polarizing beam splitter, mirrors, and quarter-wave plates. The system setting the mirrors angles can measure the angular separation of the beams with an accuracy of 10 μrad in the horizontal direction. The largest angle the system can measure is 17.5 degrees. However the polarizing beam splitter limits the maximum angular separation to ±15 degrees due to the degradation of extinction ratios. The response time for a stage, 20 ms, is limited to the response time of the liquid crystal material. The setup for constructing the deflector angle has minimized the number of components, losses, and size which will reduce the difficulty in constructing a system. In the next chapter a series of stages are incorporated to function as a beam steering system.

CHAPTER 7 SYSTEM CONSTRUCTION

This chapter discusses the construction of an optical system which is composed of cascading ten stages . The layout, tolerances, and adjustments are described followed the problems encountered at the last two stages. The electronics for testing and controlling the optical system, which includes manual angle selection and scanning in both directions, was designed and implemented with collaboration from Southern University.

Chapter 6 discussed the construction of a stage which is composed of a liquid crystal cell and a deflector angle. The liquid crystal cells are used to change the polarization, which results in angle selection. If the output of one stage is used as an input to a second stage, the result is four possible angles controlled by the two liquid crystal cells. The number of angles or beams (output directions) is 2^n, where n is the number of stages in the system. The figure below (Figure 7.1) illustrates the concept of a system composed of four sequential stages. The stages are mounted on spacers and fastened by screws.

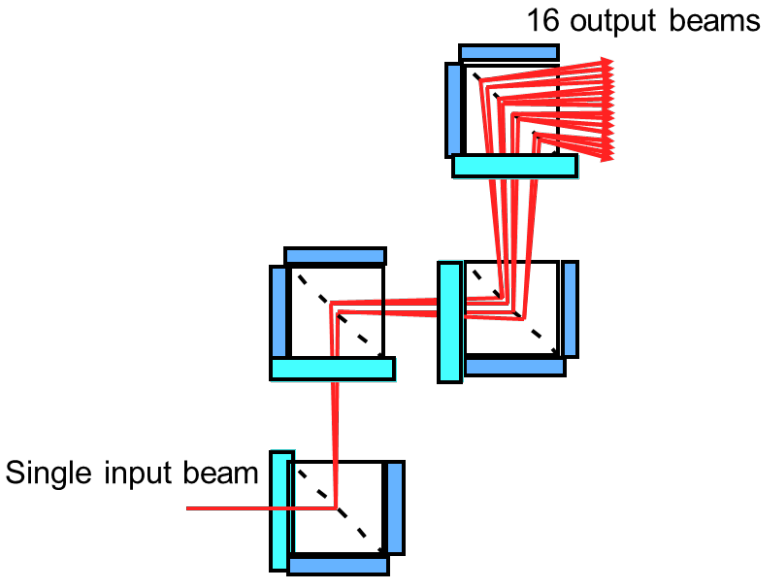

Figure 7-1: The illustration depicts an optical system composed of four sequential stages. An incident beam passing through four stages results in 16 angular displacements to select. The liquid cells are used to select the angle or output direction for clarity.

Digital circuits are used to control the signal sent to each liquid crystal cell. The digital circuits, composed of Basic Stamp processor [17] with a digital keyboard input, combined with counting circuits allow manual (user input) angle steering or sequential angle steering.

7.1 Layout of Multiple Stages

In order to minimize transverse displacements, the stages were placed close to each other. Figure 7.2 illustrates the layout of two stages mounted on spacers.

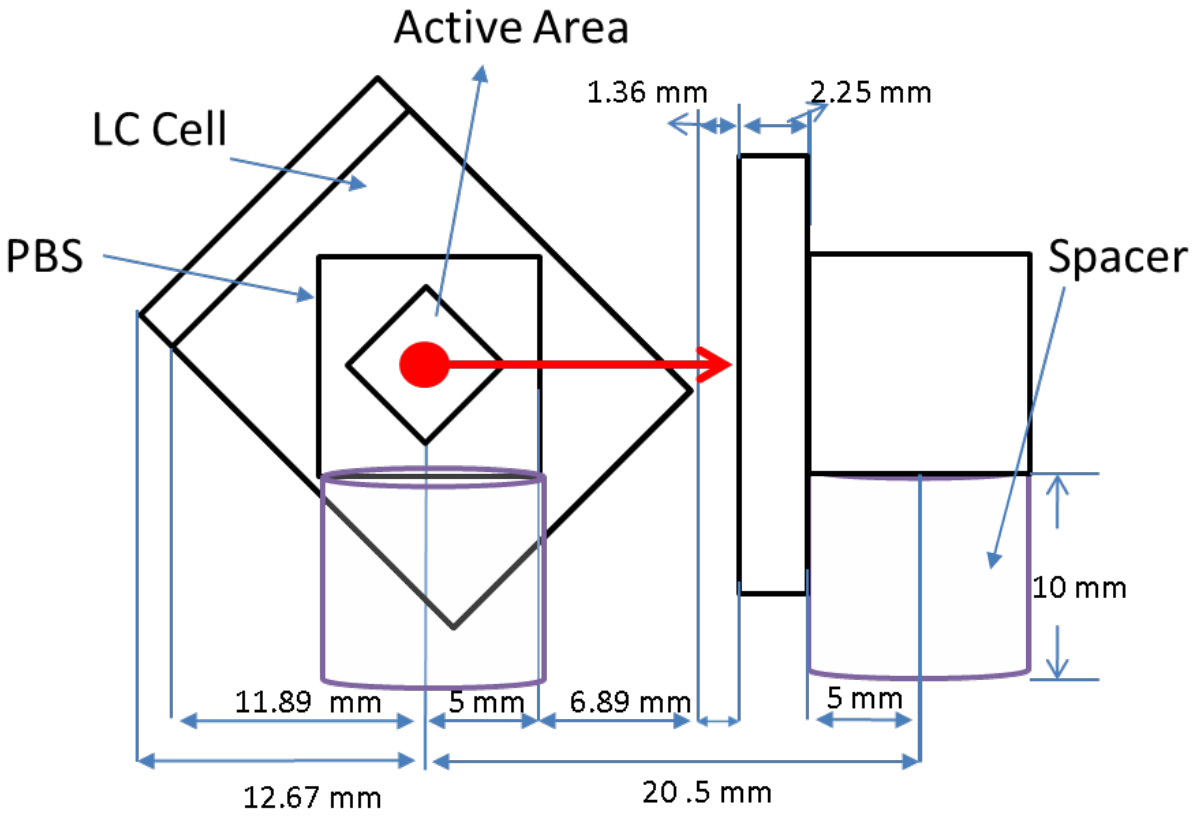

Figure 7-2: The layout for a two stage system. The distance separating the liquid crystal cells for system is 1.36 mm. However, the distance the beam travels in air from the output of the first stage to the liquid crystal cell of the second stage is 8.25 mm.

The diameter and height of the spacers are 10 mm. The separation between the center of the first spacer and second is 20.25 mm and a distance of 1.36 mm separates the edge of the liquid crystal cell in the first stage from the second. The 1.36 mm distance separating adjacent

stages prevents the liquid crystal cells from making contact with each other and allows angular rotations of the spacer to minimize offsets from fixing the spacer to the stage. The layout for a seven stage system is shown in Figure 7.3 below:

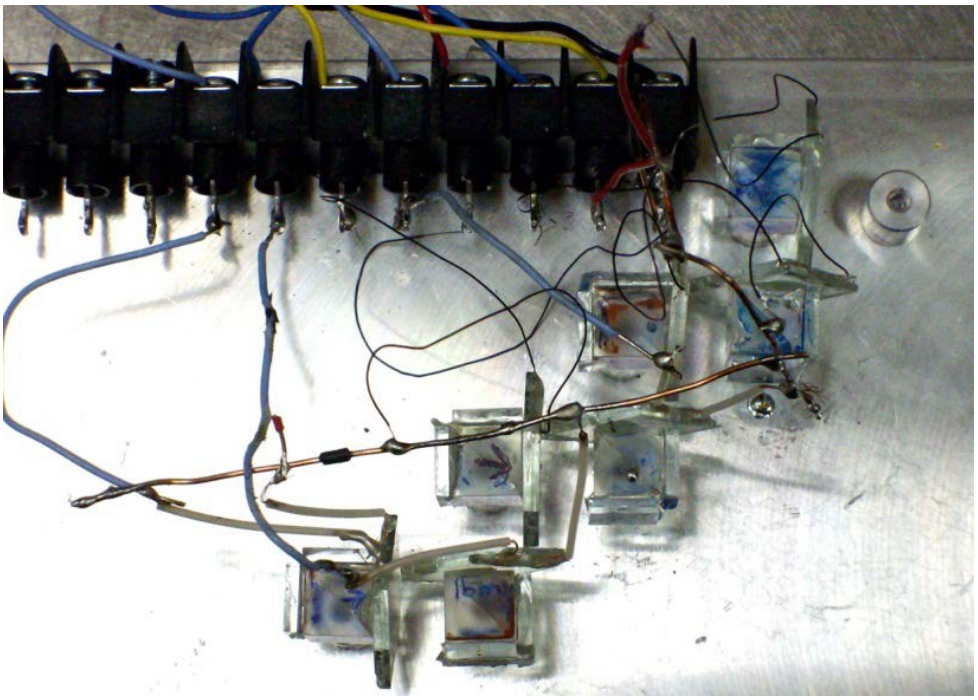

Figure 7-3: A photograph of the system layout with seven stages assembled.

7.2 Tolerances and Adjustments

Each stage is fixed on a spacer with epoxy. Variations in the wedge angle of the epoxy layer resulted in vertical displacements (Figure 7.4). Shims were inserted to minimize these unwanted displacements. The variations were considered acceptable in a linear deflector, since they didn't affect the deflection in the desired direction.

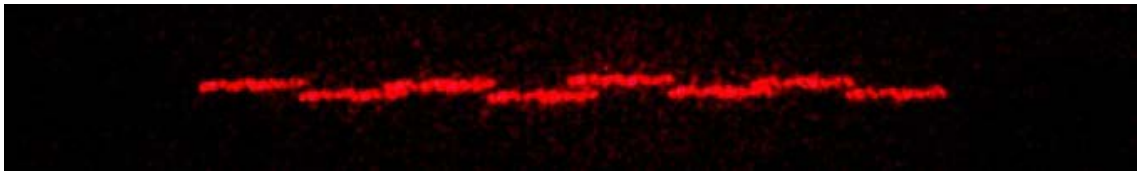

Figure 7-4: Offsets occurring in a one dimensional deflection system due to the split photodiode being unable to account for displacements in the vertical direction. The liquid crystal cells are driven in half-voltage operation to view all output angles.

7.3 Alternatives for the Last Stage

The maximum displacement, in the horizontal direction, entering the last two stages was 9.5 mm which is larger than width of the active area within the liquid crystal cell. This section discusses two alternatives for last stage. A reflective optical system was used so the linear displacements leaving a stage would remain the same the same entering the next stage. Also the liquid crystal cells for the last two stages were replaced with new cells which have an active area larger than 1 cm. and a smaller volume reducing the distance and linear displacement.

7.3.1 Reflective Optical System between Stages

Alternatively, an additional optical system was demonstrated to couple the 9^{th} stage to the 10^{th} stage without additional spreading of the beams. Figure 7.5 shows the folded telescope used to couple the stages. Parallel beams leaving the 9^{th} stage are focused by a lens on a mirror one focal length distant. They are then returned through the lens and again become parallel beams. The 9^{th} and 10^{th} stages are also one focal length from the lens, and lie in conjugate positions. Thus, the light exiting stage 9 is imaged at unit magnification on stage 10, and parallel beams return to stage 10 at the same angle at which they left stage 9.

The telescope arrangement eliminates undesired displacements due to the distance traveled in air. Therefore the optical path length is set by distance the beam travels through the optical components within the stage which is the optimum condition when the active area of the liquid crystal cell is larger than the area of the input face of the polarizing beam splitter. However the mirrors will increase the power loss per stage while increasing the systems size and cost. Additional stages using the telescope arrangement would increase the number of components in the system, size, cost, power losses, and require a complex arrangement.

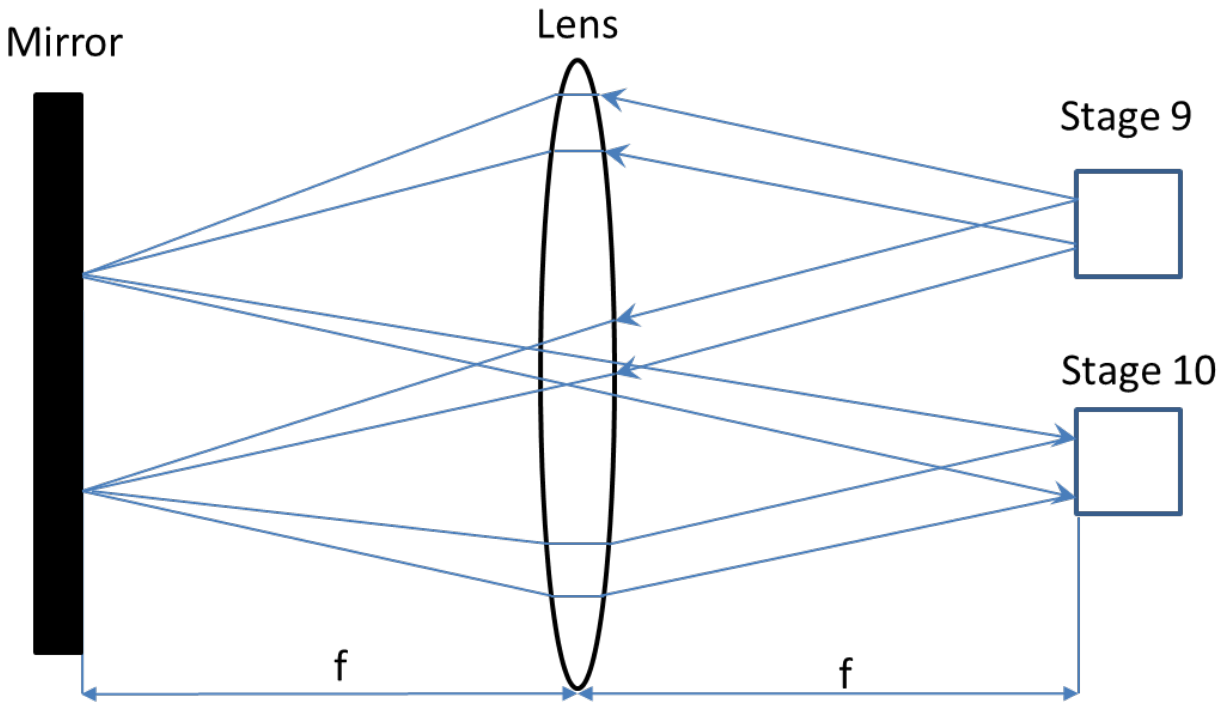

Figure 7-5: Telescope arrangement used for the tenth stage.

7.3.2 Liquid Crystal Cells with a Larger Active Area

The liquid crystal cells from Teledyne have an active area (18.5 mm x 11 my m) larger than the input face of the polarizing beam splitter. Therefore the maximum displacement entering the last stage is restricted to the area of the polarizing beam splitter.

The size of the Teledyne liquid crystal cell (20 mm x 12.5 mm x 1 mm) is smaller and requires a 90 degree orientation angle which reduces the distance separating two stages to13.25 mm, the optical path length to 15.39 mm, and maximum displacement entering the last stage 3.94 mm. Replacing the last two stages with the liquid crystal cells from Instec can decreases the distance the separating adjacent stages by 3.25 mm and reduce the maximum linear displacement at the last stage by 4.85 mm.

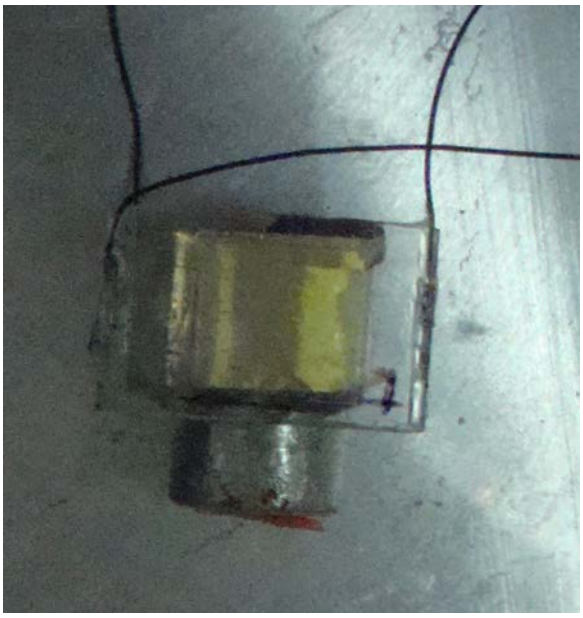

Figure 7-6: A stage with a liquid crystal cell with a larger contact area. Also, a 45 degree rotation isn't required and the area is smaller. Therefore, the distance separating the last two stages is reduced by 3.14 mm.

7.3.3 Discussion

Based on the application and specification, both options are suitable for the last two stages. The telescope arrangement limits the maximum linear displacement to the distance the beam travels through the optical components which approaches the theoretical limit. It is a suitable choice when cost and size aren't constraints. The telescope arrangement was demonstrated but replaced with the liquid crystal cells from Teledyne because the total displacement entering the last stage was larger than the active area within the liquid crystal cells.

7.4 Electronics for Stage Testing

This section will discuss the electronic systems used to drive the liquid crystal cells within a stage. A switching system was implemented to test individual stages during system assembly.

The switching system was used to test the liquid crystal cell within each stage and the individual stages effect on output directions during system assembly. Figure 7.7 is a picture of

the switching system used to test each stage during system assembly. The chassis contains the mechanical switches, an input for a function generator, and an output for sending a signal to the liquid crystal cells for each stage. The switches are connected in parallel, therefore the output signals are the same and vary with respect to the function generator.

7.4.1 Half Voltage Operation

The switching system was also used to view all output directions in the system at the same time (Figure 7.4) by reducing the amplitude of the square wave to half the threshold/operating voltage (1.5 Vpp) at a frequency of 1 kHz from the function generator.

Figure 7-7: The switchbox contains the mechanical switches, input signal from the function generator, and the output of each switch is wired to a liquid crystal cell.

7.5 Electronics for System Control

The electronic system used to control the optical system was designed and implemented by Southern University. The system is capable of selecting an output direction and scanning in both directions (± x).

The signal sent to the liquid crystal cells was controlled with digital circuits. The digital circuits, composed of Basic Stamp processor [17] with a digital keyboard input, combined with counting circuits allow manual (user input) angle steering or sequential angle steering. A free running oscillator was used to generate the signal driving the liquid crystal cells and a second oscillator (555-timer) was used to set the scanning rate (or speed) of the counting circuit.

This section will first discuss the key components within the digital system which consist of free running oscillators, user input interface, and counting circuits. A discussion of the digital system will conclude this section.

7.5.1 Free Running Oscillator

A free running oscillator was used to generate the signal used to drive the liquid crystal cells and the clock used to set the counting speed or scan rate of the optical system. Kenny Moses and Vontrel Collins from Southern University designed and implemented both oscillator networks.

The circuit for generating the square wave signal of 3Vpp at a frequency of 1 kHz is shown in Figure 7.8. The output square wave signal was sent to an analog multiplexer. The circuit contains a 741 operational amplifier which is used as a comparator, capacitor, three resistors, and two DC power supplies. There are two feedback networks in the circuit. The first feedback network, from output to input, is sent to negative input (V_-) and contains a resistor and capacitor which sets the time constant and frequency of oscillation. The second feedback network is sent to the positive input (V_+) and contains two resistors used a voltage divider which also sets the period of the square wave.

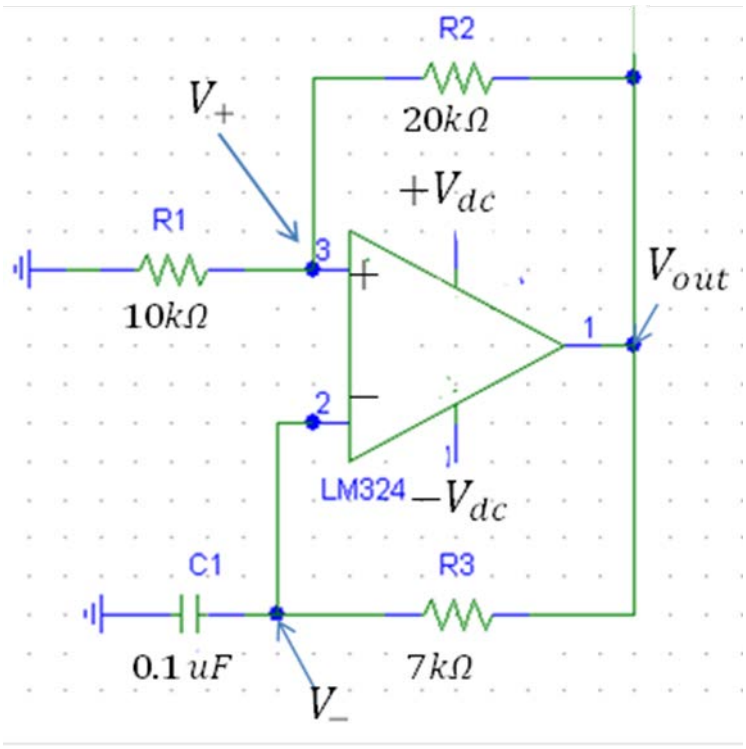

Figure 7-8: Free oscillation circuit, composed of a 741 operational amplifier, used to generate a square wave signal of 3 Vpp at a frequency of 1 kHz.

The duty cycle is fixed by the R1, R2, and the feedback loop containing R3 and the capacitor (C1) and the design equation is shown below:

$$f = \frac{1}{2R_f C * \ln(\frac{2R1}{R2} + 1)}$$

A 555 timer was used to generate a digital clock oscillating at frequency 40 Hz. The digital clock was sent to the counting circuit to set the scanning speed.

7.5.2 Selectable Output Direction

A Basic Stamp processor was programmed and interfaced with the keypad and display, by Tracey Jones from Southern University, to process a decimal number entered by a keypad and output a 10-bit binary number to the counting circuit. The electronics allow the user to manually select output directions and select the initial direction prior to scanning.

The program prompts the user in enter a decimal number from 0 to 1023 and waits for an input. After an entry is made from the keypad, the processor converts the decimal entry into a binary output which is updated to the display and sent to the counting circuit. After selecting an initial angle, the user has the option to select another angle by resetting the processor. If no angle is entered, the initial 10-bit binary number sent to the counter is 0.

7.5.3 Counting Circuit

System scanning was demonstrated with two 5-bit binary counters in which the carry bit of the first counter was sent to the second counter to function as one 10-bit binary counter. The output from the counter is a 10-bit binary number that's sent to an exclusive NOR gate. The input to the counters was a 10-bit output binary number from the processor (Section 7.5.2) in which the first five bits were passed to the first binary counter and the final five bits to the second counter. This section will discuss the additional inputs to the counter circuit and their effect on the system.

The digital clock discussed in section 7.5.1 was sent to both counting circuits. The counting circuit has four additional inputs which controls the counting circuit. The inputs to the counting circuit include a load which passed the 10-bit binary number from the processor when set to logic 0 (user input) or started counting when set to logic 1. The clear input resets the counter output to 0 when set to logic 1. The inputs for counting include the count up input to start adding by one when set to logic 1 (+ x direction) and the countdown input to start subtracting by one when set to logic 1 (- x direction).

7.5.4 Digital System

The digital system for controlling the optical system, discussed in Section's 7.1-7.3, includes the electronics discussed earlier (7.5.1-7.5.4), exclusive NOR correction, analog

multiplexers, and a switching network to control the counting circuit. The schematic for the digital system is shown below in Figure 7.9.

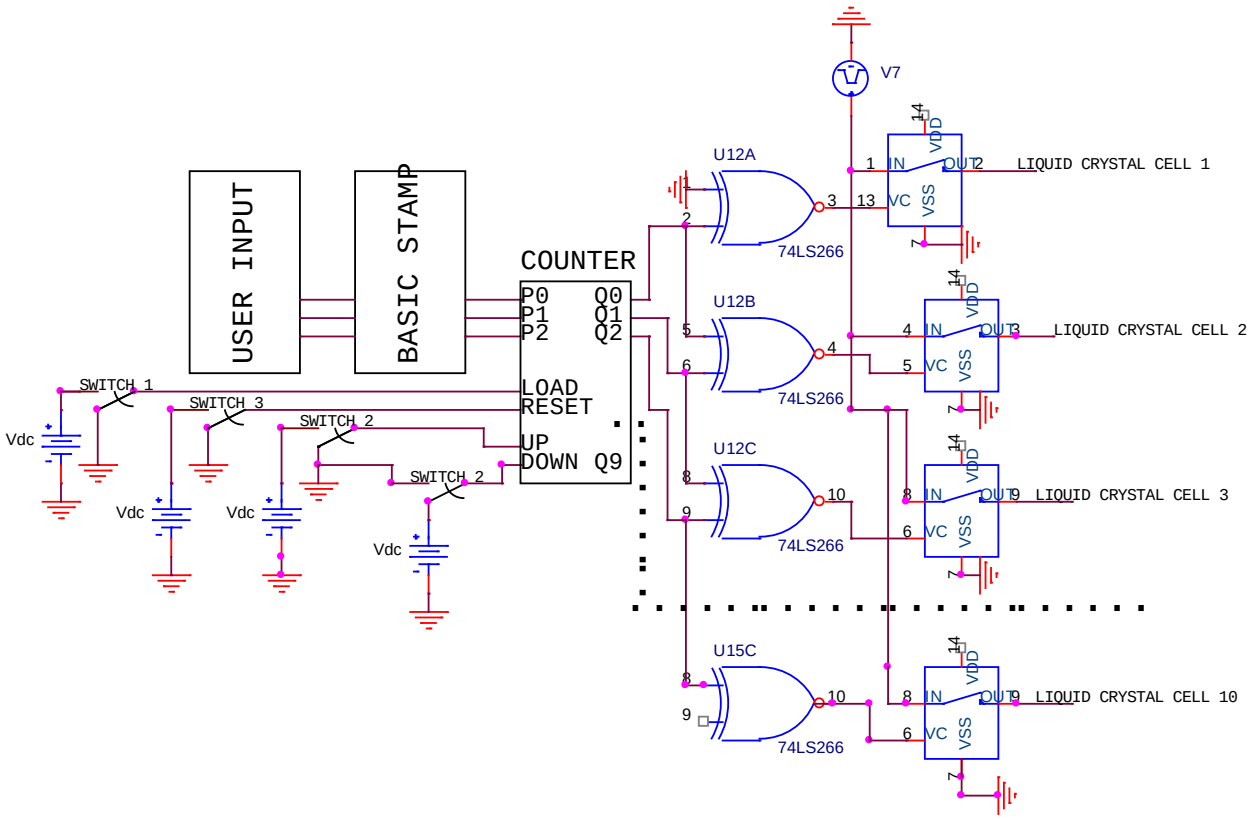

Figure 7-9: Schematic of the digital circuit used to control the optics. The square wave signal sent to the analog multiplexers comes from an op-amp oscillation circuit. The multiplexers output is passed to the liquid crystal cells.

The system requires two DC sources (± 10V) for operation. The inputs to the system are the keypad and a switching network composed of four switches. There are 10 outputs to the system which are sent to the ten stages in the optical system to drive the liquid crystal cells.

The outputs from the counting circuit were passed to an exclusive NOR network to account for the polarization changes, which are cumulative, within the optical system (Chapter 4.5). After exclusive NOR correction, the outputs are sent to an analog multiplexer (digital/analog switch). The multiplexer will pass the square wave, from the op amp oscillator

(Section 7.5.1) to the liquid crystal cell, when the input is logic 1 and remove the signal when the input is logic 0.

7.5.5 System Operation

The switching network used to control the counting circuit discussed in section 7.5.3 is composed of 4 switches that control the system. Switch 1 controls the systems mode of operation which includes scanning or manual entry of output direction by passing a logic 1 or logic 0 to the load pin of the counter. The system is capable of selecting an initial direction or starting point by setting switch 1 off to enter the direction then setting switch 1 on to start counting. Switch 2 is a double-pole double-throw switch used to control the scanning direction by controlling the count-up and count-down pins within the counter and preventing logic "1" simultaneously passed to both pins. Switch 3 is used to reset the system for entering a new output direction or continue scanning from the initial position by sending logic "0" to the processer and counter. Switch 4 is used to increase the scan rate by having both counters simultaneously count by 1. Table 7.1 provides a summary of the logic used to control the circuits.

Table 7-1: A summary of the switching network which controls the digital system. Switch 3 resets the system by setting the counter outputs to 0 while the processor prompts the user to enter an output direction. Switch 2 is double-pole double-throw switch used to select the scanning direction. The label X implies "don't' care" which implies the input has no effect on the output.

CLEAR	LOAD	UP	DOWN	QO	Q1	Q2	…Q10	
1	X	X	X	0	0	0	0	SWITCH 3
0	0	X	X	P0	P1	P1	…P10	SWITCH 1
0	1	1	0	COUNT	UP			SWITCH 2
0	1	0	1	COUNT	DOWN			SWITCH 2

An enclosure for the digital system was assembled for system packaging, protection, and organization for easy use by the operator. The picture below (Figure 7.10) is a photo of the electronic control system used to control the optical system.

Figure 7-10: The digital system used to control the optical system. The electronics are assembled into an enclosure for protection and organization.

7.6 Conclusion

In conclusion, the construction of the optical system and electronic systems, for system testing and control, was presented. An optical system composed of ten sequential stages was assembled. The system adjustments include angular changes to the system layout and changing the angle of a stage by inserting shims underneath the spacer to minimize vertical offsets. For the last two stages, liquid crystal cells with a larger active area and smaller size were used to minimize the total displacement entering the last stage.

The switching system was used to test individual stages during system assembly and view all output directions by driving the cells in half-voltage operation.

The electronic system for controlling the optical system is capable of scanning in two directions, selecting an output direction and start scanning, select a different direction, start scanning from the first position, and increase the scan rate by skipping directions. The system scan rate was 40 Hz and the total time to scan the range (1024 directions) took 25.6 seconds. The results of the linear array are presented in the next chapter.

CHAPTER 8 RESULTS OF THE LINEAR ARRAY

The results of the linear system constructed in Chapter 7 are discussed and compared to theory discussed in chapter 5. The total displacement, number of resolved locations, etc. are presented.

8.1 Cumulative Effects

The systems resolution was set to 240 μrad which was somewhat below the nominal resolution of 268 μrad. The angular separation for the first and final stage was set to 250 μrad and 128 mrad respectively. The required width, D, of the last stage was observed to be 9.5 mm, slightly larger than the theoretical estimate of 8.7 mm [31]. Table 8.1 is a summary comparing the measured results to the theoretical limits.

Table 8-1: A summary and comparison of the required deflector width, beam diameter, and resolution for the linear system compared to theory.

	Theoretical Limits		
Path Length (L) = 22.2 mm	Optimum	Exp. Setup	Measured
Beam Diameter (d)	4.3 mm	3 mm	3.2 mm
Resolution (θ)	188 μrad	268 μrad	240 μrad
Deflector width	8.3 mm	8.7 mm	9.5 mm

8.2 Number of Spots

Deflection was achieved over the full range of $2^{10} = 1024$ angular positions, or about 24.7 cm at a distance of 1 meter. Although the deflected beams had low intensity halos arising from imperfections in the optical surfaces, they were well focused and evenly spaced (Figure 8.1). The vertical offsets are due to the split photodiode was unable measure the vertical angles during assembly of the mirror angles and vertical angles introduced during system assembly from fixing the stages to spacers. It's possible to increase the number of resolved locations by reducing the separation between the stages. The number of unwanted reflections can be reduced by applying

an anti-reflection coating to the liquid crystal cells. The intensity halos can be reduced further by improving the polishing procedure, of the polarizing beam splitter, which is performed after removing the anti-reflection coating from the faces used for mirror angle assembly.

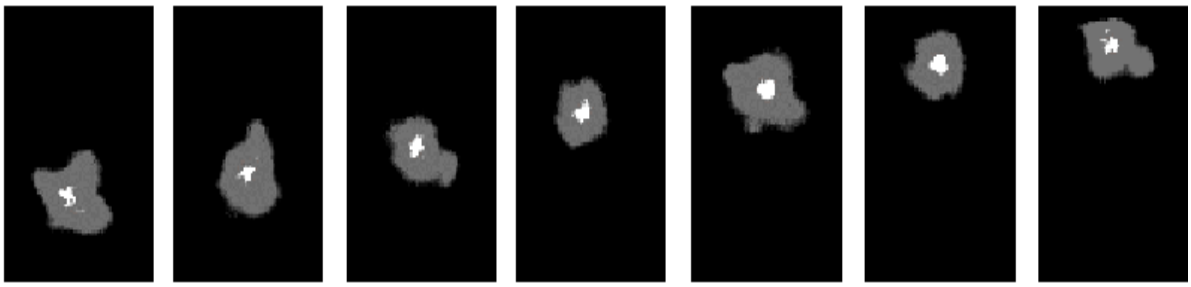

Figure 8-1: Photographs of 7 consecutive deflected beams, near the center of the deflection range. Each beam is surrounded by a low intensity halo arising from imperfections in the optical surfaces it encountered. Although the beams took very different paths through the optical system, and therefore suffered different aberrations, the bright central regions are well separated and evenly spaced.

8.3 Response Time

The response time of the liquid crystal cells was about 20 ms. Individual beam positions were selected manually from a digital keyboard, or the beams were scanned sequentially at a frequency of about 40 Hz. A time required to scan the angular range was approximately 26 seconds. The scan rate can be increased further by obtaining liquid crystal material with a faster response time.

CHAPTER 9 EXTENSION TO 2-D ARRAY

The previous chapters discussed a digital deflector that scans, or deflects, a laser beam in a line (1-D). In this chapter, the research is extended so that the laser beam can be deflected, or scanned, in two dimensions. The optical system is controlled using liquid crystal cells.

9.1 Need for Out of Plane Accuracy

The angular displacement between two beams leaving each stage is determined by the stages internal geometry and is fixed. It doesn't depend on the exact orientation of each stage. However, the average deflection does depend on stage orientation. As discussed in Chapter 7, the stages were glued to their supports. Variations in the thickness of the glue layer led to angular offsets, producing vertical displacements in the deflected beam (Figure 7.4). Those variations were considered acceptable in a linear deflector, since they didn't affect the deflection in the desired direction. However for a two dimensional deflector they must minimized, since they are equivalent to extraneous deflections in the orthogonal direction.

9.1.1 Added Adjustment Screws at Each Beam Splitter Stage

A miniature tilting table was designed and constructed to correct for any misalignment in orientation of the stage (Figure 9.1). The size of the table, 3/8 inch square, is slightly less than the 1 cm square beam splitters used in the optical stages. The table utilizes pairs of 2-56 screws at opposite diagonal corners. One pair is screwed into the upper, or tilting part of the stage and is in tension. The other pair of screws pass through the threaded holes in the table's support, and push against opposing indents in the upper or table part. These screws protrude slightly from the support. Titling about either diagonal is accomplished by loosening one screw and tightening the other screw of the diagonal.

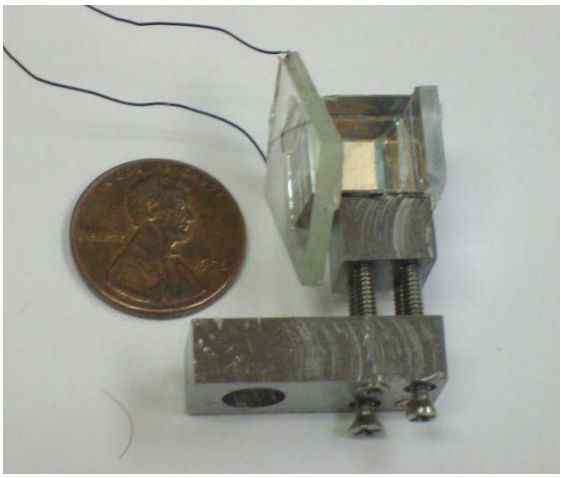

Figure 9-1: Miniature tilting table used for fine angular adjustments of each stage.

9.2 Three Dimensional Layouts of Stages

The horizontal and vertical deflections need to be interleaved which produces a complex three dimensional path. Figure 9.2 is a mechanical sketch of the deflection system, and Figure 9.3 is a photograph of the completed mechanical system before any of the optical components have been added.

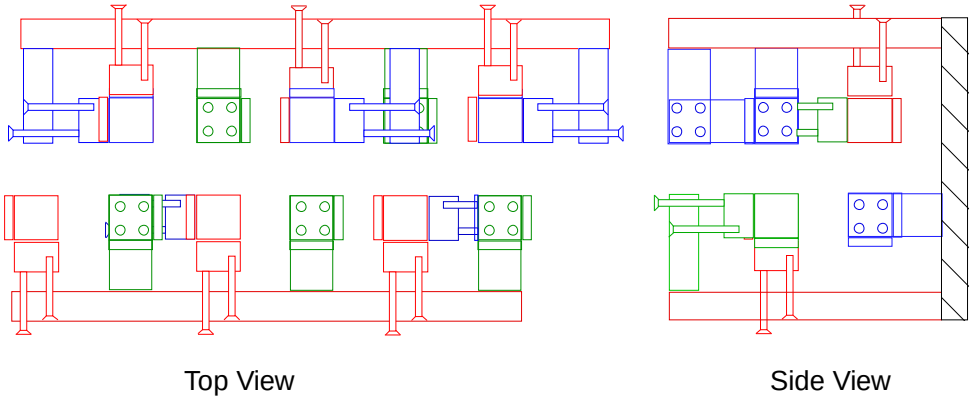

Figure 9-2: Mechanical drawing of the 16 stage layout used for 2-dimensional scanning. Color coding is used to help identify specific stages.

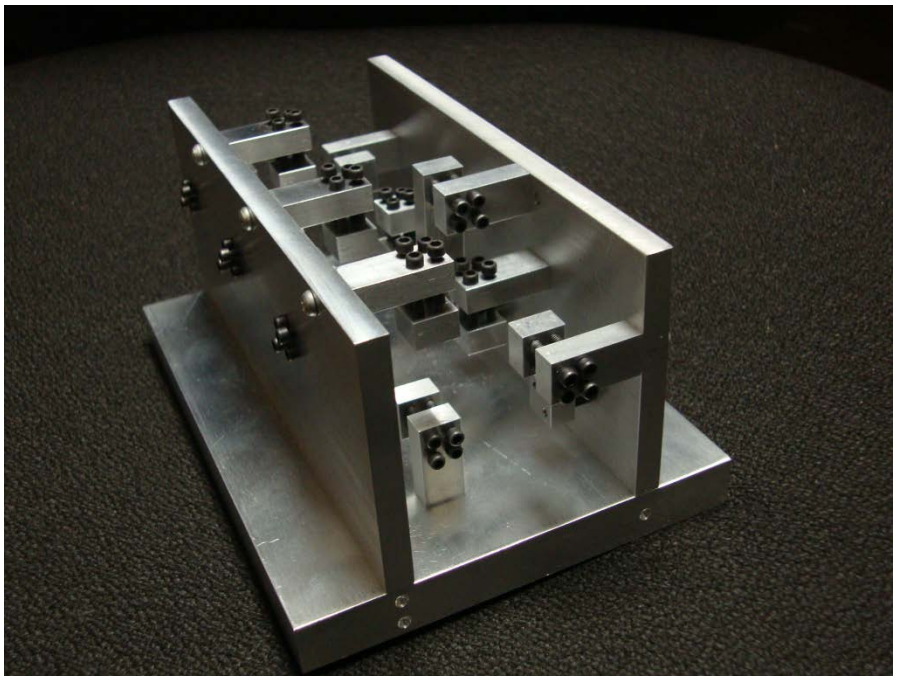

Figure 9-3: Photograph of the completed mechanical system, before introduction of the optical components.

9.3 Stage Construction

For linear deflections, the angular separation between two beams was measured using a split photo diode fixed on a digital caliper which was discussed in Chapter 5. For the two dimensional deflector the position of each beam needs to be measured in the vertical as well as the horizontal position. This was accomplished by replacing the split photo diode with a quadrant detector.

9.3.1 System Design

The quadrant detector was purchased from Edmund Optics. The quadrant detector consists of four photo detectors separated by a small distance and an active area of 2 x 2 mm^2. The four detectors correspond to four quadrants and four currents based on the position of the beam.

A beam centered on the quadrant detector will generate four equal currents in the four quadrants. If the beam deviates from the center, vertically or horizontally, the current generated by each quadrant will change. Figure 9.4 is a sketch of a quadrant detector.

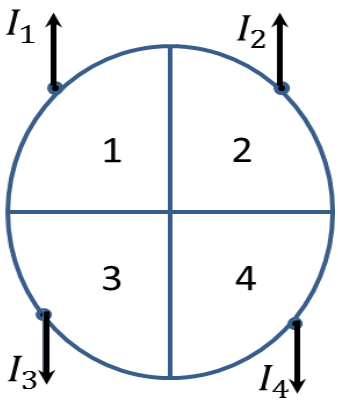

Figure 9-4: Sketch of a quadrant detector. A beam centered with respect to the quadrant detector will generate four equal currents from each detector.

For small angles, the horizontal and vertical displacements (Figure 9-5) with respect to the center of the quadrant detector are determined by the following:

$$dx = x \approx (I_2 + I_4) - (I_1 + I_3) \quad 9.1$$

$$dy = y \approx (I_1 + I_2) - (I_3 + I_4) \quad 9.2$$

9.3.2 Experimental Setup

The apparatus for measuring vertical and horizontal displacements contains the quadrant detector and electronics on the digital caliper. The electronics inputs are the four currents, generated from the quadrant detector, and the output is two voltages which correspond to the x-coordinate and y-coordinate respectively.

The electronics are composed of three stages. The first stage converts the four currents generated from the quadrant detector into four voltages. The second stage is composed of two differential amplifiers.

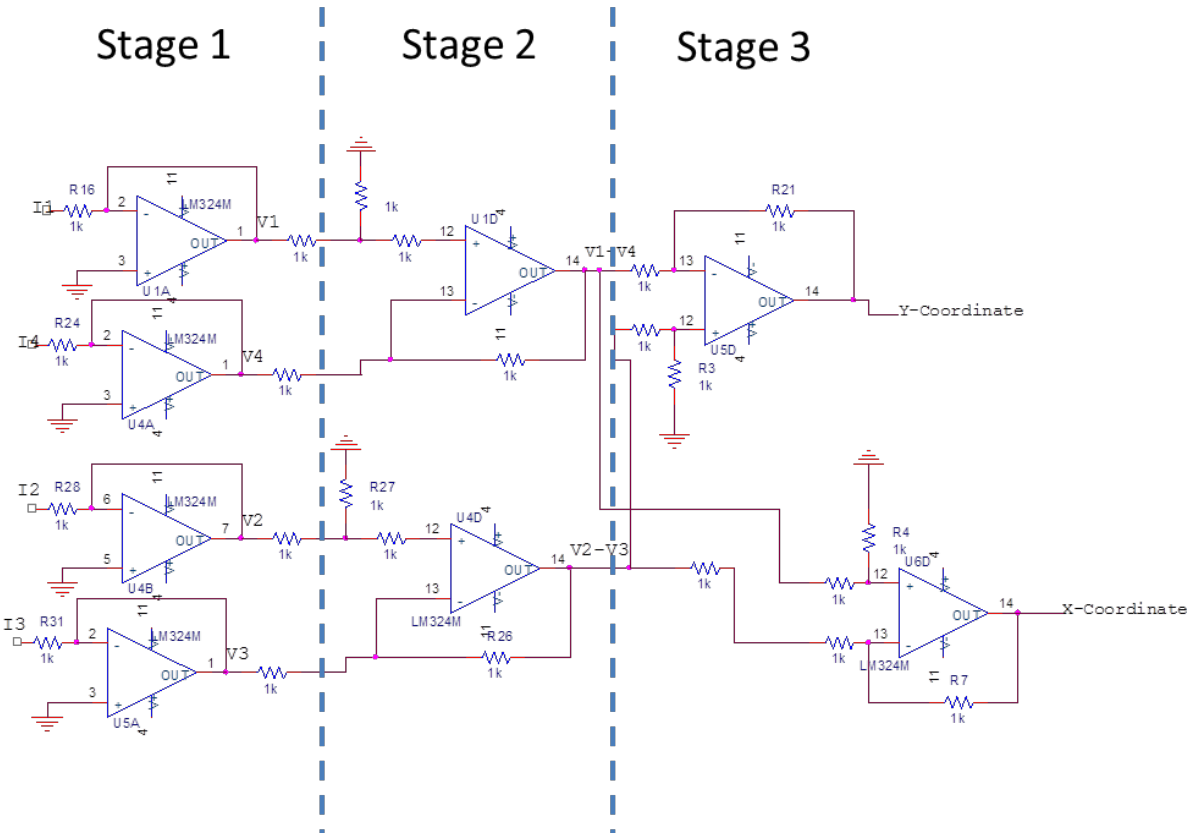

Figure 9-5: Schematic for the electronics interfaced with the quadrant detector. The electronics is composed of three stages. The inputs are the four currents while the output voltages consist of the x-coordinate and y-coordinate respectively. The output is sent to an oscilloscope.

The first differential amplifier takes the difference in voltage between the first and fourth quadrant while the second differential amplifier takes the difference in voltage between the second and third quadrant. The third stage consist of two differential amplifiers and the output consist of two voltages which correspond to the x and y coordinate.

The outputs, from the third stage, are sent to an oscilloscope. The scope is set to X-Y mode; therefore, horizontal and vertical deviations from the center of the photo detector correspond to different voltages hence different positions on the oscilloscope.

The quadrant detector, electronics, and scope setup was assembled.. The voltages scales, for the x and y coordinates, are identical and are set to 10 mV/per division. The quadrant

detector and associated electronics are mounted on a digital caliper. Initially, the beam was placed in the center of the quadrant detector. Next, minute displacements on the caliber were performed while measuring the voltage on the oscilloscope. A voltage change in 10 mV corresponds to a 50 um linear displacement in the vertical and/or horizontal direction.

9.4 Preliminary Results

The stages with the smallest angles were assembled first followed by the larger angular displacements. Offsets associated with assembly tolerances during stage construction caused spots to overlap. However, the larger angles were successful in system assembly for a smaller incident beam width. In this the preliminary results for optical system and electronics system are discussed.

9.4.1 Optical System

The incident source is a HeNe laser with a parallel beam diameter set to 1 mm. Upon exiting the optical system, the output beams are focused by a 1 meter focal length lens.

9.4.1.1 Fine Angle Results

For smaller angles, the output beams brought to focus by a 1 meter away pass through a 10x microscope objective for observation, inspection, and alignment using the tilty tables. The output beams after the first, second, and third stages are shown in Figure 9.6a-c.

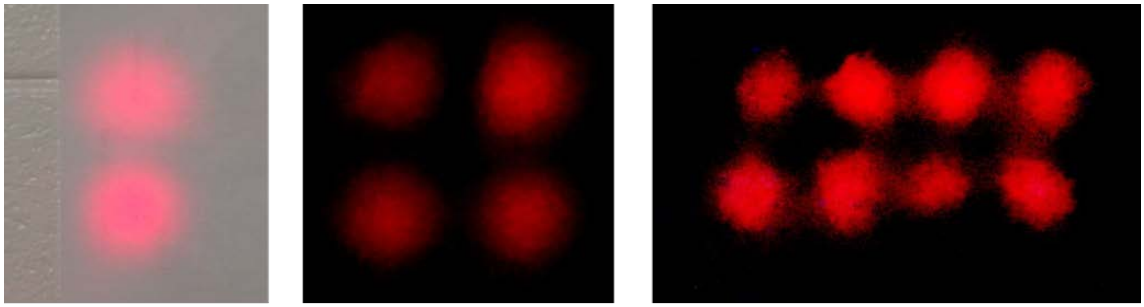

Figure 9-6: System output after assembling the a.) first stage, b.) second stage, and c.) third stage.

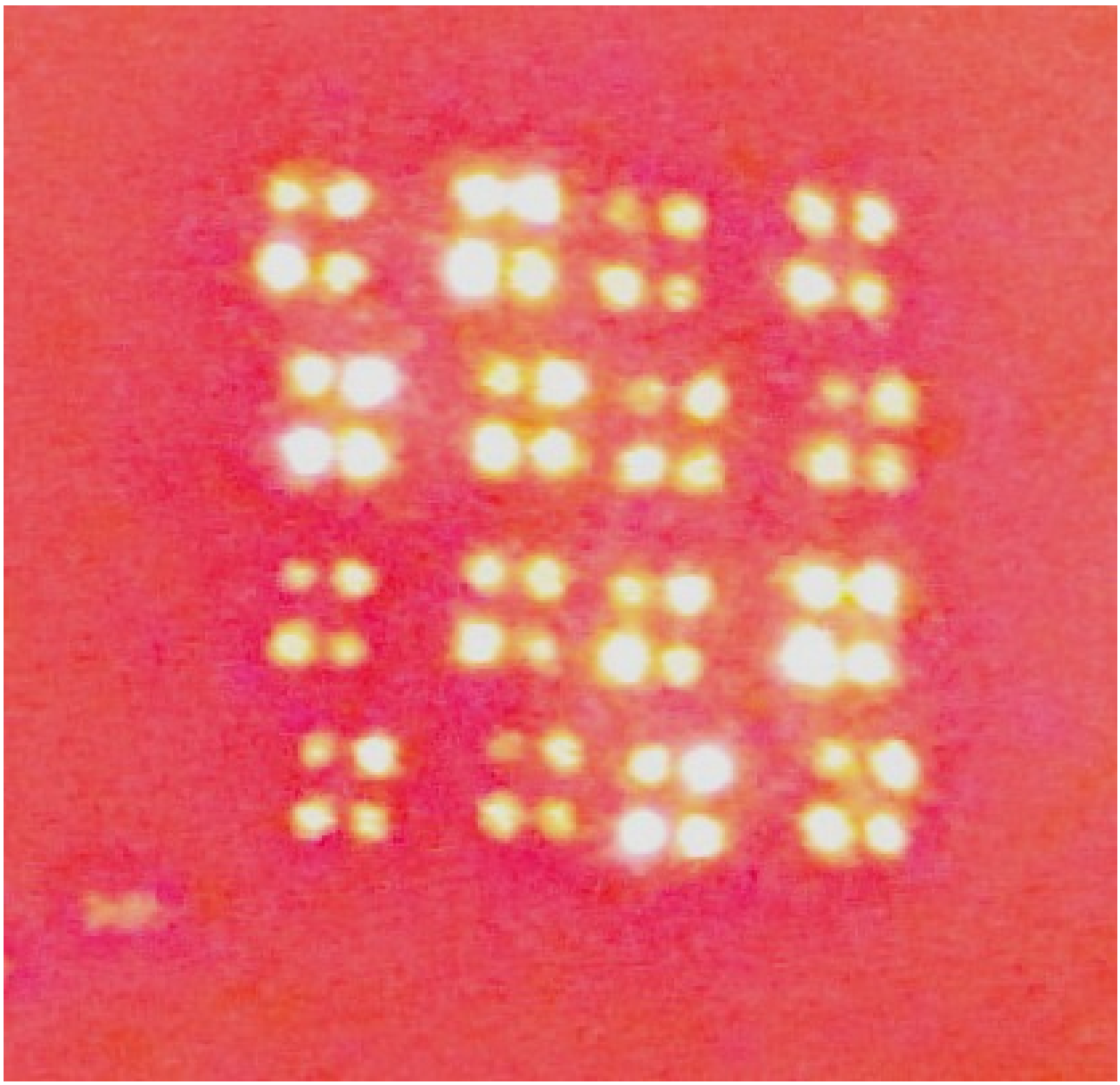

Figure 9-7: Output beams after passing through six stages.

9.5 Results

The systems resolution was set to 0.80 µrad which was somewhat worse than the nominal resolution of 0.52 µrad. The angular separation for the first and final pair of stages was set to 4 µrad and 64 µrad respectively. The optical path length between adjacent stages is 23.3 mm. The required width and height, D_x and D_y, of the last stage was observed to be 7.5 mm and 9.5 mm, slightly larger than the theoretical estimate of 8.74 mm and 6.35 mm. The power transmission

was observed to be 1.8% which was smaller than the theoretical estimate of 8%. Table 9.1 is a summary comparing the measured results to the theoretical limits.

Table 9-1: A summary and comparison of the required deflector width, beam diameter, and resolution for the two dimensional system compared to theory.

	Optimum	Exp. Setup	Measured
Beam Diameter (d)	1.09 mm	1 mm	1 mm
Resolution (θ)	0.73 µrad	0.80 µrad	0.80 µrad
Deflector Area ($\mathbf{D_y}$ x $\mathbf{D_x}$) mm	8.82 x 5.93	8.23 x 5.34	8.90 x 7.5

9.5.1 Number of Spots

Deflection was achieved over the full range, in both directions, of 2^5 x 2^5 = 32 x 32 angular positions. At a distance of 368 mm the ranges in the vertical and horizontal directions were 42 mm and 45 mm respectively.

Although the deflected beams had low intensity halos arising from imperfections in the optical surfaces, they were focused (Figure 9.8 and Figure 9.9) in full voltage operation with cross-talk. However the spots were not well focused in half-voltage operation due the problems with the liquid crystal cell at the last stage (Figure 9.10). It's possible to increase the number of resolved locations by reducing the separation between the stages and reducing the cross-talk at the last stage by replacing the liquid crystal cell. The number of unwanted reflections can be reduced by applying an anti-reflection coating to the liquid crystal cells. The intensity halos can be reduced further by improving the polishing procedure, of the polarizing beam splitter, which is performed after removing the anti-reflection coating from the faces used for mirror angle assembly.

9.6 Conclusion

The arrangement of stages for 2-D steering required a complex arrangement compared to the linear system. The stages are fixed on miniature-tilting tables to correct misalignment in stage orientation. A split photodiode was replaced with a quadrant detector to measure angular displacements in the horizontal and vertical directions. The liquid crystal cells for the last three stages required larger active area. Five vertical and five horizontal stages were assembled and a 32 x 32 array of spots was demonstrated. Additional stages could be added to increase the number of output directions with an improved setup to build stages. The digital algorithm to control the setup was verified for the six stage system. The response time of the system was 20 ms which can improve with faster polarization devices like Kerr or Pocket cell while tradeoff is size and cost.

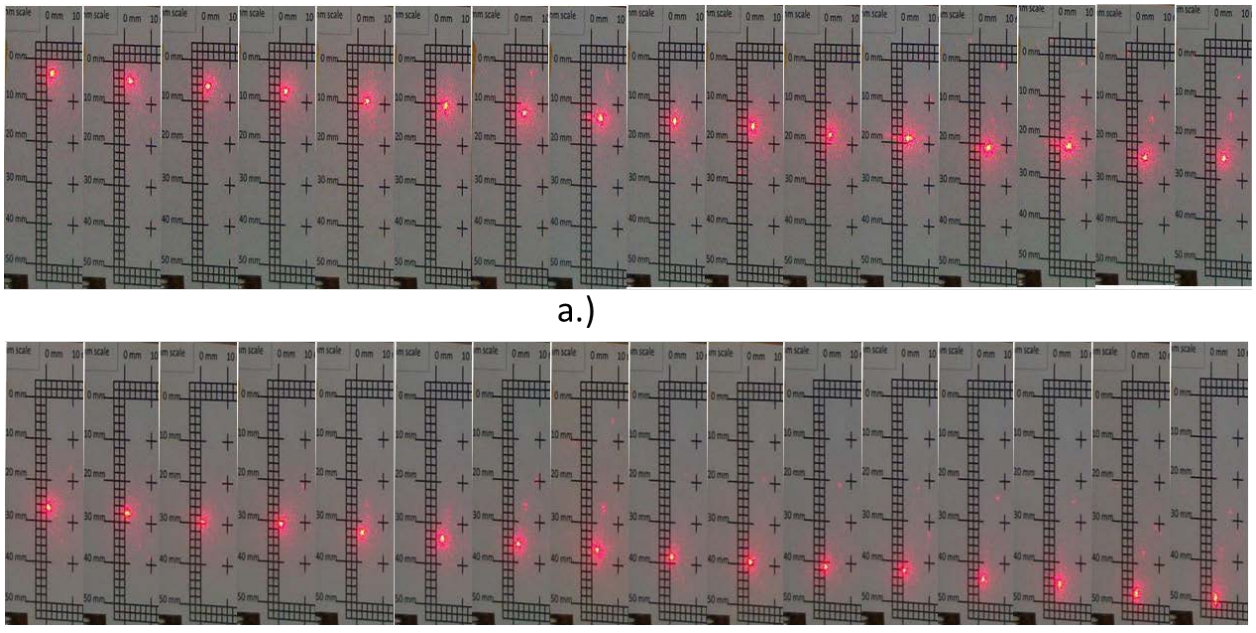

Figure 9-8: Photograph of the 1st vertical line at the output of the 2D system (32 positions). The range is 42 mm at a distance of 368 mm and the width of the focused beam was approximately 2 mm.

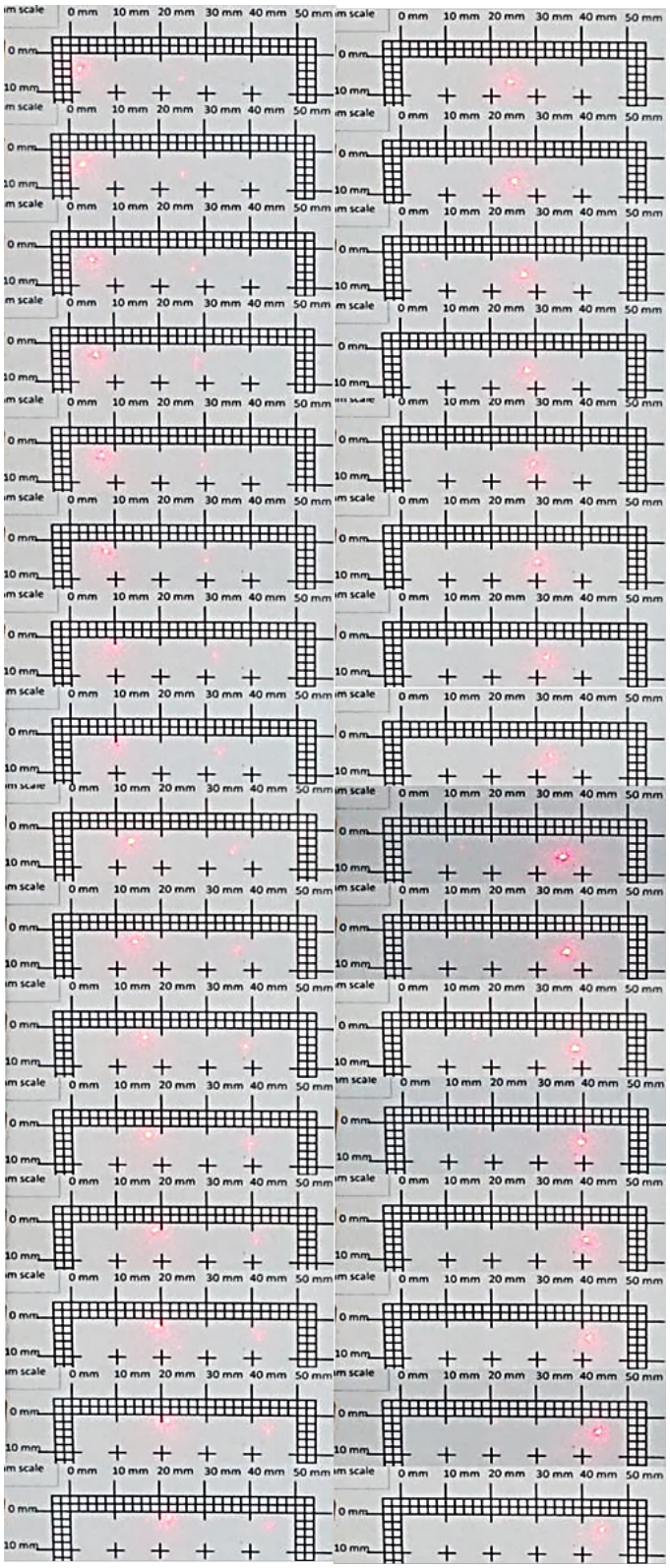

Figure 9-9: Photograph of the 32 positions in the first horizontal line. The range is 45 mm at a distance of 368 mm with a beam width of approximately 1 mm.

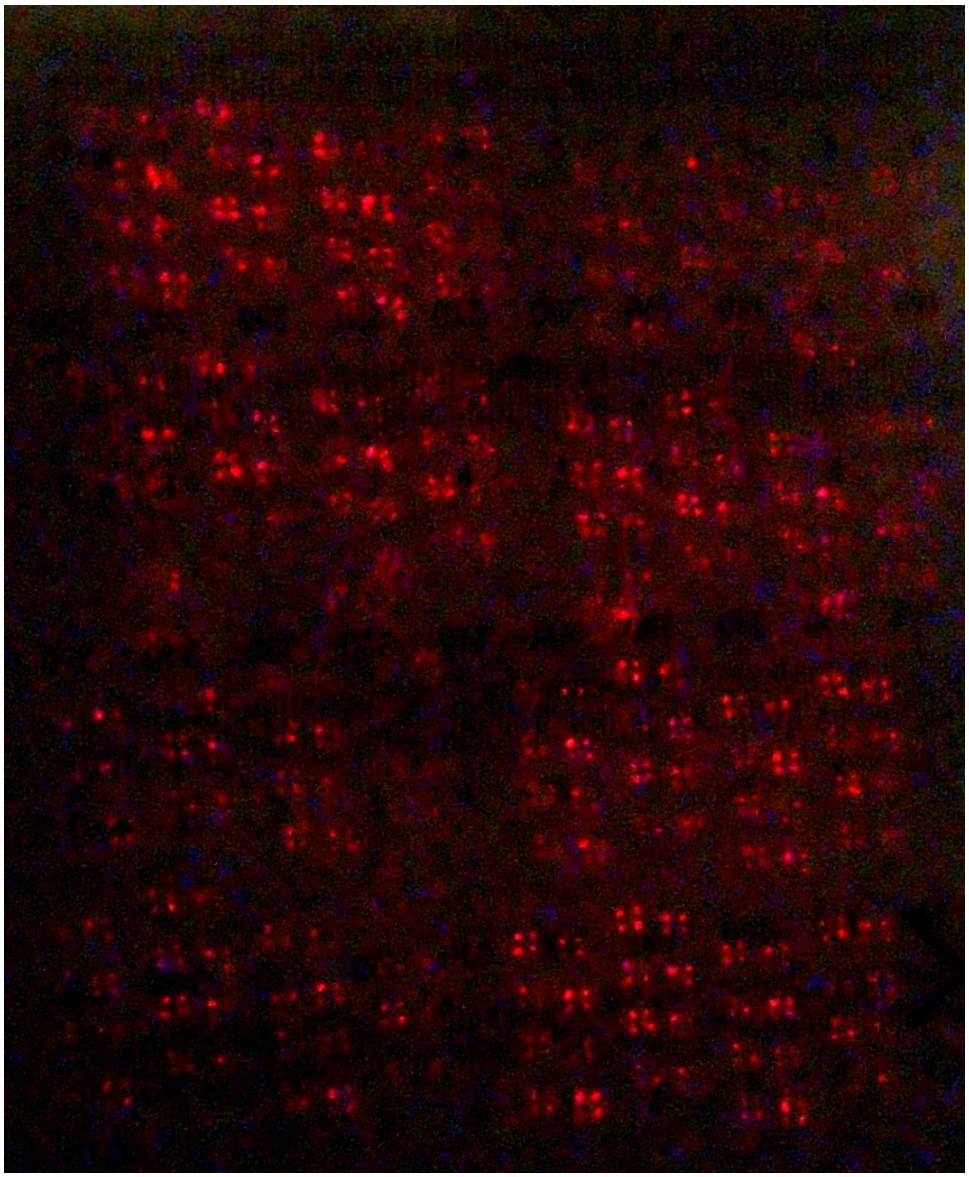

Figure 9-10: Half-voltage operation: The spots were brought to a focus at a distance of 368 mm with a beam diameter of approximately 1 mm.

CHAPTER 10 SUMMARY

A novel digital non-mechanical beam steering device, capable of steering in a line and plane, was demonstrated. The combination of a voltage controlled polarizer and a deflector angle was used to change the direction of a beam of light by controlling the polarization. The deflector angle consisted of a polarizing beam splitter used in double pass operation in which the angular separation was set by the angle of mirrors. The voltage controlled polarizer was a twisted nematic liquid crystal cell.

A system was composed of several cascaded stages. The range, and maximum angular separation, was limited by the extinction ratio of the polarizing beam splitter cubes. The number of output directions increased by a factor of 2 at each stage. The incident beam and all displacements must fit within the last stage. The optical path length is predominately set by the size of the polarizing beam splitter cubes. The response time for the system is restricted to the response time of the liquid crystal cells. In this chapter, brief reviews of the assembled systems are discussed, and a comparison is made to the state of the art and recommendations for future work.

The angular separations between the beams are set by mirror angles and are independent of the wavelength.

Digital circuits were implemented to control the output direction. By keeping track of polarization changes throughout the system, we found XNOR correction between a binary input and the liquid crystal cells was required to select directions. An electronic system for entering an output direction or scanning in both directions was designed and implemented by Southern University.

10.1 Linear Beam Steering System

A linear beam steering system has been assembled in which a HeNe laser beam passes through ten sequential stages. The incident source was expanded to a parallel beam with a diameter of 3.2 mm. The path length from one stage to the next is 22.2 mm and the minimum angle was set to 248 μrad.

The beam splitter cubes were 10 mm on a side. Except for the last two stages, the active area was set by available liquid crystal cells to a 5 mm diamond shape. A full 10 mm square liquid crystal cell was used at the 9^{th} and 10^{th} stage. 1024 deflected beams were well resolved.

The liquid crystal cells have a measured response time was 20 ms. The linear system scanned at a rate of 40 Hz. Therefore, a time of 25.6 seconds was required to scan the entire line or sequentially scan all positions. .

10.2 2-D Array

Five vertical and five horizontal stages were assembled and a 32 x 32 array of spots was demonstrated. Based off the study conducted from the linear array, modifications were required for the 2-D beam steering setup. Adjustment screws were added at each beam splitter stage to prevent periodic offsets. The system for measuring mirror angles was modified, by using a quadrant detector, for accurate horizontal and vertical displacements. However the accuracy of mirror mount holding the L-bracket restricted the accuracy of angular separations in the vertical direction.

10.3 Comparison to the "State of the Art"

The systems discussed were able to point in one direction by driving the liquid crystal cells in full voltage operation or several directions by driving the liquid crystal cells in half-voltage operation. The response time for changing the beam of light's direction is limited by the relaxation time of the liquid crystal material. Replacing the liquid crystal cells with Pockel or

Kerr cells can improve the response time at the expense of size and cost of the system. Mechanical beam systems are not able to point in several directions at the same time.

10.4 Recommendation for future work

This topic can be extended to a thorough theoretical model of the cross-talk as function of input angles and switching speed of the liquid crystal cell and the polarizing beam splitter. Additional topic extensions include combining liquid crystal cell polarization gratings with our methods to expand the maximum angle and scanning range.

REFERENCES

1. High Speed Two Axis Gimbal, General Dynamics, http://www.gd-imaging.com

2. Pollshuk A., Pelded U., Missim M., Golub M., Arnon S., Wide-Range, high-resolution optical steering device; Optical Engineering, Vol. 45 No 9, Sept. 2006.

3. Beam Steering Using Liquid Crystals; Boulder Nonlinear Systems, Inc.; May 2001

4. DeSandre L., Gruniesen M., Rotge J., Dymale R., Lubin D.; Phased Array Diffractive Wavefront Control System for Continual Agile Beam Steering and Tracking; Proceedings of SPIE; Vol. 5553, Pages 83-101, 2004

5. Tabiryan, N.V., Nersisyan S.R.; Large-angle beam steering using all-optical liquid crystal spatial light modulators; Applied Physics Letters; Vol. 84, Num 25, June 2004.

6. Tuantranont, A., Bright V.M., Zhang B.J., Zhang W., Neff J.A., Lee Y.C.; Optical beam steering using Mems-controllable microlens array; Sensors and Actuators A; Vol. 91, 363-372, 2001.

7. Karl Lambrecht Corporation, 4204 N. Lincoln Ave. Chicago IL 60618, Calcite Wollaston prism Modal No. MW2A-10-5, catalog description at www.klccgo.com

8. Feldman M., El-Amawy A., Srivastava A., Vaidyanathan R.; Adjustable Wollaston-like prisms; Review of Scientific Instruments, Vol. 77, 2006

9. Qingkun, Z., et al. (2008). Design of Fast Steering Mirror systems for precision laser beams steering. Robotic and Sensors Environments, 2008. ROSE 2008Refai, H. H., et al. (2007).

10. "Digital micromirror device for optical scanning applications." Optical Engineering **46**(8): 085401-085401.

11. C. Schwarze, R. V., D. Carlson, E. Schundler, T. Evans and J. Engel (Sept 2005). Risley-Prism Based Compact Laser Beam Steering for IRCM, Laser Communications, and Laser Radar, Critical Technology.

12. Schwarze, C. A NEW LOOK AT RISLEY PRISMS. Photonic Spectra**:** 5. (2006).

13. Sánchez, M. G., David (2006). Control laws for a three-element Risley prism optical beam pointer. Free-Space Laser Communications VI, SPIE.

14. Chen, C. B. (2007). "Beam steering and pointing with counter-rotating grisms", *Proc. SPIE* 6714, Adaptive Coded Aperture Imaging and Non-Imaging Sensors, 671409.

15. Yang, Y. (2008). "Analytic Solution of Free Space Optical Beam Steering Using Risley Prisms." Journal of Lightwave Technology **26**(21): 3576-3583.

16. Yu, F. T. S., et al. (2004). Refractive beam steering, SPIE. **5560:** 282-292.

17. McManamon, P. F., et al. (2009). "A Review of Phased Array Steering for Narrow-Band Electrooptical Systems." Proceedings of the IEEE **97**(6): 1078-1096.

18. N. V. Tabiryan and S. R. Nersisyan,"Large-angle beam steering using all-optical liquid crystal spatial light modulators",Appl. Phys. Lett. 84, 5145 (2004).

19. Roland E. Juhala and George Dube, *"Refractive Beam Steering"*, Proc. SPIE 5528, 282 (2004), DOI:10.1117/12.559865

20. Hamley, I., "INTRODUTION TO SOFT MATTER", John Wiley & Sons, 2000.

21. Kawamoto, H.; , "The history of liquid-crystal displays," *Proceedings of the IEEE* , vol.90, no.4, pp.460-500, Apr 2002.

22. Flynn Castles, Stephen M. Morris, Damian J. Gardiner, Qasim M. Malik, and Harry J. Coles,"*Ultra-fast-switching flexoelectric liquid-crystal display with high contrast*," J. Soc. Inf. Display 18, 128 (2010)

23. Vladimir G. Chigrinov, *"Liquid Crystal Applications in Photonics"*, Proc. SPIE 7232, 72320P (2009)

24. Saleh B.E.A., Teich M.C. (2007), "Fundamentals of Photonics" (2nd Edition), John Wiley & Sons, p 232-234.

25. Arines Justo, *"Impact of Liquid Crystal in Active and Adaptive Optics"*, Materials 2009, 2, 549-561.

26. Becker, W., et al., "Liquid Crystals for Active Matrix Displays", Merck Inc., www.merck.com

27. Instec Inc**.,** 5589 Arapahoe Ave. #208 Boulder, CO 80303, Liquid-Crystal Cells Model No. LC1-6.8, catalog description at www.instec.com

28. Kelly. S. and O'Neill, "Handbook of Advanced Electronic and Photonic Materials and Devices", Vol.7: Liquid Crystals, Display and Laser Materials, Academic Press, (2000) , ISBN 012-513757-5

29. Norland Products, 2540 Route 130, Suite 100, Cranbury, NJ 08512 Model No. NOA 68, catalog description at http://www.norlandprod.com/adhesives/noa%2068.html.

30. Parallex Inc., 599 Menlo Drive, Rocklin, CA 95765, Model No. BS2-IC, catalog description at http://www.parallax.com

31. From equation (2.17) a somewhat better choice of θ_1 would be 188 urad, corresponding to a 4.3 mm diameter beam and D = 8.3 rather than 8.7 mm**.**

32. D. Hebert, P. Cantu, C. Washington, O. Ajala, and M. Feldman, “High Capacity Digital Laser Beam Steering System”, Rev. Sci. Instrum. 82, 116101 (2011).

33. J. Larry Pezzaniti and R. Chipman, "Angular dependence of polarizing beam-splitter cubes," Appl. Opt. 33, 1916-1929 (1994).

34. Watson, E. A., et al. (1999). "Applications and requirements for nonmechanical beam steering in active electro-optic sensors." 216-225.

35. McManamon, P. F., et al. (1996). "Optical phased array technology." Proceedings of the IEEE **84**(2): 268-298.

36. McManamon, P. F. and E. A. Watson (2001). Design of optical phased array beam steering with limited dispersion. Aerospace Conference, 2001, IEEE Proceedings.

37. Shi, J., et al. (2004). "Switchable optical phased prism arrays for beam steering." 102-111.

38. Stockley, J. and S. Serati (2005). Multi-access laser terminal using liquid crystal beam steering. Aerospace Conference, 2005 IEEE.

39. Tholl, H. D. (2006). "Novel laser beam steering techniques." 639708-639708.

40. Kelly, J. (2007). Applications of Liquid Crystal Technology to Telecommunication Devices, Optical Society of America.

41. Jarrahi, M., et al. (2008). "Optical switching based on high-speed phased array optical beam steering." Applied Physics Letters **92**(1): 014106.

42. Xiaozhang, W., et al. (2010). Progress and analysis of the liquid crystal phased array technology in ladar. Laser Physics and Laser Technologies (RCSLPLT) and 2010 Academic Symposium on Optoelectronics Technology (ASOT), 2010 10th Russian-Chinese Symposium on.

43. Serati, S. and J. Stockley (2002). Advanced liquid crystal on silicon optical phased arrays. Aerospace Conference Proceedings, 2002. IEEE.

44. CASIX Inc, P.O. Box 1103 Fuzhou Fujian 350014, China, Narrowband Polarizing Beamsplitter model CBS0101-632.8 nm, catalog description at www.casix.com.

45. Saleh B.E.A., Teich M.C. (2007), “Fundamentals of Photonics” (2nd Edition), John Wiley & Sons, p 209-214.

46. L. Li and J. Dobrowolski, "Visible broadband, wide-angle,thin-film multilayer polarizing beam splitter," Appl. Opt. **35**, 2221-2225 (1996).

47. Quarter-Wave Plate, Anchor Optics (Catalog # 27341), http://www.anchoroptics.com

48. First-Surface Mirrors, Edmund Optics (Catalog #45517), http://www.edmundoptics.com

49. Liquid crystal material provided by Teledyne Scientific, Dr. Miland Mahajan

50. Ball bearing load ratings and lifetime calculations, NMB technology,

51. Quarter-Wave Plates (Retarder), Edmund Optics (Catalog #85-022), www.edmundoptics.com

52. Polarizing Beam Splitter Cube, Edmund Optics (Catalog #47-777), www.edmundoptics.com

APPENDIX A MEASUREMENT OF CROSS-TALK VS. ANGULAR ROTATION OF THE POLARIZING BEAM SPLITTER

The measured cross-talk in a polarizing beam splitter as the input angle deviates from the normal limits the maximum angular separation within a stage. Recall from Chapter 5.1 that rotating the polarizing beam splitter changes the angle of incidence, which increases the power of the unwanted polarization (cross-talk). For high extinction ratios (T_H/R_V) the cross talk is negligible. Cross talk (R_V) from rotating the polarizing beam splitter is an unavoidable, inherent property of the system, which limits the maximum steering angle.

An experiment was performed to test the power of the unwanted polarization (cross-talk) and extinction ratio as the incident angle increased. The experimental setup is shown in Figure A.1.

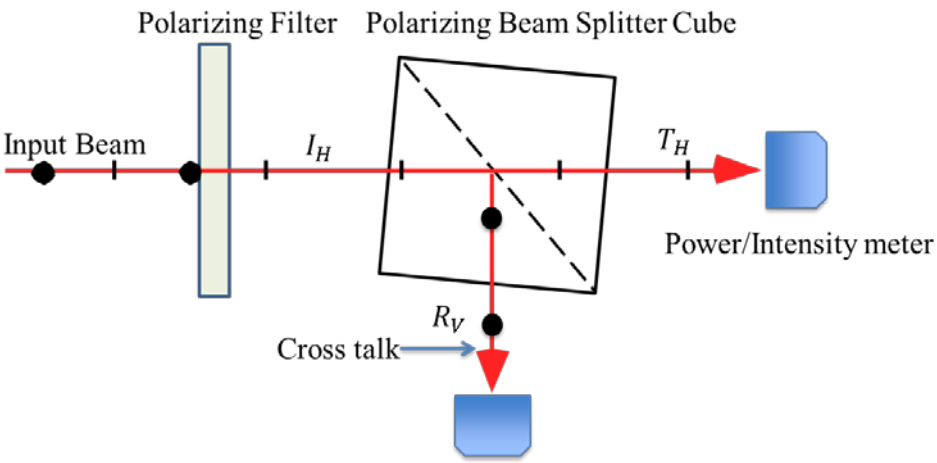

Figure A.1: Experimental layout to measure cross-talk and the incident angle increases.

The input beam is a HeNe laser which passes through a polarizing filter, to define the incident polarization, prior to entering the polarizing beam splitter. The polarizing beam splitter from CASIX was fixed on a goniometer to change the incident angle of the beam splitter [43]. Power measurements are taken at both output faces of the polarizing beam splitter for measuring the transmitted power (T_V) and reflected power (R_V).

The polarizing filter was set to only allow light from a HeNe laser vertically polarized to pass prior to entering the polarizing the beam splitter. The initial angle between the polarizing beam splitter and the incident source was set to 90 degrees. Next, the beam splitter was rotated while continuing to measure the power at both output faces of the polarizing beam splitter.

Results

The cross-talk which is the power of the reflected beam within the polarizing beam splitter, vs. the angular rotation of the polarizing beam splitter is shown in Figure A.2. The minimum reflected power (cross-talk) occurs when the angle of incidence is normal to the polarizing beam splitter ($\Theta_{PBS} = 0$).

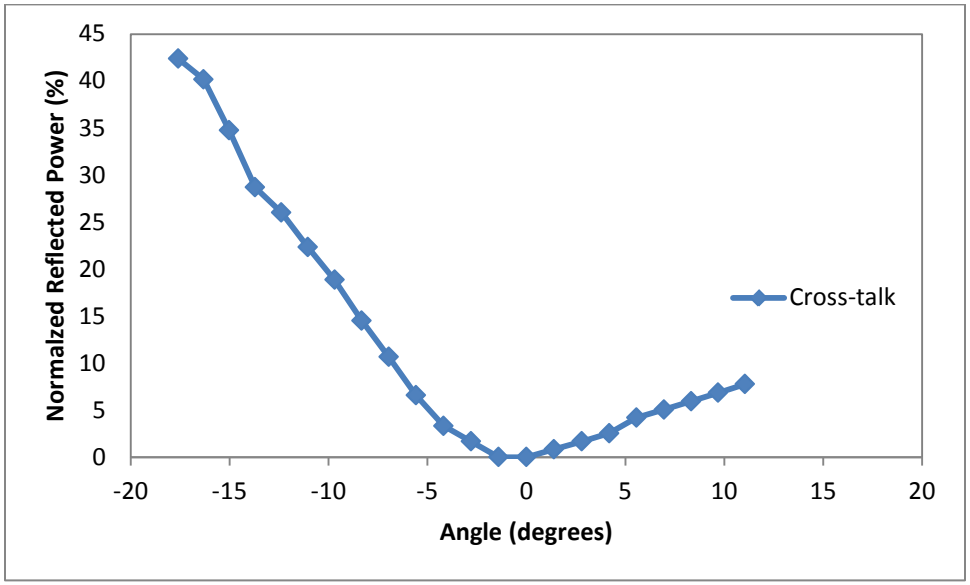

Figure A.2*:* Measurement of the reflected power (vertically polarized), cross-talk, as the angle of the polarizing beam splitter varies from normal incidence.

As the angular rotation of the polarizing beam splitter increases the power of the reflected (vertically polarized), un-wanted beam, increases. For rotation angles less than ±5 degrees the cross talk (reflected power) is small.

Similarly the power for the transmitted beam is high for small rotation angles (Figure A.3). For larger angular rotations, the power of the transmitted beam decreases while the power of the unwanted reflected beam (cross-talk) increases.

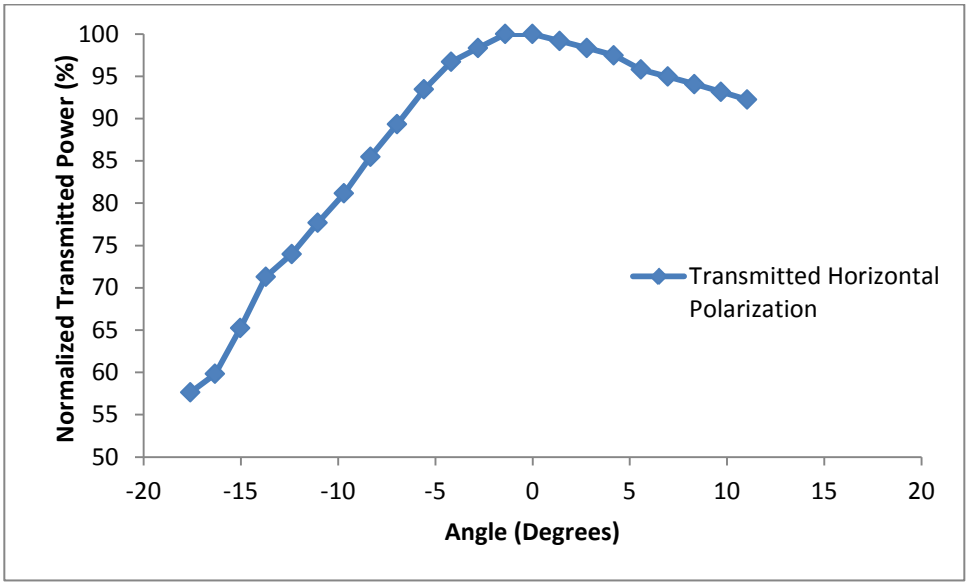

Figure A.3*:* Measurement of the transmitted beam (horizontally polarized) as the angle of the polarizing beam splitter varies from normal incidence.

The extinction ratio is very high when the incident beam is normal to the surface of the polarizing beam splitter. However the extinction ratio is reduced as the angle increases (Figure A.4).

The power of the unwanted polarization, cross talk, increases as the rotation angle of the polarizing beam splitter increases. However a rotation of the polarizing beam splitter is required to separate the output beams (at an angle). The maximum angle of deflection is limited due to the degradation of the extinction ratios of the polarizing beam splitters at larger angles. There are additional losses due to absorption and scattering as the angle increases.

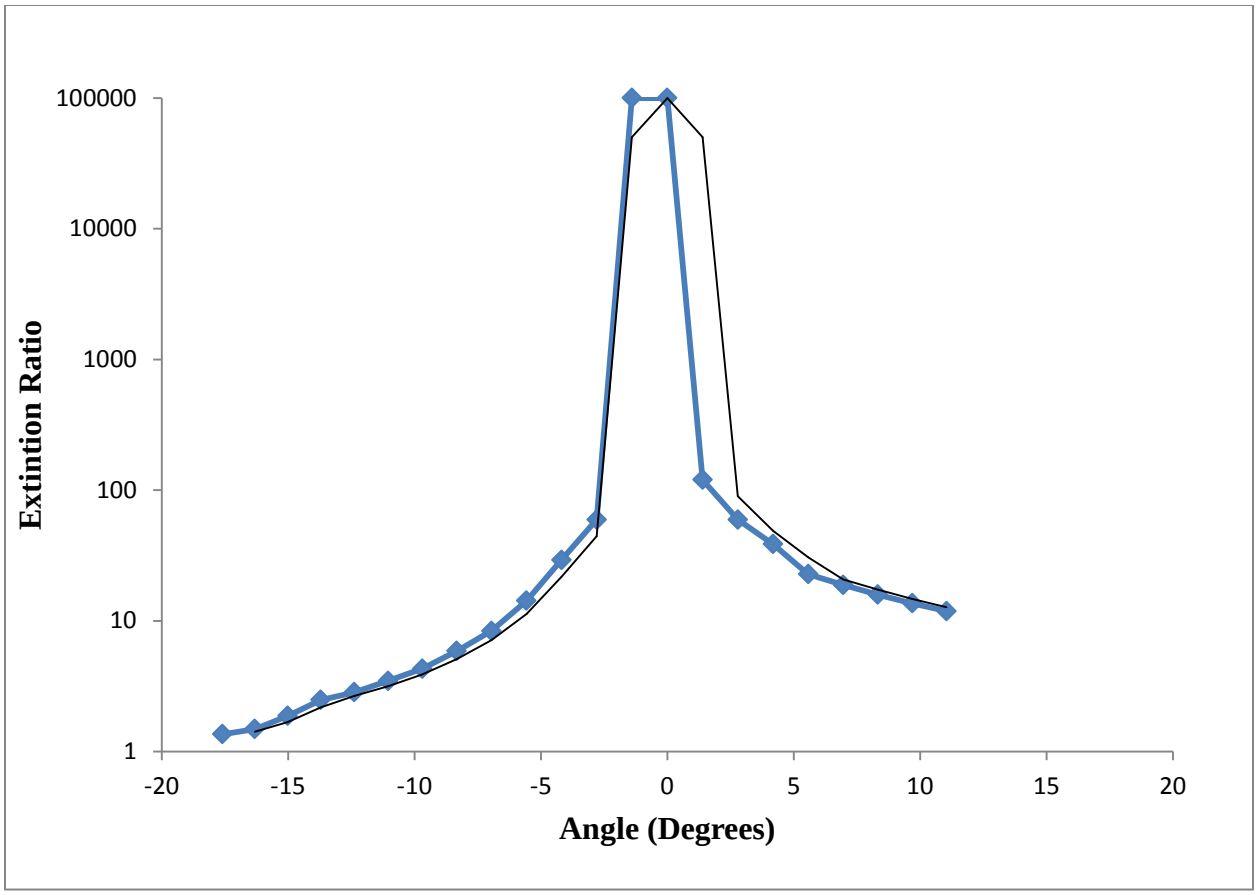

Figure A.4*:* Measurement of the extinction ratio as the angle of the polarizing beam splitter varies from normal incidence.

APPENDIX B DEVIATIONS OF THE 45-DEGREE ROTATION AND ACTIVE AREA OF THE LIQUID CRYSTAL CELL

An experiment was performed to test the cross-talk, of a polarizing beam splitter, as the angle of the liquid crystal cell deviates from a 45 from degree orientation angle and active area of the liquid crystal cell.

The setup is similar to the experiment for testing cross-talk in the polarizing beam splitter except the Liquid crystal cell is rotated instead of the polarizing beam splitter. The liquid crystal cell initial angle was set to 45-degrees then increases to 90-degress. The power of the unwanted-polarized beam and the transmitted beam was the measured.

Deviations from the liquid crystal cell active area

An experiment was performed to test the cross-talk of the liquid crystal cell, as a function of position, when the beam misses the active area. The LC cell is fixed at a 45-degree angle. The setup is similar to the experiment for testing cross-talk vs. angular rotation of the LC cell except a linear translation stage replaced the tool used to rotate the LC cell. The layout for the experiment is shown in Figure B.1. Small deviations from the active area have a small effect on the polarization efficiency.

The power loss was measured for 24 empty liquid crystal cells within the active area and outside the active area. The average power loss was larger within the active area of the liquid crystal cell was 15.12% and the average power loss outside the active area was 11.91%.

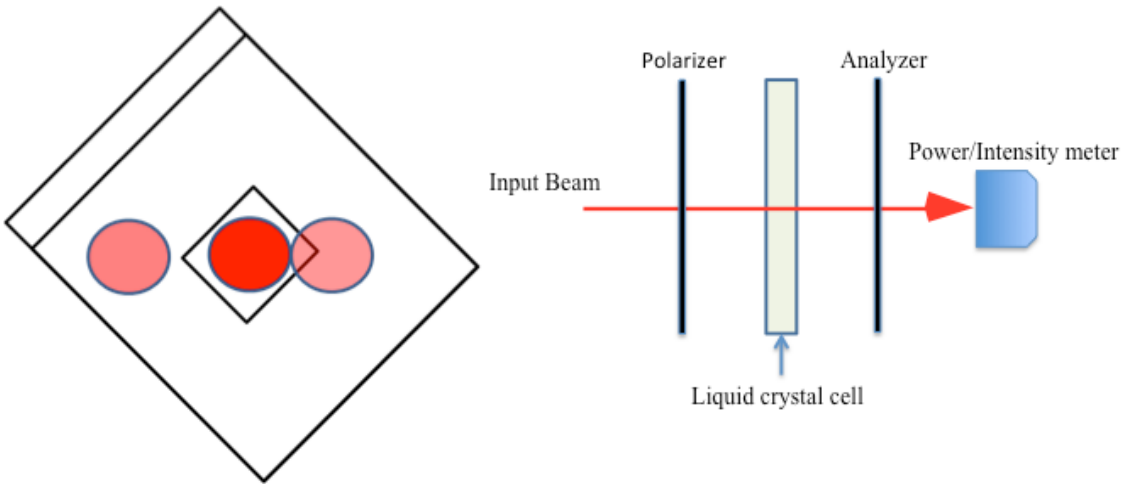

Figure B.1: Experimental setup to measure the cross-talk as the beam moves in the liquid crystal cell.

APPENDIX C MEASUREMENT OF LIQUID CRYSTAL CELL RESPONNSE TIME

This section discusses the measured response time of the liquid crystal cells from Instec and Teledyne. The measured response time for the liquid crystal cells from Instec was 20 ms while the measured response time for the cells from Teledyne was 12 ms.

The setup consists of an incident beam, polarizer, analyzer, function generator, switch, power meter, and an oscilloscope. The incident beam passes though the stage and an intensity meter is placed at the stages output to measure the power of beam. An oscilloscope is set to scope trace receives the power measurement from the intensity meter. Initially, a signal is sent to the liquid crystal cell, square wave a 1.5 V_{pp} at a frequency of 1kHz, then removed.

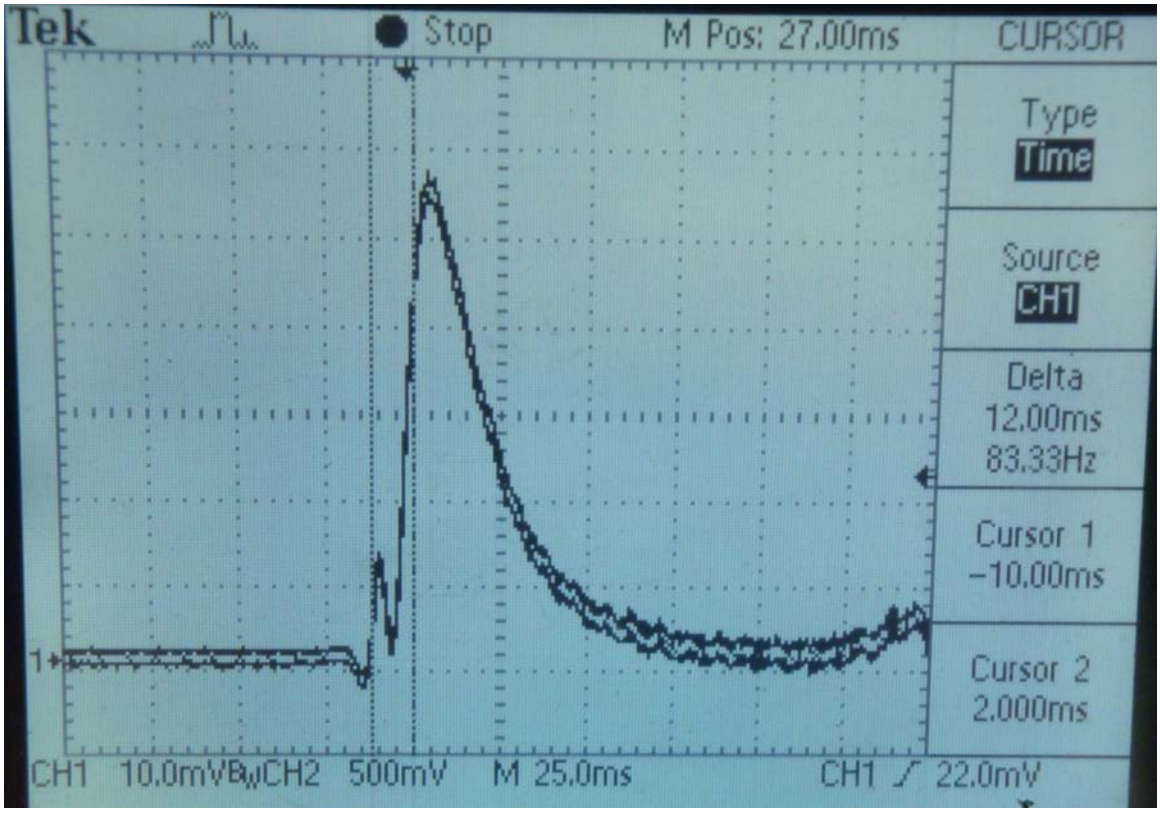

Figure C.1: The measured response time (relaxation time) of the liquid crystal material within the liquid crystal cell, provided by Teledyne, was approximately 12.0 ms.

APPENDIX D MEASUREMENT OF OUTPUT DIRECTIONS VS. POSITION

The figure below shows the output positions after seven stages, for the linear system.

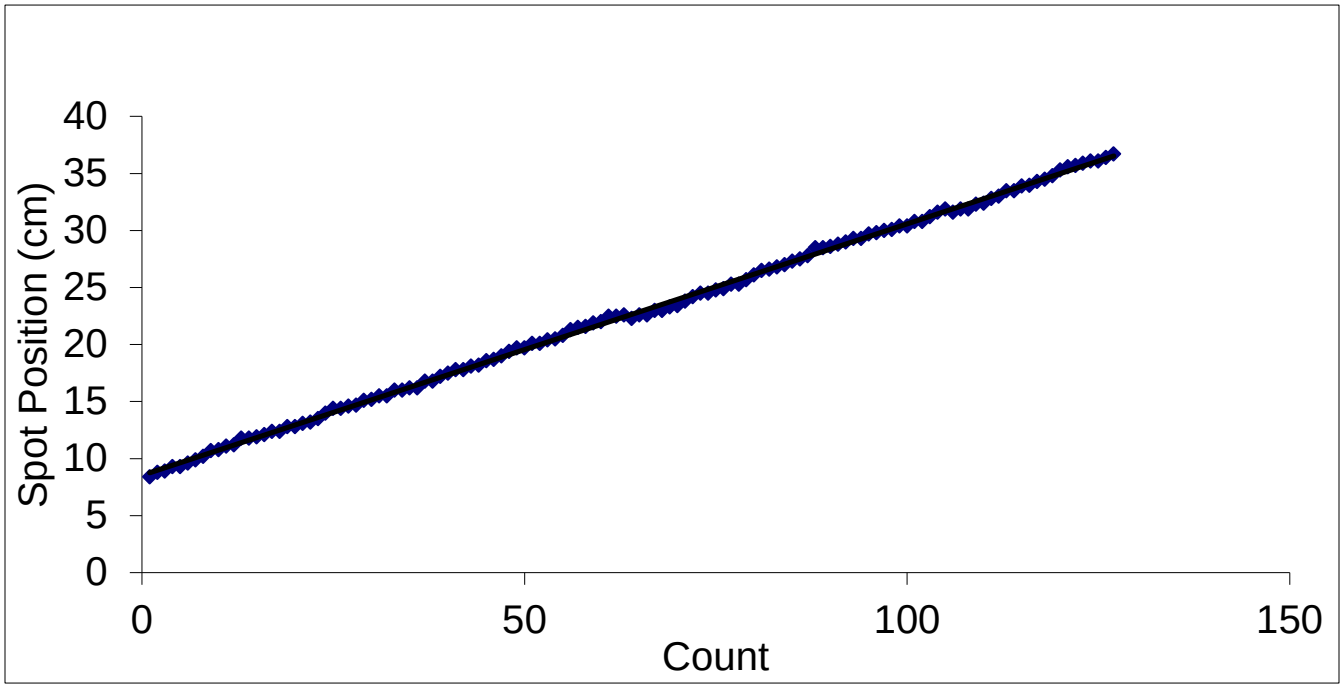

Figure D.1: Measurement of position vs. beam location after assembling seven stages.

APPENDIX E MAXIMIMUM DISPLACEMENT COMPARISION

This section will compare the maximum displacement at the last stage for a two dimensional system for interleaving vertical and horizontal stages vs. having all vertical stages followed by the horizontal stages (non-interleaving). A quick summary of the study is initially presented. Next a 20 stage system composed of ten vertical and horizontal stages is presented followed by the optimum design for the system. Similarly the maximum displacement for the 10 stage two dimensional system discussed in Chapter 9 is presented.

20 stage ideal

Using the small angle approximation Table E.1 contains a summary of interleaving vs. not interleaving vertical and horizontal stages within a 20 stage two dimensional system. The initial angular separation between stages is set to 0.25 urad and the optical path length between adjacent stages is 23.2 mm. The maximum displacement at the last stage when the vertical and horizontal stages are interleaved is 17.68 mm and 11.75 mm respectively. The maximum displacement at the last stage when the vertical and horizontal stages are not interleaved is 65.21 mm and 5.88 mm respectively.

Optimum/Ideal Design

The optimum/ideal design for the 20 stage two demsional system discussed in the previous section would have an optical path of 13 mm between adjacent stages, hence the maximum displacement, in both directions, for an interleaved and a non-interleaved system will decrease (Table E.2). The maximum displacement in the vertical and horizontal directions has reduced to 11.4 mm and 7.59 mm, when vertical and horizontal stages are interleaved which implies the volume of the polarizing beam splitter at the last stage must increase(Table 3). A practical length for a polarizing beam splitter cube for the last stage would be 15 mm.

Table E.1: The maximum displacement for 2D system using the small angle approximation. The initial angle is set to 0.25 μrad and the optical path length is 23.2 mm between adjacent stages. a.) The vertical and horizontal stages are interleaved. b.) The first ten stages consist of vertical angles followed by horizontal stages for the final ten stages.

Interleaved

Stage	Displacement (mm)	Stage	Displacement (mm)
y_1	0.1102	x_1	0.1044
y_2	0.1972	x_2	0.1856
y_3	0.348	x_3	0.3248
y_4	0.6032	x_4	0.5568
y_5	1.0208	x_5	0.928
y_6	1.6704	x_6	1.4848
y_7	2.5984	x_7	2.2272
y_8	3.712	x_8	2.9696
y_9	4.4544	x_9	2.9696
y_{10}	2.9696	x_{10}	
y	17.6842	x	11.7508

Non-Interleaved

Stage	Displacement (mm)	Stage	Displacement (mm)
y_1	0.1102	x_1	0.0522
y_2	0.2088	x_2	0.0928
y_3	0.3944	x_3	0.1624
y_4	0.7424	x_4	0.2784
y_5	1.392	x_5	0.464
y_6	2.5984	x_6	0.7424
y_7	4.8256	x_7	1.1136
y_8	8.9088	x_8	1.4848
y_9	16.3328	x_9	1.4848
y_{10}	29.696	x_{10}	0
y	65.21	x	5.88

The maximum displacement in the vertical and horizontal directions has reduced to 42.16 mm and 3.79 mm, when vertical and horizontal stages are not interleaved. However the volume of polarizing beam splitter cube is very large (45 to 50 mm^3) and expensive in a practical design.

Experimental Setup

This section briefly discusses the maximum displacement in the vertical and horizontal directions for the 10 stage, or five interleaved pairs, two dimensional system discussed in Chapter 9. The optical path between adjacent stages was set 23.3 mm while the initial angle was set to .4 urad. Table E.3 shows the the displacement at the final stage associated with each stages contribution to the maximum displacement and the maximum displacement in both

directions. In principle the maximum displacement in the vertical and horizontal directions is 7.70 mm and 4.83 mm respectively.

Table E.2: The optimum design for a two dimensional system containing ten vertical and ten horizontal stages. The initial angle is set to 0.25 urad and the optical path length between adjacent stages is 13 mm.

Interleaved

Stage	Displacement (mm)
y_1	0.07125
y_2	0.1275
y_3	0.225
y_4	0.39
y_5	0.66
y_6	1.08
y_7	1.68
y_8	2.4
y_9	2.88
y_{10}	1.92
y	11.43

Stage	Displacement (mm)
x_1	0.0675
x_2	0.12
x_3	0.21
x_4	0.36
x_5	0.60
x_6	0.96
x_7	1.44
x_8	1.92
x_9	1.92
x_{10}	
x	7.59

Non-Interleaved

Stage	Displacement (mm)
y_1	0.07125
y_2	0.135
y_3	0.255
y_4	0.48
y_5	0.90
y_6	1.68
y_7	3.12
y_8	5.76
y_9	10.56
y_{10}	19.2
y	42.16

Stage	Displacement (mm)
x_1	0.03375
x_2	0.06
x_3	0.105
x_4	0.18
x_5	0.30
x_6	0.48
x_7	0.72
x_8	0.96
x_9	0.96
x_{10}	0
x	3.79875

Table E.3: The table shows theoretical maximum displacement, in both directions, for the 10 stage two dimensional system which was discussed in Chapter 9. Also the displacement at the final stage associated with each stages contribution to the maximum displacement is listed.

2D-System (initial angle: 4 urad)		
Stage	**Displacement (mm)**	
	y-dir.	x-dir.
1. y_1	0.8388	
2. x_1		0.7456
3. y_2	1.3048	
4. x_2		1.1184
5. y_3	1.864	
6. x_3		1.4912
7. y_4	2.2368	
8. x_4		1.4912
9. y_5	1.4912	
10. x_5		
Max	**7.70**	**4.83**

VITA

Daniel Hebert was born in New Iberia, Louisiana in 1981. He graduated from the University of Louisiana of Lafayette, in 2004, with bachelor's degree in Electrical Engineering within the Computer Engineering option. In 2007, he received a master's degree in Electrical Engineering from Louisiana State University. He has been enrolled in the doctoral program in the Department of Electrical and Computer Engineering since 2007 with a minor in Physics.

His research interest include applied-optics, electro-optics, MEMS, and lithography. Outside of academia, he enjoys jogging, reading, and cooking.